Die approbierte Originalversion dieser Dissertation ist an der Hauptbibliothek der Technischen Universität Wien aufgestellt (http://www.ub.tuwien.ac.at).

The approved original version of this thesis is available at the main library of the Vienna University of Technology (http://www.ub.tuwien.ac.at/englweb/).

TECHNISCHE UNIVERSITÄT WIEN

VIENNA UNIVERSITY OF TECHNOLOGY

DISSERTATION

Low-Complexity Timing Synchronization and Equalization Techniques for ATSC Digital Terrestrial Television Reception

ausgeführt zum Zwecke der Erlangung des akademischen Grades
eines Doktors der technischen Wissenschaften

unter der Leitung von

o.Univ.-Prof. Dipl.-Ing. Dr.techn. Herbert Grünbacher
Institut für Technische Informatik (E182)

eingereicht an der

Technischen Universität Wien
Fakultät für Informatik

von

Thomas Wilson MEng (Oxon) CEng
Matrikelnummer: 0527662
Nordwestbahnstrasse 35a/13
A-1020 Wien

Wien, im März 2008

Kurzfassung

Die vorliegende Arbeit beschreibt den Entwurf eines Demodulators für den Empfang von digitalen, ATSC-konformen Fernsehsignalen. Entwickler von Massenprodukten wie digitalen Empfängern sind konfrontiert mit gegensätzlichen Anforderungen wie niedrige Produktionskosten, bestimmt durch die Größe des Halbleiterbausteine, verbunden mit hoher Leistungsfähigkeit. Schlussendlich wird eine effiziente Lösung angestrebt, bei der die Fernsehbild- sowie die Audiowiedergabe akzeptabel sind. Ziel ist es ein bestmögliches Preis/Leistungsverhältnis der digitalen Schlüsselkomponenten zu erzielen.

Rundfunksignale sind Signale sind Störungen im Übertragungskanal ausgesetzt. Um einen fehlerfreien Datenempfang erzielen zu können, müssen die Störungen des Datenkanals und deren Auswirkungen bestmöglich minimiert werden. Ein Entzerrer, ein Teil des Empfängers, vermindert diese Beeinträchtigungen, indem er die Intersymbolstörung (ISI) verringert. Die Takterzeugung ist eine weitere kritische Funktion eines digitalen Empfängers. Sie hat die Aufgabe sich an die Taktrate des Senders anzupassen und diese fortwährend beizubehalten, um eine optimale Symbolphase sicherzustellen und Fehler bei der Symbolerkennung zu minimieren.

Diese Dissertation konzentriert sich auf die Aufgaben der Synchronisierung und Entzerrung des Eingangssignals. Die Ergebnisse stellen einen Fortschritt im Bereich der Algorithmen für niedrig-komplexe Signalverarbeitung, sowie im Entwurf von System-on-Chip (SoC) Architekturen für drahtlose digitale Kommunikationssysteme dar.

Abstract

The work addresses the design of a demodulator for reception of terrestrial American Television Standards Committee (ATSC) digital television (DTV) signals. Designers of mass market receivers face the opposing demands of low implementation cost in terms of silicon area, and high performance, judged ultimately by the proportion of locations at which acceptable TV picture and audio reception can be obtained. The objective is therefore a favorable utility/cost ratio of the key digital components.

Broadcast signals are subject to disturbances arising from the transmission channel, the impact of which must be minimized if accurate data reception is to be achieved. An equalizer within the receiver compensates for these impairments by reducing inter-symbol interference (ISI). Another critical function of a digital receiver is to reconstruct and maintain a digital clock at the same rate as the transmitter, in order to ensure optimal symbol phase and minimize symbol detection errors.

The thesis focuses on synchronization and equalization of the input signal, and presents advancements in the state of knowledge of low-complexity signal processing algorithms and System-on-Chip (SoC) architecture design for wireless digital communication systems.

Summary

The ATSC digital television standard and modulation scheme was originally developed to contend with typical multipath propagation characteristics considerably more benign than those since experienced “in the field”. This mandates a larger and more sophisticated equalizer than that employed in the first ATSC prototype, on the basis of which the standard was accepted for nationwide adoption in the United States of America.

In particular the span and power of echoes in median and worst-case scenarios is significantly higher than anticipated, with several consequences: (i) an equalizer capable of contending with the extended echo profile now dominates the demodulator silicon area; (ii) the periodically-transmitted training sequence is too short to resolve the channel impulse response and consequently fully populate the equalizer coefficients; and (iii) the extended length of the equalizer increases the delay within the timing control loop. These factors motivate the development of efficient equalizer structures, reference-free coefficient-setting techniques and delay-robust timing control.

Measures to reduce the equalizer size are considered. A feedback structure theoretically yields a lower mean-square error (MSE) than a conventional linear equalizer for a given number of coefficients. In addition, the group delay is shorter, with positive repercussions on timing control. However, although reference-data-free (“blind”) techniques are well established for linear equalizers, the situation is more complicated for feedback structures. The coefficients may converge to sub-optimal solutions in decision feedback equalizers (DFEs) when incorrect decisions are fed back. Linear-feedback equalizers (LFEs) are immune to this, but instead they exhibit inferior error rates under some noise conditions and have a higher computational complexity. In the course of the thesis it is demonstrated how a reduced-complexity LFE can provide superior performance to its DFE counterpart (where the definition of performance in the context of DTV reception is analyzed). A novel low-complexity high-performance blind algorithm is presented for coefficient adaptation of a LFE.

The spacing of filter coefficients is an important consideration: the maximum theoretical spacing is the symbol period, which corresponds to the minimum number of equalizer coefficients required for a given echo coverage and thus the lowest implementation complexity. However, such an approach constrains the choice of timing recovery technique and is reported to be sensitive to timing phase. It is shown that symbol rate equalization and timing recovery techniques can be used for ATSC reception and an efficient means of timing control is demonstrated. Use of in-phase, rather than complex symbols, further reduces the computational requirements.

Cost-effective implementation of the required functionality provides opportunities for receiver designers to achieve significant product differentiation through innovations in demodulator component design [1, 2]. Rather than aiming to attain as close to theoretical reception performance as possible, the objective of the work was to design a system satisfying commercial demands: good performance at low cost.

The critical algorithms were developed within Matlab; subsequently a complete system-level model was constructed in SystemC. This enabled verification of system performance under challenging channel conditions and conformance to the ATSC recommendations.

Acknowledgement

I would like to thank my parents for encouraging me to pursue doctoral studies.

I would also like to acknowledge On Demand Microelectronics AG and the Vienna University of Technology for their ongoing support during the course of this work.

This work was sponsored as part of FIT-IT Co-operative Research Project 810196, jointly funded by On Demand Microelectronics AG, Austria and the Bundesministeriums für Verkehr, Infrastruktur und Technologie, Austria.

Contents

1 Introduction 1

1.1 Chronology 2

1.2 Contribution of the Thesis 2

1.3 Organization of the Thesis 2

2 ATSC Digital Television System 4

2.1 Wireless Communication Systems 5

2.1.1 Bandwidth Limitation 5
2.1.2 Multipath Propagation 6
2.1.3 Noise 7

2.2 Data Encoding 8

2.3 Data Frame Structure 9

2.4 8-Vestigial Sideband Modulation 10

2.5 Performance Requirements 12

2.5.1 SNR and TOV 12
2.5.2 AWGN Criterion 13
2.5.3 Eye Diagram 14
2.5.4 Channel Ensembles 15

3 Receiver Architecture 16

3.1 System Overview 16

3.1.1 Implementation 16
3.1.2 Complexity 17

3.2 RF Tuner 17

3.3 Front-End 17

3.3.1 Analog to Digital Conversion 18
3.3.2 Automatic Gain Control 18
3.3.3 Matched Filtering 19
3.3.4 Carrier Frequency and Phase Control 19
3.3.5 Pilot Removal 19
3.3.6 Interpolator 20

3.4 Demodulator 26

3.4.1 Timing Synchronization 27
3.4.2 Equalization 27
3.4.3 Demapper 28

3.5 Decoder 28

4 Timing Recovery 29

4.1 Foundations 29

4.1.1 Structure 29
4.1.2 Implementation Complexity 32
4.1.3 Performance Measures 32

4.2 Timing Error Detector 33

4.2.1 Fundamental Concepts 33
4.2.2 Segment Sync-based Approaches 34

4.2.3 Non-Segment Sync-based Approaches ... 37
4.3 Control Loop ... *39*
4.3.1 Loop Filter ... 39
4.3.2 Controller ... 39
4.4 Proposed Approach ... *40*
5 Equalization ... 41
5.1 Model ... *41*
5.2 Design Considerations ... *42*
5.2.1 Structure ... 42
5.2.2 Data Types ... 44
5.2.3 Coefficient Spacing ... 45
5.2.4 Filter Lengths ... 45
5.3 Coefficient Adaptation ... *45*
5.3.1 Criterion ... 46
5.3.2 Channel Estimation ... 47
5.3.3 Iterative Adaptive Algorithms ... 47
5.4 Blind Equalization ... *49*
5.4.1 Bussgang Algorithms ... 50
5.4.2 Convergence ... 52
5.5 Improved Blind Equalization for ATSC ... *52*
5.5.1 LFE ... 53
5.5.2 Reduced-Complexity Coefficient Updates ... 54
5.5.3 Dispersion Coefficient ... 55
6 Simulations ... 57
6.1 Models ... *57*
6.2 Timing Recovery ... *57*
6.2.1 Steady-State Performance ... 57
6.2.2 Transient Performance ... 59
6.3 Equalization ... *60*
6.3.1 Extended Feedforward Filter ... 60
6.3.2 Coefficient Quantization ... 61
6.3.3 Phase Offset Compensation ... 62
6.3.4 ATSC Channels ... 63
6.3.5 Choice of Feedback Signal ... 66
6.3.6 Dispersion Coefficient ... 68
7 Conclusions and Outlook ... 71
7.1 Main Advancements ... *72*
7.1.1 Timing Synchronization ... 72
7.1.2 Blind Feedback Equalization ... 72
7.2 Outlook ... *73*

Glossary

Abbreviations

ACATS	Advisory Committee on Advanced Television Service
ADC	Analog Digital Converter
AGC	Automatic Gain Control
ASIC	Application Specific Integrated Circuit
ATSC	Advanced Television Systems Committee
ATTC	Advanced Television Test Center
AWGN	Additive White Gaussian Noise
BER	Bit Error Rate
BW	Bandwidth
CIR	Channel Impulse Response
CMA	Constant Modulus Algorithm
CPU	Central Processing Unit
DA	Data-Aided
DAC	Digital to Analog Converter
DC	Direct Current (0Hz)
DCT	Discrete Cosine Transform
DD	Decision-Directed
DFE	Decision Feedback Equalizer
DSL	Digital Subscriber Line
DSP	Digital Signal Processor / Digital Signal Processing
DTV	Digital Television
ELD	Early-Late Detector
FB	Feedback
FEC	Forward Error Correction
FF	Feedforward
FIR	Finite Impulse Response
FPGA	Field-Programmable Gate Array
FSE	Fractionally-Spaced Equalizer
GA	Grand Alliance
HDTV	High-Definition Television
ICI	Inter-Carrier Interference
IF	Intermediate Frequency
IIR	Infinite Impulse Response
ISI	Inter-Symbol Interference
LFE	Linear Feedback Equalizer

LMS	Least Mean Squares
MAP	Minimum a-posteriori
ML	Maximum-Likelihood
MM	Mueller and Muller
MMSE	Minimum Mean-Square Error
MPEG	Motion Picture Experts Group
MSE	Mean-Square Error
NCO	Numerically-Controlled Oscillator
NDA	Non Data-Aided
NTSC	National Television Systems Committee
PAM	Pulse Amplitude Modulation
PDF	Probability Density Function
PLL	Phase Lock Loop
ppm	parts per million
PSD	Power Spectral Density
QEF	Quasi Error-Free
RAM	Random Access Memory
RF	Radio Frequency
RLS	Recursive Least Squares
RMS	Root-Mean Square
ROM	Read-Only Memory
RRC	Root-Raised Cosine
RS	Reed-Solomon
SE	Sign-Error
SER	Symbol Error Rate
SGA	Stop-and-Go Algorithm
SINR	Signal to Interference-plus-Noise Ratio
SNR	Signal to Noise Ratio
SoC	System-on-Chip
SSE	Symbol-Spaced Equalizer
TBD	Trace-Back Depth
TED	Timing Error Detector
TOV	Threshold of Visibility
TV	Television
UHF	Ultra High Frequency
VHF	Very High Frequency
VLSI	Very Large-Scale Integration
VSB	Vestigial Sideband
ZF	Zero Forcing

List of Figures

Figure 2.1 Digital Terrestrial Television Broadcasting model [1] 4
Figure 2.2 Trellis-Coded 8-VSB RF/Transmission system 4
Figure 2.3 Relative position of the Physical Layer relative to Transmitter and Receiver 5
Figure 2.4 Simplified Transmission/Reception model 6
Figure 2.5 DTV multipath channel (time-domain) [9] 7
Figure 2.6 Frequency impairment in 8-VSB ATSC RF Spectrum [10] 7
Figure 2.7 Data Frame structure [1] 10
Figure 2.8 8-VSB data sequence 10
Figure 2.9 Double Sideband spectrum of 8-VSB Signal at IF 11
Figure 2.10 Nominal channel occupancy 12
Figure 2.11 MPEG-2 transport stream segment error rate variation with SNR [3] 13
Figure 2.12 Variation of SER with SNR 14
Figure 2.13 Eye diagram 14
Figure 2.14 Echo Amplitude/Delay profile 15
Figure 3.1 ATSC 8-VSB Receiver 16
Figure 3.2 Frequency down-conversion in the Front-End 18
Figure 3.3 Field-captured ATSC spectra [10] 19
Figure 3.4 Farrow structure for cubic Interpolator 23
Figure 3.5 Farrow structure 23
Figure 3.6 Piecewise Parabolic Farrow structure with α=0.5 24
Figure 3.7 Impulse responses of Farrow filter implementations 25
Figure 3.8 Frequency responses of Farrow filter implementations 25
Figure 3.9 Comparison of interpolator implementations. 26
Figure 3.10 Generic demodulator structure 27
Figure 3.11 ATSC 8-VSB Receiver 28
Figure 4.1 Illustration of Oscillator phase noise 29
Figure 4.2 Feedforward Timing Recovery 30
Figure 4.3 Feedback Timing Recovery 30
Figure 4.4 Analog Timing Recovery 31
Figure 4.5 Hybrid Timing Recovery 31
Figure 4.6 All-Digital timing control 32
Figure 4.7 Structure of Timing Recovery loop 32
Figure 4.8 Segment sync correlator S-curve 34
Figure 4.9 Early-Late Detector S-curve (values 1 and 3) 35
Figure 4.10 Early-Late Detector S-curve (values 2 and 4) 36
Figure 4.11 S-curve of Early Late Detector as applied by Kim 36
Figure 4.12 Mueller and Muller S-curve SNR variation 38

Figure 4.13 Mueller and Muller S-curve standard deviation 38
Figure 4.14 Sawtooth function 40
Figure 1 Simplified model of Channel and Equalizer 42
Figure 5.2 Linear transversal equalizer 43
Figure 5.3 Feedback equalizer structure 44
Figure 6.1 SystemC Front-End and Demodulator implementation 57
Figure 6.2 Comparison of Timing Error Detectors 58
Figure 6.3 Effect on SER of Interpolator compensation 58
Figure 6.4 Equalizer frequency response for Interpolator compensation 59
Figure 6.5 Convergence of Timing Recovery loop 59
Figure 6.6 Feedforward coefficient values 60
Figure 6.7 Histogram of Equalizer output symbols 61
Figure 6.8 Required SNR at TOV versus coefficient wordlength. 61
Figure 6.9 Effect of coefficient wordlength on convergence time 62
Figure 6.10 Variation of coefficients with symbol timing phase 63
Figure 6.11 Equalizer output SNRs for ACATS Ensembles A-F 65
Figure 6.12 SER curves for ACATS Ensemble A channel 67
Figure 6.13 Comparison of LFE implementations (Brazil B, 21.1dB SNR) 67
Figure 6.14 Implied Dispersion Coefficient 68
Figure 6.15 AWGN performance of DFE 68
Figure 6.16 Further simulations with optimal Dispersion Coefficient 69
Figure 6.17 Variation of (DFE) SER with dispersion coefficient close to the TOV. 70

List of Tables

Table 1 ATSC Data Encoding and Framing Parameters 9
Table 2 ATSC 8-VSB Modulation Parameters 11
Table 3 Complexity of low-order Farrow implementations (per interpolant) 24
Table 4 Computational increase of a LFE relative to a DFE 53
Table 5 Computational complexity of a DFE 54
Table 6 Complexity of full-precision coefficient update 54
Table 7 Complexity of sign-error coefficient update 55
Table 8 ACATS Echo Ensembles used by ATTC 64
Table 9 Equalizer (LFE) performance at TOV 65
Table 10 Brazil Echo Ensembles 66

1 Introduction

The advanced television systems committee (ATSC) system was designed to allow digital transmission of high-quality video and audio signals in MPEG-2 data packets with improved power and bandwidth efficiencies compared with the existing analog system. Following extensive laboratory and field testing of a prototype receiver developed by the "Grand Alliance" (GA) consortium, the ATSC system was formally approved as the digital television (DTV) standard for the United States on December 24th, 1996, with a scheduled switch-off of analog TV (NTSC) broadcasts on February 17th, 2009. It has been successfully adopted in Canada and Mexico, and is currently undergoing evaluation for possible deployment in other Latin American countries considering a similar transition.

The ATSC DTV standard incorporates considerable flexibility for broadcasters by defining 18 different allowable picture formats, of which six are high definition TV (HDTV). These allow for different levels of picture quality, picture sizes and frame rates, with up to five channels of high-quality audio.

Compared with the its analog predecessor, the digital system exhibits improved robustness to impulse noise, co-channel interference (from other DTV channels or legacy analog NTSC signals) and signal distortion arising from multiple path propagation in the transmission channel. The last of these arises when the receiver signal comprises superimposed signals arriving from two or more paths from the transmitter, such as a direct path and a reflection off a building, which have different lengths and thus arrive out of phase with one another. In analog TV this phenomenon is perceived as a superposition of multiple pictures known as "ghosting"; in DTV it degrades the digital bitstream rendering the picture completely unwatchable unless corrected.

Digital signals are inherently immune to low levels of noise whose amplitude is less than half the distance between the discrete levels, and is therefore automatically removed when the symbols are quantized prior to decoding. At higher noise levels, forward error correction (FEC) applied to the transmitted signal permits quasi-error-free operation of the receiver down to low signal-to-noise ratios. In contrast to analog TV signals which degrade with increasing interference and noise, DTV pictures exhibit a more sudden transition.

Three "helper" signals are periodically inserted into the ATSC data stream to assist reception under imperfect transmission conditions: a constant-level pilot for carrier acquisition and a Segment Sync for synchronizing the data clock in both frequency and phase. In addition, a Frame Sync is added for data framing and to assist compensation of channel distortion by an equalizer; it facilitates calculation of the channel impulse response, which can be used to set of equalizer coefficients. Its length of 832 symbols allows resolution of echoes up to 24μs either side of the dominant signal path, which was assumed to be sufficient when the standard was ratified. Since then considerably longer echoes have been observed in practice, rendering the training sequence insufficient in isolation for populating equalizer coefficients. This mandates the use of additional (or alternative) coefficient-setting techniques using the non-training data.

The necessity for longer echo cancellation capability also increases the required equalizer length far beyond that originally anticipated, raising challenges in the areas of convergence time, signal-to-noise ratio performance and equalizer stability. It emphasizes the desirability of implementations featuring the opposing characteristics

of low-complexity and high performance. A key requirement in meeting this objective is to minimize the sample rate through the equalizer, despite a penalty in channel inversion performance, robustness to timing phase and increased risk of converging local minima compared with higher sample-rate alternatives. This constraint on the sample rate also restricts the available design options for timing synchronization.

1.1 Chronology

The GA consortium's prototype receiver [3] was demonstrated in 1994. The first commercial DTV receivers in 1998 and 1999 experienced problems with tuner overload and multipath equalization, which were addressed in later designs. In 2001, the so-called "4th Generation" 8-vestigial sideband (8-VSB) receivers exhibited good outdoor DTV characteristics. By 2005 the next generation performed well indoors due largely to improvements in tuner design, carrier and clock synchronization and multipath cancellation [4].

More than a decade after the introduction of the ATSC standard, design of compliant receivers is still a fertile area for research and innovation. Of particular interest are channel equalization and timing recovery, both of which are critical to successful operation and differentiate products in terms of performance and implementation cost [5].

1.2 Contribution of the Thesis

The thesis presents innovations in the fields of channel equalization and timing synchronization techniques, with a focus on 8-VSB ATSC DTV receivers. However, the techniques developed have a wider applicability, because they do not rely on ATSC-specific data sequences.

By considering the minimum SNR required to obtain a quasi-error free (QEF) picture, rather than the symbol error rate (SER) at all SNRs, it is shown that a linear feedback equalizer (LFE) exhibits superior performance to a decision feedback equalizer (DFE). The increase in complexity associated with processing unquantized values in the equalizer's feedback filter is mitigated by use of a hard-limited algorithm. Further performance improvement is obtained by adjusting the dispersion coefficient within a blind algorithm to incorporate the effect of noise in the received signal; a result that has wider implications for blind equalization.

A symbol-rate equalizer with real-only coefficients filtering only the in-phase portion of the input signal exhibits a relatively low implementation cost for a given echo coverage. An all-digital symbol-rate timing synchronization scheme is presented, which combines the benefits of reduced component count and improved performance compared with the technique in the GA prototype. This is achieved by measuring the timing error on quasi-random data rather than the periodic synchronization byte. Overall, the system exhibits a lower timing jitter and consequently implementation loss, while its ability to operate on unknown multi-level data renders it a desirable solution in the broader field of PAM communication systems.

1.3 Organization of the Thesis

The ATSC DTV system is introduced in Chapter 2 in the context of wireless communications; section 2.1 introduces the main impairments experienced during terrestrial transmission, which explains the motivation behind the data encoding and modulation techniques (sections 2.2 to 2.4) employed in ATSC transmission. The recommended

multipath echo span coverage and resilience to channel ensembles and noise of a commercial receiver are then discussed. The performance measures described in section 2.5 provide a means of comparing design alternatives.

Chapter 3 covers the main signal processing stages within a DTV receiver and their relative positions. The subject of receiver architecture design begins with a discussion on complexity measures in section 3.1.2, understanding of which is vital to appreciation of the innovations described in later chapters. After a system overview in section 3.1, the remainder of the chapter concentrates on the main functions of a demodulator. Particular attention is paid to the various topologies for timing recovery systems; due to the relative merits of an all-digital implementation, interpolation techniques (section 3.3.6) are discussed in detail, and a structure with favourable characteristics is presented.

Timing recovery is then analysed in more detail in chapter 4. After a survey of the main concepts in all-digital timing recovery (section 4.1), applicable symbol-rate timing measurement techniques (section 4.2) are described. Control of the interpolator for timing phase and frequency synchronization is described in section 4.3, before innovations in this area are presented in section 4.4.

Chapter 5 explores applicable equalization techniques: the objective is first clarified in section 5.1; then architectural considerations are covered in section 5.2. Several methods for coefficient adaptation are analysed in section 5.3 in the context of ATSC reception. A deeper evaluation of blind equalization techniques in the following section (5.4) provides the necessary background for understanding the approach taken and its improvement over the state-of-the art (section 5.5).

The designs are verified by means of simulations, results of which are presented in chapter 6. First the models and the test methodology are described in section 6.1, with an explanation of the critical design parameters. Then results for the timing recovery and equalization techniques are given in sections 6.2 and 6.3, clearly illustrating their improvement over existing methods.

Chapter 7 concludes with a summary of the main advancements in the fields of timing synchronization (section 7.1.1) and blind feedback equalization (section 7.1.2). As the topic is of considerable interest to researchers and design teams, a number of possible areas for future research are suggested in section 7.2.

2 ATSC Digital Television System

In order to make most efficient use of the channel capacity, the raw video and audio streams are first compressed by sophisticated algorithms such as the Discrete Cosine Transform (DCT), motion estimation and frame prediction according to the MPEG-2 standard (Motion Picture Experts Group). Audio is compressed following the Dolby Digital AC-3 standard. From the resulting data sequences, a service multiplexer constructs an MPEG-2 transport stream containing video packets, audio packets, and ancillary data packets (Figure 2.1).

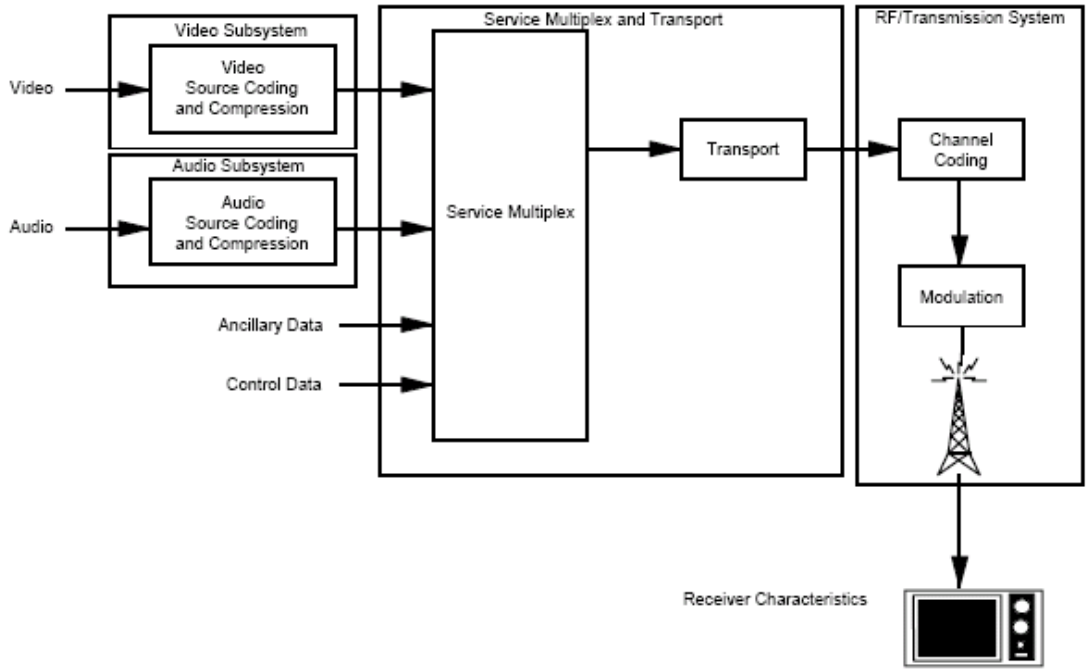

Figure 2.1 Digital Terrestrial Television Broadcasting model [1]

The transport stream data rate is maintained at a constant 19.28Mbits/s by adding additional null packets if necessary, and divided into 187 byte data segments (the "payload"), headed by an MPEG-2 sync byte. The transmitter passes the MPEG-2 packets through a channel encoder, modulator and a high power amplifier, to produce a RF broadcast signal (Figure 2.2).

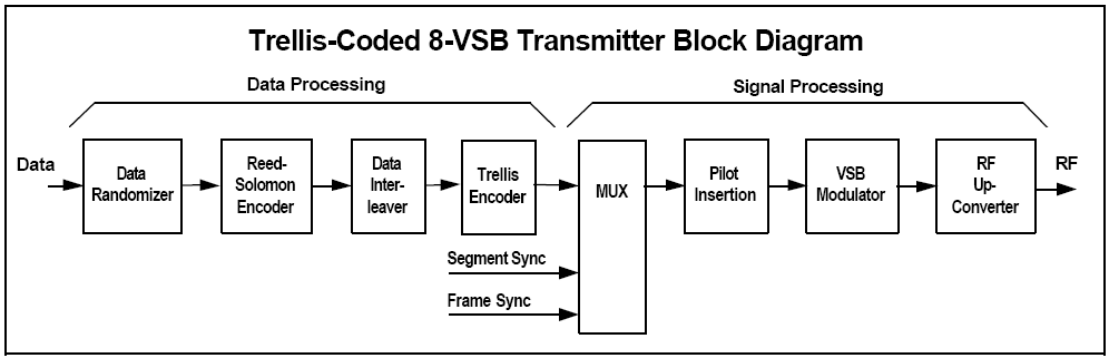

Figure 2.2 Trellis-Coded 8-VSB RF/Transmission system

This work focuses on aspects of the *physical layer*; a subset of the RF transmitter/receiver system. This comprises a modulator that converts a sequence of data bits

into a continuous-time waveform suitable for transmission over the airwaves, the *communication channel*, and a demodulator within the receiver, whose role is to reconstruct this sequence as accurately as possible (Figure 2.3).

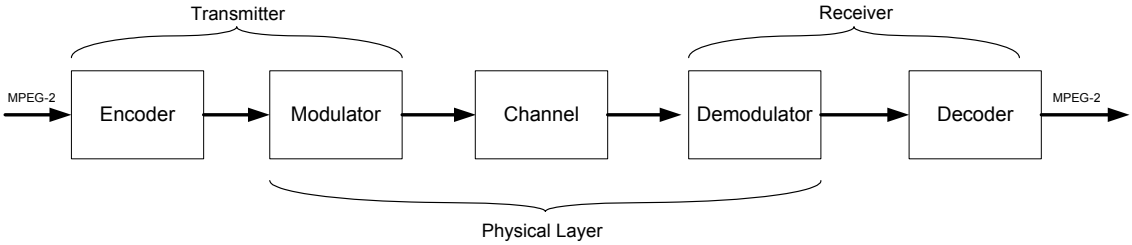

Figure 2.3 Relative position of the Physical Layer relative to Transmitter and Receiver

2.1 Wireless Communication Systems

Wireless communications appear in many different applications, such as terrestrial radio links (e.g. military communications), mobile phones, wireless networks, broadcast, global positioning systems (GPS) and satellite links. Despite their apparent diversity, all of these have in common several challenges arising directly from the physical separation (the "channel") between the transmitter and receiver, and indirectly from measures in the transmission process applied in order to convey as much information as possible in the minimum frequency bandwidth.

Impairments resulting from the channel include attenuation of the signal due to the physical distance and medium between transmitter and receiver, and interference from background noise and other signals. The net effect of these is to reduce the signal-to-noise ratio (SNR) of the received signal. Objects blocking the path further lower the SNR, while multiple reflections of the signal introduce further complications, introduced in section 2.1.2 and discussed in much detail through the thesis.

Indirect challenges include the need to reconstruct a digital clock at the receiver corresponding to that driving the digital-to-analog converter (DAC) at the transmitter, which is necessary in order to determine the information-bearing digital signal values. In addition, signals transmitted on adjacent frequency bands may interfere with the band of interest, resulting in a significant impairment. (This topic is beyond the scope of the work described here.)

The character and severity of these effects depends on the communications system and the nature of the transmission channel.

2.1.1 Bandwidth Limitation

The symbol pulses must be shaped before transmission in order to reduce their spectral width and thus permit transmission over a bandwidth-limited channel. Otherwise interference between the symbols occurs due to "ringing" in time either side of the pulse, thus obscuring the clear divisions between the symbol levels. Filtering with a Nyquist filter band-limits the signal while maintaining orthogonality of the pulses, thereby preserving the original symbol values at the sampling instants. Between sampling instants, the total RF waveform envelope is the summation of the ringing of previous and future symbols.

2.1.2 Multipath Propagation

Multipath propagation is the phenomenon where a signal transmitted from an antenna travels over multiple paths of different lengths, resulting in an ensemble of signals at different power levels displaced in time at the receiving antenna. The combination of time delays correspond to frequency-dependent power attenuation and may considerably raise the error rate at the receiver unless compensated [6]. In DTV systems, there tend to be only a few dominant paths [7], and the signal is said to be *sparse*.

The main forms of propagation phenomena are:

- Reflection off smooth surfaces.
- Transmission through buildings, walls, etc..
- Diffraction at solid edges.
- Scattering on rough surfaces.
- Shadowing due to large objects, such as hills.

In this thesis, multipath propagation is considered to be a linear system as depicted in Figure 2.4: a source signal from a transmitter is subject to multipath propagation and noise before reaching a receiver.

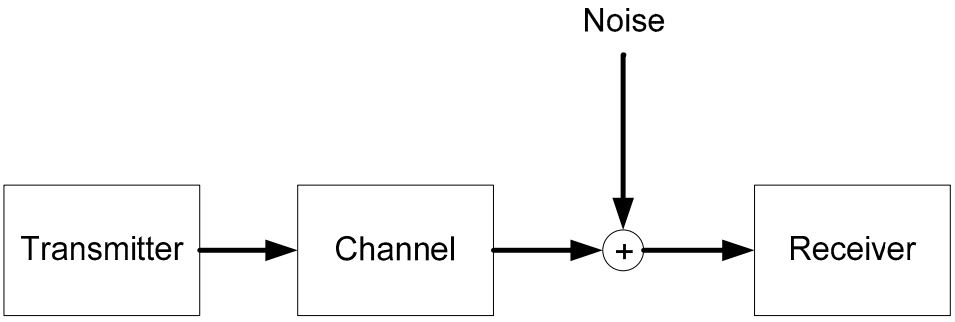

Figure 2.4 Simplified Transmission/Reception model

The *coherence time* of a system is an indicator of the rate of change of a channel [8], defined as:

$$T_c = \frac{0.5}{f_{Doppler}}. \qquad 2.1$$

As the Doppler frequency specified in the performance recommendations [9] is 0.05Hz, the coherence time is 10s. This is sufficiently long for the channel to be considered stationary. The *coherence bandwidth* refers to the signal bandwidth above which frequency-selective attenuation due to the maximum echo span T_m would occur [8]:

$$BW_c = \frac{0.5}{T_m} \qquad 2.2$$

The maximum expected echo span in ATSC is from -10μs to +40 μs [9], leading to a coherence bandwidth of 10kHz. As this is significantly lower than the transmitted signal bandwidth of 6MHz, the channel is highly frequency selective. Figure 2.5 illustrates a typical field-captured channel impulse response. The axes are normalized

to the dominant path (highest power), which is not the first signal to reach the antenna: lower power pre-echoes in the region –3μs to –2μs arrive before it. A post-echo at +16μs is also visible.

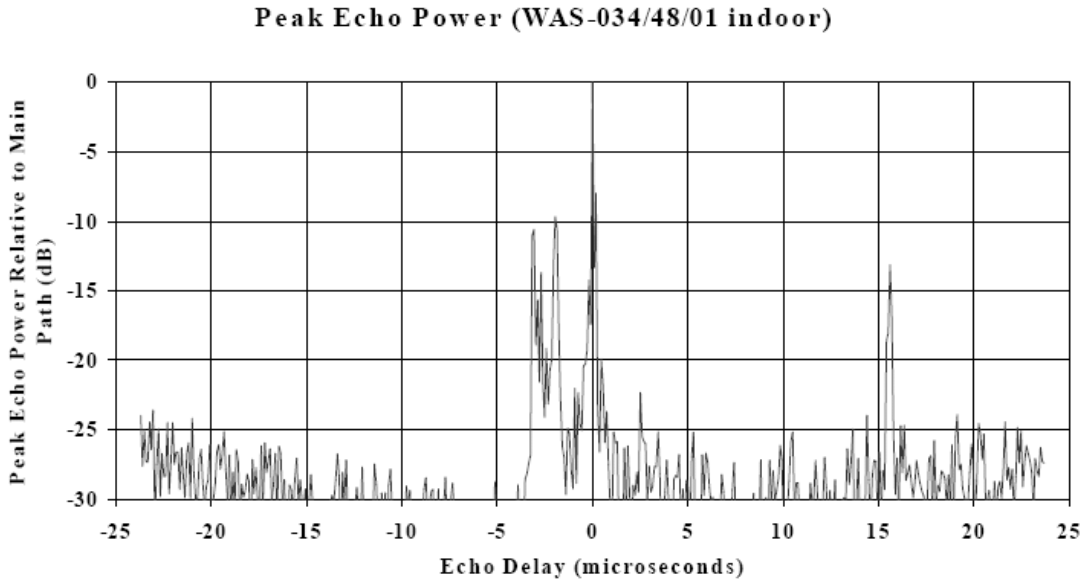

Figure 2.5 DTV multipath channel (time-domain) [9]

Figure 2.6 illustrates the frequency-domain distortion arising from a field-captured channel. In this case the overlaid (dotted) line represents the transmitted signal, whereas the received signal illustrates non-uniform passband attenuation.

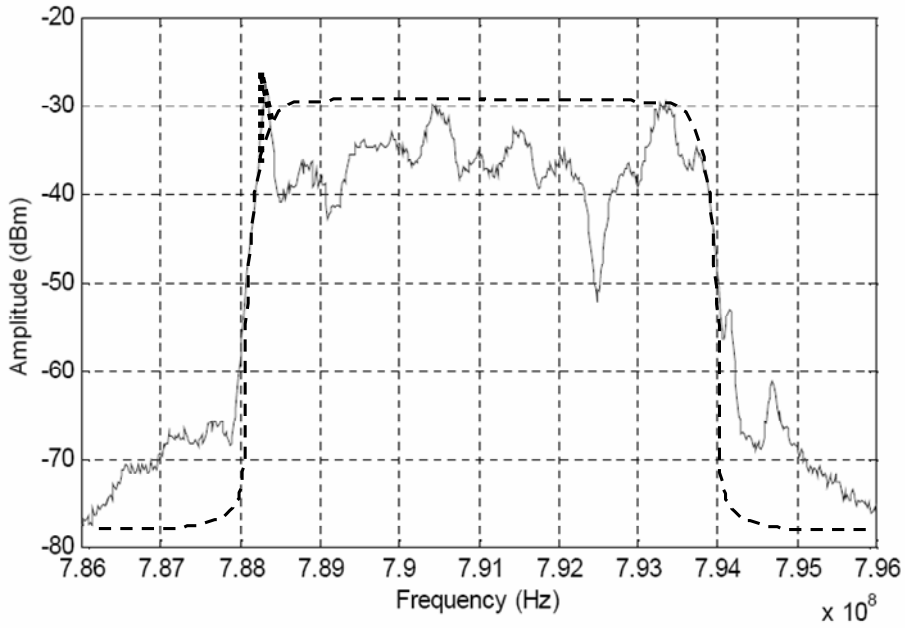

Figure 2.6 Frequency impairment in 8-VSB ATSC RF Spectrum [10]

2.1.3 Noise

Noise is one of the principal impairments in 8-VSB signals [11]. It is useful to distinguish between the main sources that arise in ATSC DTV systems.

- The largest contribution is *broadband noise*, which is caused by random fluctuations and crosstalk in the same bandwidth as the transmitted signal.
- *Amplitude and phase errors* arise when the signal gain or phase changes at the transmitter or receiver as a function of instantaneous variations in the signal magnitude. This is a non-linear effect that generates inter-modulation terms outside the assigned channel ("spectral re-growth") and reduces the SNR measured at the receiver.
- *Implementation noise* is introduced by non-idealities at both transmitter and receiver, normally due to limited numerical precision in operations and storage, and approximations and truncations in computational functions (e.g. non-flat group delay or frequency response in filters). Tracking loops, such as timing synchronization, introduce jitter and act as noise sources. Equalizers enhance noise as well as signal power; even with an infinite length equalizer it may not be possible to invert a channel perfectly. Consequently trade-offs between complexity and performance are required in any equalizer design. The stochastic nature of their input data sequences leads to low-level fluctuations in their coefficients when adapted by an algorithm; even "idle" coefficients– those not involved in signal compensation–vary randomly at a low level and contribute noise.

In the remainder of the thesis only the predominant sources of noise are considered, namely the implementation loss and broadband noise, modelled as AWGN. (The total contribution of other sources is estimated to be between 27dB and 29dB SNR, which is considerably less than the expected AWGN levels [11].)

Sub-systems within commercial products are inherently imperfect, either due to manufacturing limitations or cost constraints; good system design is the process of ensuring that such compromises are chosen so as to provide satisfactory performance at an acceptable cost.

Most sources of implementation noise are independent and consequently contribute to the total noise power. The corresponding increase in input SNR required to obtain a given SER compared with an ideal receiver is collectively known as the "implementation loss". A receiver with superior performance has a lower implementation loss, because it exhibits a lower SER for a given input SNR, translating to a wider range of sites at which it produces a QEF picture. Alternatively, if an acceptable implementation loss is specified, it makes commercial sense to use this "budget" in areas that will most significantly reduce manufacturing costs (e.g. by lowering the required silicon area for filters by using the minimal numbers of short-wordlength coefficients).

2.2 Data Encoding

Error correction techniques protect the data from corruption due to imperfections in the modulator/demodulator sub-system, and more significantly due to ISI arising from noise and distortion within the transmission channel.

Successful analog-to-digital conversion requires a high percentage of the received samples to fall within the analog-to-digital conversion (ADC) range to avoid "clipping". In addition, the mean signal level should occupy a significant proportion of the available dynamic range in order to prevent quantization effects from impairing the SNR. However, a conflicting consideration is that it is advantageous to use as few bits' numerical precision per converted sample in order to keep unit costs low in the

context of a mass-market DTV receiver. Thus it is advantageous for the signal to be transmitted with a low peak-to-average ratio, which is achieved by employing a data randomizer as the first step within the encoder, which reduces the likelihood of long sequences of 0s or 1s and flattens the spectrum of the transmitted signal. This also lowers the demands on the AGC, minimizes interference into adjacent channels, and protects against complications that might otherwise occur in the receiver tracking loops.

Forward Error Correction (FEC) is applied within a Reed-Solomon encoder, which adds twenty parity bytes to the end of each data segment, extending the length from 187 to 207 bytes. This provides error correction capability of up to 10 byte-errors per data segment corrupted during transmission, and in conjunction with the data byte convolutional interleaving is particularly effective for burst noise correction. Next the data segments (but not the segment and frame syncs) are spread out over 52 data segments to a depth of 1/6 of a frame (4ms) within a convolutional interleaver. The bytes of each segment are moved to different segments, distributed evenly among the group. This prevents against strings of consecutive bit corruption (such as "shot noise") up to 193μs, because at the receiver they are converted into many short errors, which can all be corrected within the corresponding Reed-Solomon decoder in the receiver. Finally, protection against burst noise in the channel is achieved by 2/3 rate trellis encoding: a redundancy bit is added to every two data bits, with state transitions governed by a four-state Ungerboeck code.

Table 1 ATSC Data Encoding and Framing Parameters

Segment Length (including sync)	832 symbols
Segment Sync Duration	4 symbols
Frame Sync Duty Cycle	1/313
Bits per Symbol	3
Trellis Coding Rate	2/3
Reed-Solomon FEC	T=10 (207,187)

2.3 Data Frame Structure

A pilot, segment syncs and a training sequence (the "Field Sync") are added to the signal in order to assist data reconstruction within the receiver.

A Data Frame is formed by multiplexing the channel-coded data and Segment Sync and Field Sync symbols, as defined in [1] and illustrated in Figure 2.7. A data frame comprises of two Data Fields, each of which contains 313 Data Segments. A Data Segment is split into four Segment Sync Symbols and 828 data and FEC symbols, except the first Data Segment of a Data Field, where the data symbols are replaced by a known synchronization pattern: the "Field Sync". The latter is primarily a set of known pseudo random sequences, which can be used to train the coefficients of the receiver's equalizer up to ±24ms of the dominant signal path.

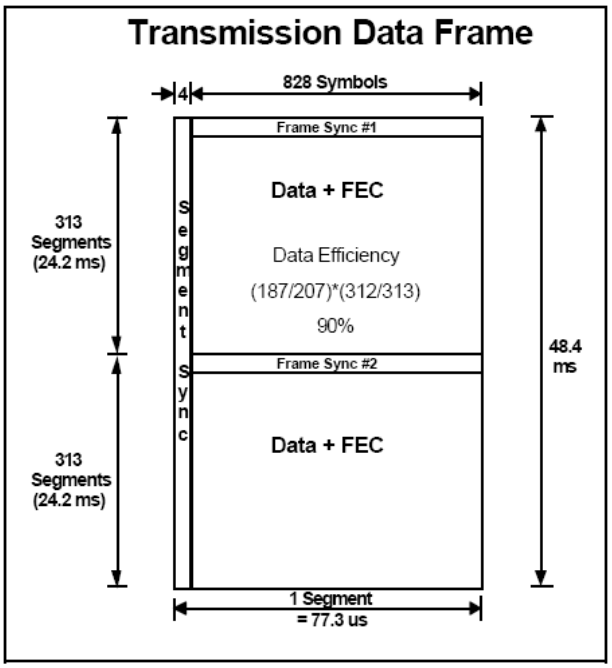

Figure 2.7 Data Frame structure [1]

In the terrestrial broadcast mode, the signal is a form of pulse amplitude modulation (PAM) with an alphabet of eight symbol levels {–7, –5, –3, –1, +1, +3, +5 +7}. Due to randomizing of the binary data distribution in the transmitter, the 8 symbol levels are equiprobable with zero mean.

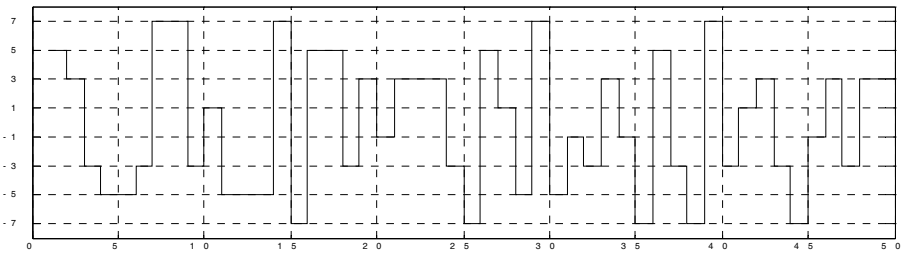

Figure 2.8 8-VSB data sequence

A periodic 4-symbol sequence {+5, –5, –5, +5} is inserted at the start of every 832-symbol segment (replacing the MPEG-2 packet sync byte) in order to assist symbol clock recovery and data segment delineation. The pulse is designed to be easily extracted from the quasi-random data sequences by a correlator.

A low-level pilot intended to aid carrier recovery is created by adding a DC value of 1.25 to the baseband data. This appears as a peak in the spectrum after modulation, contributing 0.3dB to the total transmitted power.

2.4 8-Vestigial Sideband Modulation

This section describes 8-VSB modulation and illustrates how its application to ATSC DTV results in efficient spectrum utilization. The main parameters are summarized in Table 2.

Table 2 ATSC 8-VSB Modulation Parameters

Channel Bandwidth	6.0 MHz
Excess Bandwidth	11.5 %
Symbol Rate	10.762 MHz
Payload Data Rate	28.9 Mbps
Gross Payload	21.52 Mbps
Pilot Power Contribution	0.3 dB
Peak/Average Power (99.9%)	6.3 dB

The eight-level signal containing data, syncs and DC pilot is amplitude modulated onto an intermediate frequency (IF) carrier, typically at a standard frequency (44 MHz in the U.S.). As the original baseband signal contains real-only values, the resulting spectrum is symmetrical, as illustrated in Figure 2.9 (taken from [12]). As the lower half is a mirror image about the IF, and the sidelobes on both sides are scaled copies of the centre spectrum, it contains redundant information.

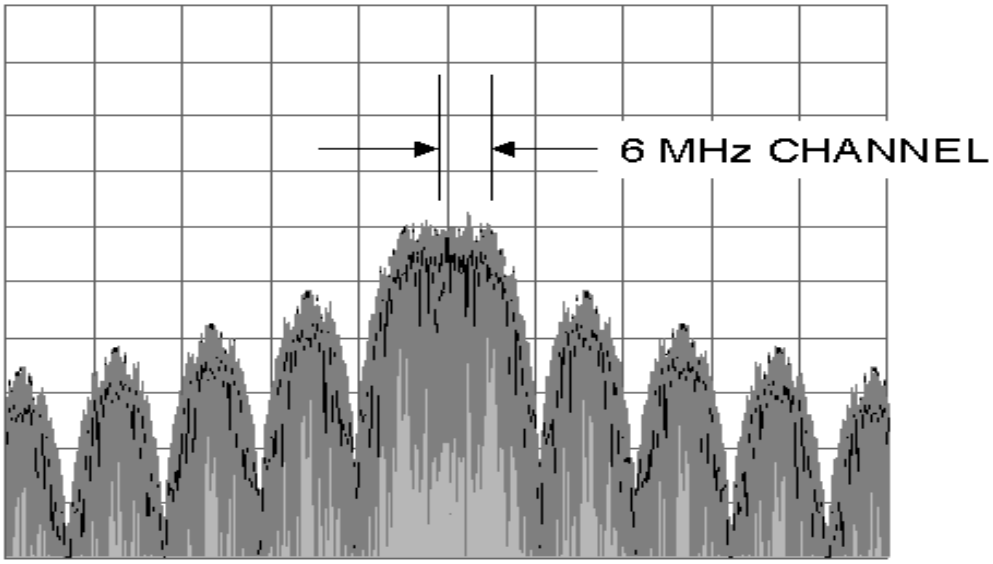

Figure 2.9 Double Sideband spectrum of 8-VSB Signal at IF

The redundancy is removed by bandpass filtering this signal, to leave only the upper half of the central lobe. This operation can be combined with pulse-shaping (described in section 2.1) by employing a root-raised cosine (RRC) filter. As the RRC and the raised cosine are both Nyquist filters, this allows a second RRC to be used as a matched filter at the receiver, so that transmit and receive filters have the combined response of a raised-cosine filter.

The data rate at the output of the trellis coder is 10.76Msymbols/s; thus the band of interest is 10.76/2 = 5.38MHz. The RRC filter parameter alpha determines the width of the transmission regions. In ATSC, this excess bandwidth is specified as 11.5%, resulting in a 6MHz channel bandwidth signal (the same bandwidth as legacy NTSC transmissions). Although this leads to a wider bandwidth requirement, it lowers the

specifications of the hardware implementation in terms of filter requirements and the precision of the sampling clock.

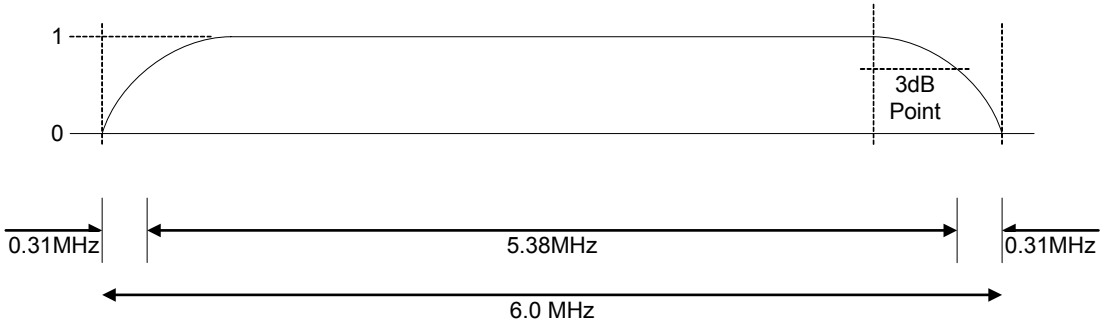

Figure 2.10 Nominal channel occupancy

The corresponding transmitted spectrum is shown in Figure 2.10. This illustrates the flat main lobe with a RRC roll-off at either end. Samples are fed at a constant symbol rate to a DAC, which generates a signal suitable for the RF up-converter to translate to the desired channel in the VHF or UHF bands.

2.5 Performance Requirements

Analog transmission systems such as NTSC experience a gradual degradation of picture and audio quality as the signal level (and consequently the SNR) decreases. Multipath propagation causes "ghosts" on the television screen which correspond to superimposed versions of the transmitted signal, delayed and attenuated by differing amounts depending on the paths between transmitter and receiver. These can only be perceived as resembling the original picture because the transmitted signal directly conveys picture information without first being encoded. In contrast, the digital ATSC signal originates from an MPEG-2 encoded stream, the bits of which are subject to further FEC encoding before modulation and transmission. As a result, the transmitted signal in no way resembles picture information until FEC and MPEG-2 decoding reconstruct the original audio-visual sequence. Thus the mechanisms of signal corruption are entirely different compared with the analog system: degradations in the received signal manifest as symbol errors following demodulation; FEC decoding corrects bit errors to an extent (depending on their rate of occurrence and character); finally, individual byte errors within the MPEG-2 stream appear as picture (or audio) errors over multiple video frames, due to the interdependence of frames. Thus the resulting audiovisual quality is highly sensitive to even small numbers of errors following FEC decoding. However, the powerful coding/decoding techniques produce quasi-error-free sequences from demodulated streams with a relatively high SER. Above a threshold, however, the error correction fails rapidly with a catastrophic impact on the audio-visual sequence.

2.5.1 SNR and TOV

ATSC has defined the point at which MPEG-2 segment errors first become observable to expert viewers[1] as the "threshold of visibility" (TOV) [13]. In the immediate region of the TOV, the MPEG-2 error rate is highly sensitive to SNR and exhibits the

[1] The FCC Advisory Committee on Advanced Television Service (ACATS).

"cliff effect" characteristic of error-corrected digital communication systems. The position of the TOV is dependent both on the channel impairment and the receiver implementation. In AWGN, this point occurs at a SNR of 14.9dB (Figure 2.11) for the GA prototype receiver, which has since been accepted as a standard requirement. A superior receiver tends to move the whole curve towards the left, and a multipath propagation channel to the right; residual distortion or amplified noise acts as an internal noise source (the more hostile, the further it would move). As the video quality is unacceptable at SNRs below TOV, and perceptibly perfect above, the threshold SNR at TOV provides a useful figure of merit for comparing receiver implementations. (Another is the ability to compensate for multipath channels, which is discussed in section 2.5.4.) Above this point, the error rate is very low because of the FEC, and consequently differences between receivers in this region have negligible impact on the user experience.

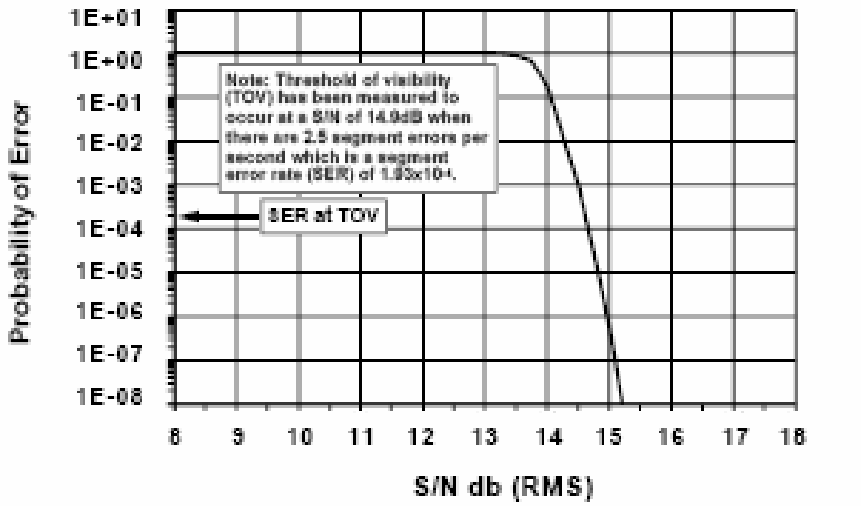

Figure 2.11 MPEG-2 transport stream segment error rate variation with SNR [3]

2.5.2 AWGN Criterion

When comparing demodulator subsystems, it is more insightful to use a more sensitive indicator of relative performance than the MPEG-2 error rate: the SER of the quantized equalizer output. This has a shallower gradient and thus permits analysis with a finer resolution in the region of interest (SNR at TOV).

Figure 2.12 depicts the theoretical relationship between SER and SNR for transmission of 8-VSB data over a noisy (AWGN) channel. A real system deviates from this curve in a similar manner to (but more pronounced than) the MPEG-2 error rate (Figure 2.11). The SNR/TOV point for the GA prototype system (the AWGN criterion) is seen to lie 0.3dB to the right of the Shannon limit; the separation represents the *implementation loss* arising from quantization, phase noise and non-ideal components [14]. This manifests itself in a digital receiver as the input signal SNR increase required to attain the same SER as an ideal receiver at a specified operating point. The 0.3dB implementation loss at TOV is taken as the performance constraint under AWGN.

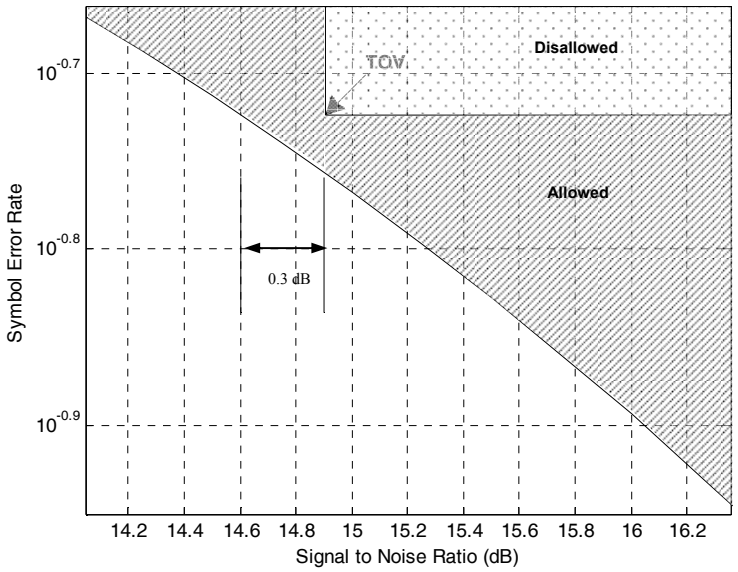

Figure 2.12 Variation of SER with SNR

2.5.3 Eye Diagram

The term "channel eye" refers to the plot on an oscilloscope that is observed if consecutive portions of a received continuous PAM signal are superimposed. It provides a useful qualitative visualization of the ISI and the effect of distortion on the probability of error. Figure 2.13 is an eye diagram covering multiple transitions of 8-VSB shown over two symbol periods. The vertical line of white spaces in the centre indicates that the levels of the received symbols may be individually discerned. Its horizontal symmetry signifies a choice of sampling phase that maximizes the probability of correct symbol identification.

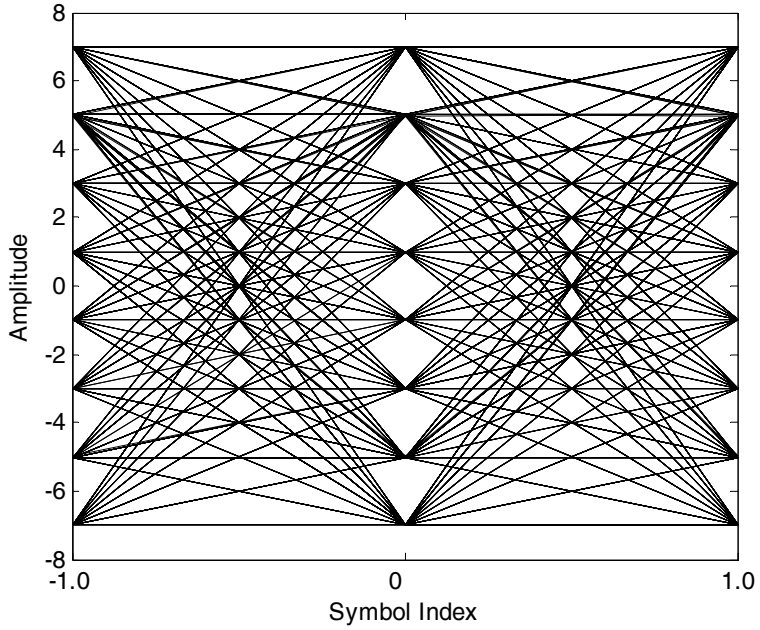

Figure 2.13 Eye diagram

2.5.4 Channel Ensembles

The AWGN performance criterion was described in section 2.5.2. When considering resilience to multipath channels, this becomes a secondary factor after the range and complexity of channels that can be handled by the system. ATSC publishes guidelines for receiver performance [9], specifying the minimum recommended echo delay/attenuation capability, and provides a set of profiles obtained from field measurements to facilitate comparison of equalizer designs under realistic conditions.

The darker line in Figure 2.14 [9] indicates the required echo power compensation within the mandatory coverage range from -10µs to +40µs. At the extremes, the echo powers are -5dB and -6dB relative to the dominant path, respectively. The region covered by the grey line is an optional extension. As the focus of the work was on developing the architecture and algorithms within the context of a receiver with acceptably high performance and low complexity, only the mandatory (black) region was considered. (It was not an objective to create a system robust to all channel ensembles.)

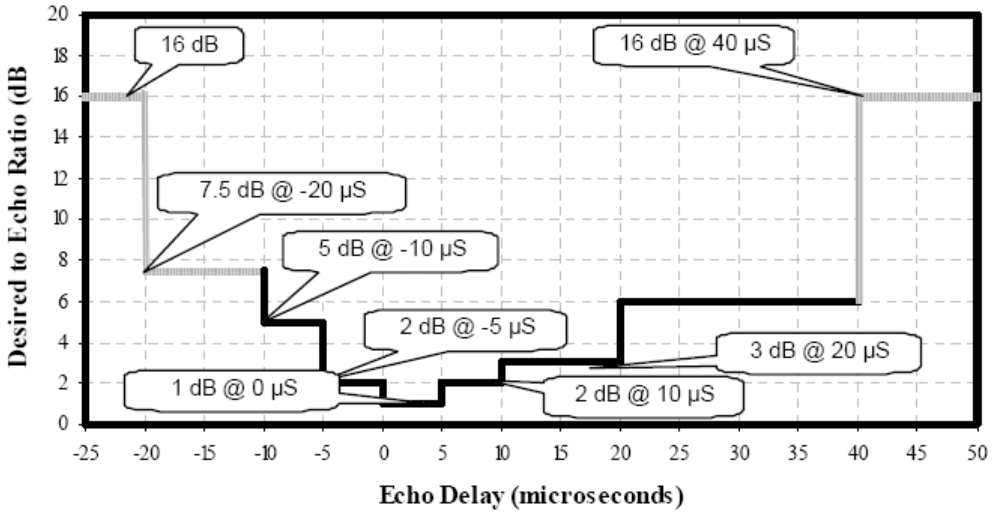

Figure 2.14 Echo Amplitude/Delay profile

3 Receiver Architecture

This chapter provides an overview of receiver architecture and draws attention to subsystems that will subsequently be analysed in more depth. In order to understand the advances in timing synchronization and equalization, it is important to appreciate their interaction and roles within the system as a whole. (However, it is not the intention to describe optimal designs for all parts of the receiver.)

3.1 System Overview

The ATSC 8-VSB receiver reverses the operations of the encoder and modulator, as illustrated in Figure 3.1. It consists of: Front-End, Demodulator, FEC Decoder and the Transport Layer decoder. In this work, the focus is on the first two of these.

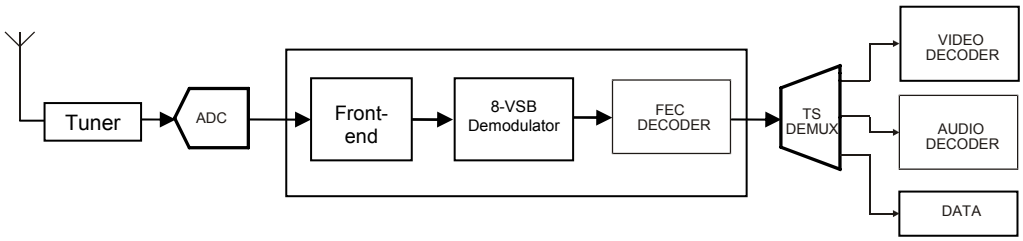

Figure 3.1 ATSC 8-VSB Receiver

3.1.1 Implementation

As in many signal processing systems, DTV receivers comprise heterogeneous components, where the functionality is achieved by a hybrid of hardware and software subsystems:

- Analog circuits, such as filters and amplifiers. Modern receivers contain a minimum of analog components, instead performing most operations digitally where possible. This typically leads to a smaller silicon requirement and therefore superior cost efficiency.
- ADCs and DACs.
- Software-programmable DSPs, which perform vector-oriented tasks such as filtering, modulation and gain control.
- Microprocessors to carry out non-repetitive or control-oriented tasks and implement protocol stacks, system software and interface software.
- Application-specific integrated circuits (ASICs) are limited to high-throughput tasks such as equalization, filtering, synchronization and channel decoding. ASICs typically exhibit the lowest power dissipation because they are dedicated and optimized for a particular purpose.
- Hardware accelerators, which compute demanding signal processing algorithms unsuited to cost-effective implementation in DSPs. These may to some extent be programmable or configurable (for example, coefficients of a digital filter).
- Programmable ROM and RAM.

The division of signal processing tasks depends on the application. As a HDTV receiver requires massive parallelization and pipelining in order to process its high

signal bandwidth in real-time, an ASIC implementation leads to a lower cost for mass-market volumes. [14]

3.1.2 Complexity

In the context of this thesis, the term complexity refers to the computational cost associated with a sequence of steps that achieve a desired functional outcome. This may be viewed on several levels: the *architectural* level, referring to the structure and choice of subsystems; the *algorithmic* level, pertaining to the algorithm or combination of algorithms used; and the *implementation* level, where the underlying arithmetic operations are considered. All of these affect the ultimate computational complexity of a signal processing system, as measured by the number and precision of arithmetic operations required to generate each output sample. [14] The number of bits associated with the input, internal calculation and output of each operation directly contributes to the total gate count and thus determines the silicon area. The number of operations per second determines the minimum clock speed required for real-time processing and consequently the operational power, which increases approximately with the square of the clock speed. Parallelization of repeated operations offers the designer the possibility to lower the clock speed and reduce the power at the cost of a greater silicon area. However, such trade-off decisions are beyond the scope of this thesis, where the discussion is limited to the number and precision of operations required to achieve a certain performance objective.

Reduced to the arithmetic level, one observes a clear hierarchy of operations: divisions are very expensive in terms of hardware, and to be avoided unless absolutely necessary, particularly in the critical signal path. Assuming fixed point arithmetic, multiplications are achieved by sequentially shifting-and-adding one operand relative to another, with the number of iterations proportional to the wordlength (number of bits representing each value). Thus it is clear that an addition of two numbers requires a fraction of the computation associated with their multiplication. A subtraction can be considered synonymous with addition in complexity terms, because it involves the same operation except with the sign of one operand altered. Identification of whether a number is less than, greater than or equal to zero can be accomplished simply by testing the most significant bit of a number, or by ANDing the individual bits. Finally, a delay (as found in a finite impulse response (FIR) filter, for example) is implemented as a buffer and constitutes minimal complexity.

Multiplications are assumed to consist of iterative shift-and-add operations, in order to facilitate comparisons of algorithmic operations.

3.2 RF Tuner

The DTV signal is first received at an antenna and then converted by a RF tuner from the 54MHz to 794MHz spectrum to a standard IF frequency. A 6MHz bandpass filter attenuates the adjacent channels. In the worst case, where two high-power analog channels flank a single lower-power DTV channel, the power difference of the three contiguous channels may be similar. This increases the complexity of the subsequent frequency down-conversion and sampling required to avoid aliasing of the adjacent channels into the signal bandwidth.

3.3 Front-End

The purpose of the Front-End is to bring the signal down from IF to baseband. As the IF signal is centred on 44MHz (in the USA), a conceptually-simple approach would

be to sample at above double the maximum frequency of interest (for example, 100MHz), and then down-convert and decimate the signal through digital processing. However, the complexity of the front-end can be reduced by undersampling at 25MHz. As illustrated in Figure 3.2a, the channel of interest lies at IF between 41 and 47MHz at the tuner output. On either side there are adjacent channels: a DTV channel to its left and an analog NTSC channel to its right. Sampling at 25MHz causes a reflected version of the frequency band in the region 37.5MHz to 62.5MHz to be brought down to DC (Figure 3.2b). The DTV channel lies between 3MHz and 9MHz, surrounded by the adjacent bands (originally at 35-41MHz and 49-55MHz) which have folded into themselves, but not into the signal band. Digital bandpass filtering isolates the DTV channel (Figure 3.2c). Modulation with a numerical oscillator just below 9MHz brings the DTV signal to baseband, concurrently reflecting it into the correct orientation with the pilot at DC (Figure 3.2d).

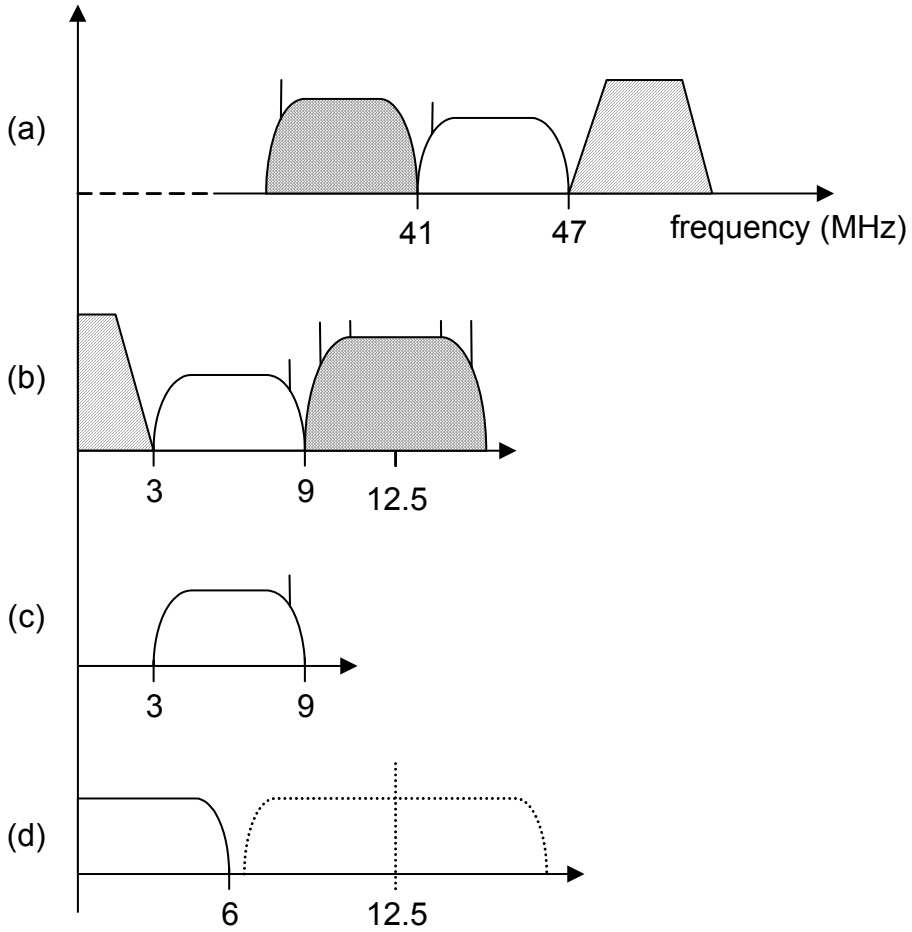

Figure 3.2 Frequency down-conversion in the Front-End

3.3.1 Analog to Digital Conversion

The signal input to the ADC is at IF. [14] The ADC is clocked by a crystal oscillator, typically with a tolerance of 100 parts per million (ppm) from its nominal value. In some digital communications receivers, the phase of the ADC may also be controlled.

3.3.2 Automatic Gain Control

The silicon area and power consumption of a digital system are to a first approximation proportional to the wordlength [14], defined as the number of bits assigned the

digital representation of each sample value. Thus in cost-effective systems such as mass-market electronic products, it is highly desirable to minimize the wordlength.

The dynamic range of digital signal processing systems is limited by the wordlength, and it is thus desirable to maintain the level of the signal at the ADC to maximize the usage of the available range without exceeding it. Control of the signal level of the analog signal prior to digitization is therefore essential if this is to be achieved. As the power of the broadcast signal measured at the receiver antenna is highly dependent on its geographical location and the power in the adjacent channels, this process must be automated. It can be performed either within the tuner, or the gain within the tuner controlled from the digital front-end by utilizing average power of the received signal. In addition, a further digital scaling may be applied following the ADC for fine-resolution control.

3.3.3 Matched Filtering

Matched filtering with a filter (whose impulse response is a time-reversed version of the transmit filter's impulse response) is necessary in order to minimize ISI. The RRC filter is most economically implemented in the digital domain on the baseband signal after interpolation prior to adaptive equalization; otherwise the performance of the auto-regression techniques used for adapting the equalizer coefficients may be compromised [5].

3.3.4 Carrier Frequency and Phase Control

A local oscillator within the Front-End varies the frequency and phase of the down-converted signal and is controlled using a phase-locked loop (PLL), which is used in wideband (e.g. >50kHz) mode for frequency acquisition and narrowband (1kHz) mode for fine frequency and phase tracking. The control signal is generated from a frequency/phase error detector located after the channel equalizer, and may utilize both the binary frame sync and sliced random data in its operation. Performing the frequency and phase tracking in this way allows a low-accuracy (more cost-effective) RF tuner to be used.

3.3.5 Pilot Removal

The DC offset is subtracted from the received signal prior to equalization. [3] As the extent of pilot attenuation due to the fading channel may vary considerably with the channel (as illustrated by a comparison of the spectra in Figure 3.3), a PLL tracks the DC level of the incoming signal and varies the subtraction accordingly.

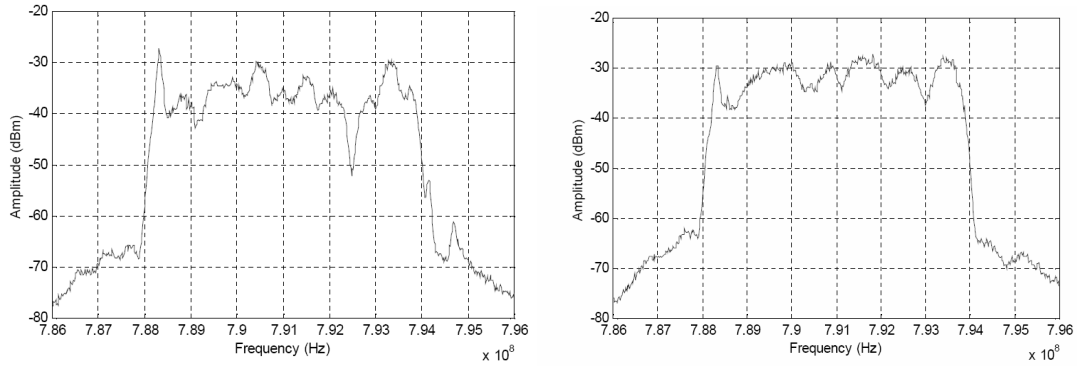

Figure 3.3 Field-captured ATSC spectra [10]

3.3.6 Interpolator

The undersampling technique described in section 3.3 allows the ADC to sample at 25MHz with the band of interest situated between DC and 6MHz. Conversion of the sample rate to the symbol rate (or a multiple thereof) as required within the demodulator is carried out by digital interpolation. In addition to sample rate conversion, the interpolator can be controlled so as to track the timing phase and frequency. Such an approach has become increasingly cost-effective compared with analog techniques due to technological improvements.

The objective of time domain interpolation is to reconstruct as accurately as possible the symbol values that would have been obtained if the analog waveform been sampled at different instants. A precondition is that the samples (obtained every T_S) contain the full information in the bandwidth B of interest present in the analog signal prior to sampling. Thus

$$\frac{1}{T_S} \geq 2B\,. \tag{3.1}$$

Theoretically, this would permit reconstruction of the underlying analog waveform *y(t)* by an ideal interpolator:

$$y(t) = \sum_{m=-\infty}^{\infty} x(mT_S) \cdot h_I(t - mT_S)\,, \tag{3.2}$$

where

$$h_I(t) = \frac{\sin(\pi t / T_S)}{\pi t / T_S} \tag{3.3}$$

is the impulse response of the ideal interpolating filter, and

$$H_I(f) = \begin{cases} T_S, & |f| < 1/2T_S \\ 0, & |f| > 1/2T_S \end{cases} \tag{3.4}$$

is its frequency-domain transfer function, $x(mT_S)$ is the sampled input signal at index m, and T_S is the sample period. Sampling this continuous signal *y(t)* at instants T_i would yield interpolants:

$$y(kT_i) = \sum_{m=-\infty}^{\infty} x(mT_S) \cdot h_I(kT_i - mT_S)\,. \tag{3.5}$$

If the indices are redefined in terms of a basepoint index

$$m_k = \mathrm{int}\left[k \cdot \frac{T_i}{T_s} \right] \tag{3.6}$$

and an associated fractional interval

$$\mu_k = k \cdot \frac{T_i}{T_s} - m_k \tag{3.7}$$

such that

$$y(kT_i) = y\left[(m_k + \mu_k) T_S \right], \tag{3.8}$$

equation 3.5 can be rearranged to give:

$$y(kT_i) = \sum_{i=-\infty}^{\infty} x\left[(m_k - i)T_S\right] \cdot h_I\left[(i + \mu_k)T_S\right], \qquad 3.9$$

in which the index i is computed as

$$i = \text{int}\left[k \cdot \frac{T_i}{T_s}\right] - m, \qquad 3.10$$

where int[x] represents the highest integer less than or equal to x.

A new sample is read into the filter every T_s seconds, while outputs are generated at the interpolated rate T_i based on an associated fractional delay value and index to the input delay line. The calculation of suitable m_k and μ_k values is discussed in the context of timing synchronization in section 4.3.2.

Ideal reconstruction would mandate an interpolating filter with an infinite impulse response. In practice this is unrealizable, but a causal time-domain digital filter suffices. In the frequency domain this corresponds to minimizing the power of folded aliases into the information-bearing frequency band of the signal. For a finite-length filter with $(I = I_2 - I_1 + 1)$ taps, equation 3.9 becomes:

$$y(kT_i) = \sum_{i=-I_1}^{I_2} x\left[(m_k - i)T_S\right] \cdot h_I\left[(i + \mu_k)T_S\right]. \qquad 3.11$$

Limitation of the filter lengths cause its frequency response to differ from the ideal described above, leading to distortion in the time-domain signal. The problem is that the spectrum of the signal samples contains periodic images spaced apart by $1/T_s$; these must be suppressed prior to resampling in order to minimize aliasing into the band of interest (up to $1/2T_s$) during resampling at rate $1/T_i$, when images spaced apart by $1/T_i$ are introduced. As T_i/T_s is irrational, the aliases are uncorrelated and constitute interference. It is therefore desirable to attenuate the power of the folded images. An additional source of distortion arises from the non-flat passband filter response (which can however to some extent be compensated by filters downstream of the interpolator or within the equalizer).

3.3.6.1 Classical Interpolation

Many of the classic texts limit the discussion of interpolation to either pure integer rates or rational fractions, typically with fixed interpolation ratios implemented in FIR or infinite impulse response (IIR) filters. A simple way to interpolate by a rational number (N/M) is to insert N-1 zeros between each original sample, and then low-pass filter and extract every Mth value. This is computationally expensive, because the low-pass filter operates on the upsampled stream and therefore not practical for a high-throughput system.

3.3.6.2 Polyphase filtering

Polyphase filtering achieves the same effect by running the interpolation FIR at the original sampling rate rather than at the upsampled rate, thus reducing the associated computation by a factor of N. However, additional noise and ISI are introduced into the signal due to the necessary approximation by a finite-length FIR. In the context of

digital communication systems, the final SER is a more important measure than traditional metrics such as passband ripple, stopband response and transition bandwidth as optimization criteria. Filter coefficients yielding a low SER can be determined through simulation or obtained from pre-computed tables.

3.3.6.3 Fractional delay interpolation

The techniques described so far are not amenable to time variation, limiting them to systems with fixed sample rate conversion. Another approach is to implement the interpolator as a fractional delay μ which can be varied on consecutive samples. So-called fractional delay filters are used in many signal processing applications where or time variation is required or the sampling-rate cannot be expressed as an integer ratio.

Interpolation can be accomplished by incrementing or decrementing the fractional delay by a fixed amount on successive symbols. As the impulse response of a fractional delay is a sinc function, it must in a realizable implementation be truncated and weighted by a window function (e.g. Kaiser or Dolph-Chebyshev). Coefficients yielding a maximally-flat frequency response can be calculated from the Lagrange formula for polynomial interpolation.

The objective is first to approximate $x(t)$ close to kT_i with an underlying polynomial $P(k(t))$, and then to calculate interpolants at values $P(kT_i+\mu)$. The approximating polynomial naturally varies with each I-point set of input samples. Lagrange formulae are used for determining suitable polynomials of odd degree.

Coefficients corresponding to each value of μ are typically pre-computed and stored in a ROM look-up table; therefore the fractional resolution attainable depends upon the number of stored coefficient sets. On each new sample the corresponding set is transferred to the filter structure. This is a labour-intensive process which may limit the speed of operation.

3.3.6.4 Farrow Technique

An efficient realization of Lagrange interpolation for high-speed VLSI implementations was developed by Farrow [15]. Rearranging the coefficients yields a z-domain transfer function of the interpolator as a polynomial in μ.

This allows the use of fixed coefficients; thus only the μ value–rather than a complete set of coefficients–needs to be transferred on each sample, and is thus more efficient for rapidly changing between fractional delays. The fractional resolution is therefore limited only by the wordlength rather than the number of coefficient sets, unlike the other techniques described previously. Unit delays and multipliers can be shared between coefficients, thereby reducing the overall complexity. An additional benefit of the Farrow structure is that it simultaneously performs anti-alias filtering, eliminating the need for a separate lowpass filter prior to the interpolator.

The generalized Farrow structure for a Nth-order interpolator is illustrated in Figure 3.4. Each of the N+1 columns contains M pre-computed coefficients arranged in a FIR filter (Figure 3.5).

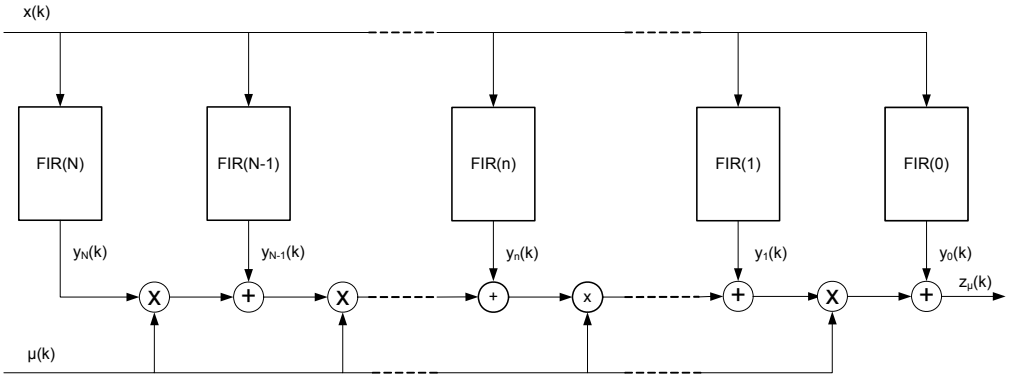

Figure 3.4 Farrow structure for cubic Interpolator

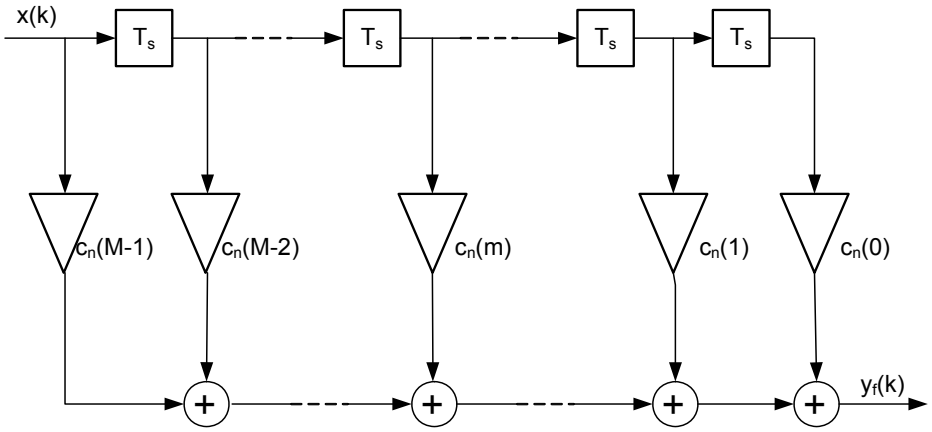

Figure 3.5 Farrow structure

The input to the structure is a stream of digital samples *x(m)* at double the baud rate or above (to prevent aliasing), which are processed by the structure so as to produce output data samples *z(k)* at baud rate for a given fractional delay *μ(k)*. Thus:

$$z_\mu(k) = \sum_{n=0}^{N} \mu^n y_n(k), \qquad 3.12$$

with intermediate values:

$$y(k) = \sum_{m=0}^{M-1} x(k-m) \cdot c_n(m-M+1). \qquad 3.13$$

The order *N* and FIR filter length *M* can be chosen to provide acceptable performance versus implementation complexity (size, area, power, CPU cycles etc) for a given application. A higher order is normally associated with superior performance.

The parameter *μ(k)* indicates the fractional delay that will be applied to the current input sample. If *μ(k)* is constant, the effect of the structure is to apply the same fractional delay to all samples. If it increases over successive samples, the output is downsampled relative to the input. If it decreases, the output is upsampled. If it is used for resampling (either up or down), the index *m* must be appropriately adjusted every time the parameter *μ* crosses a 0.0 or 1.0 boundary, as *μ* is normally restricted to the

range 0.0 to 1.0. The calculation of μ is discussed further in the chapter on timing synchronization.

Three structures are considered: 1st order (linear), 2nd order (piecewise parabolic) and 3rd order (cubic). For the 2nd order structure, two values of the design parameter α are investigated: 0.43, which provides excellent integrity; and 0.5, which exhibits inferior performance but leads to a particularly simple realization where many of the costly multiplication operations can be replaced by less computationally demanding addition (or subtraction).

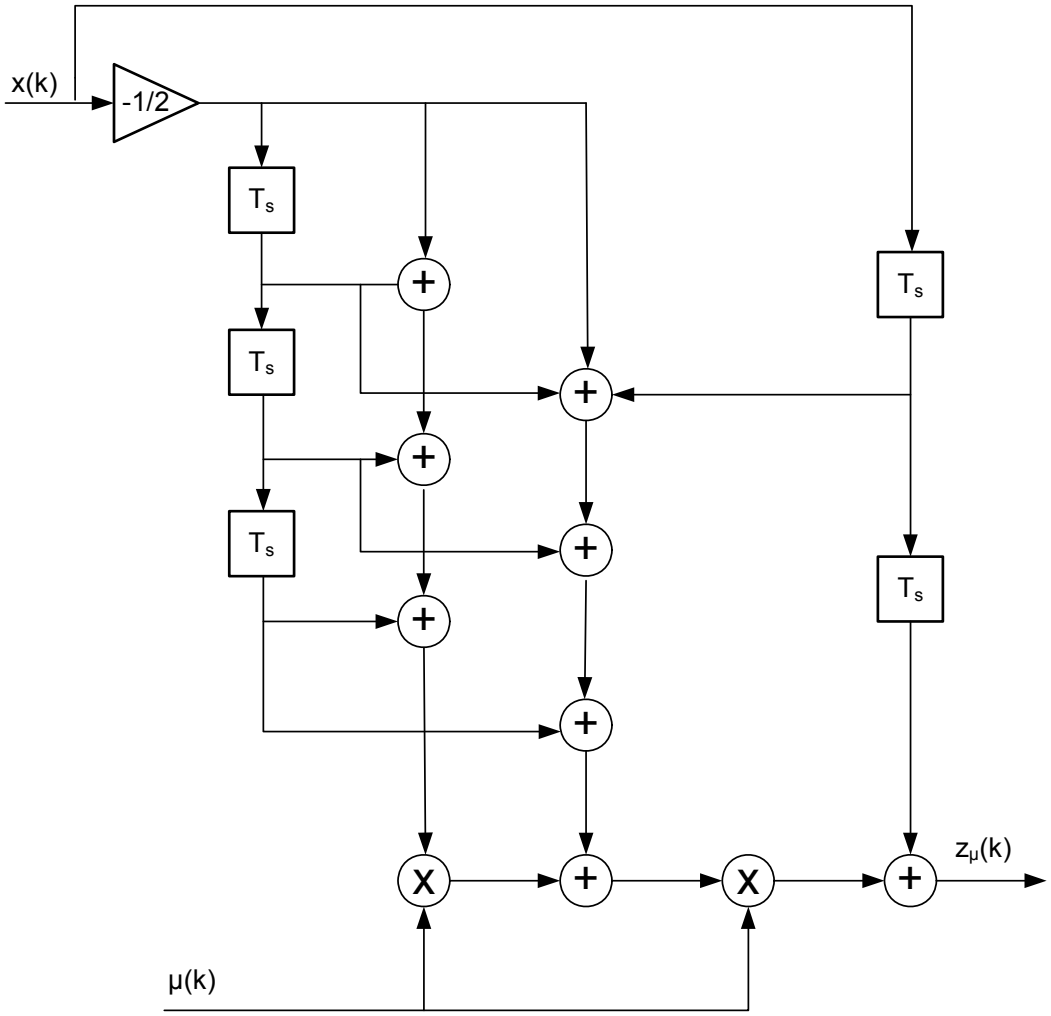

Figure 3.6 Piecewise Parabolic Farrow structure with α=0.5

Simplifications of cubic structures are also possible for certain choices of coefficients where symmetries and repeated values are present.

Table 3 Complexity of low-order Farrow implementations (per interpolant)

Order	Delays	Additions	Multiplications
(1) Linear	1	2	1
(2) Parabolic (alpha=0.43)	3	12	12
(2) Parabolic (a=0.5)	5	9	2
(3) Cubic	3	15	16

Desirable characteristics include a wide passband, sharp cut-off in the transition region and nulls on harmonics of the sampling frequency, in order to ensure minimal distortion of the original signal, while simultaneously attenuating spectral images that would otherwise alias back into the baseband. Figure 3.8 confirms this to be the case, as the four filters under consideration have a broad main lobe and nulls coincident with harmonics of the input. The linear (first order) filter is clearly inferior to the others based on these criteria.

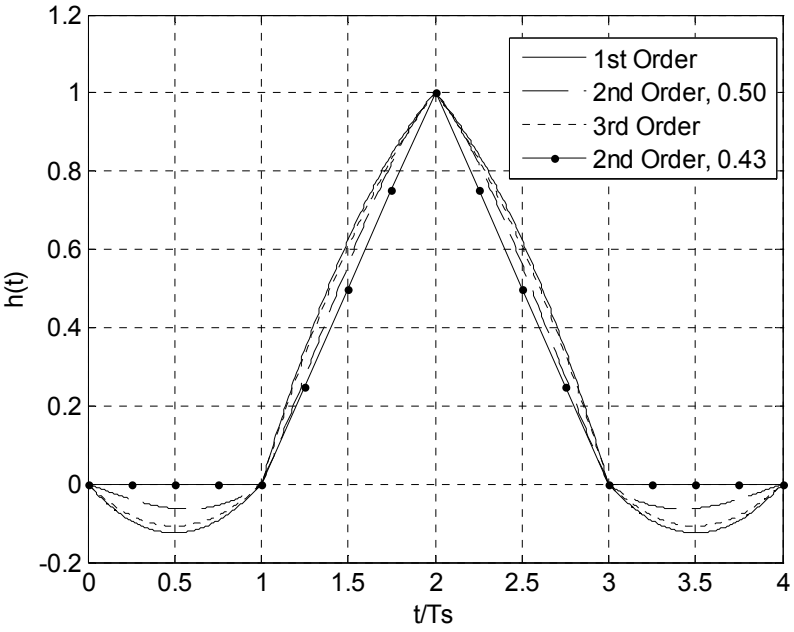

Figure 3.7 Impulse responses of Farrow filter implementations

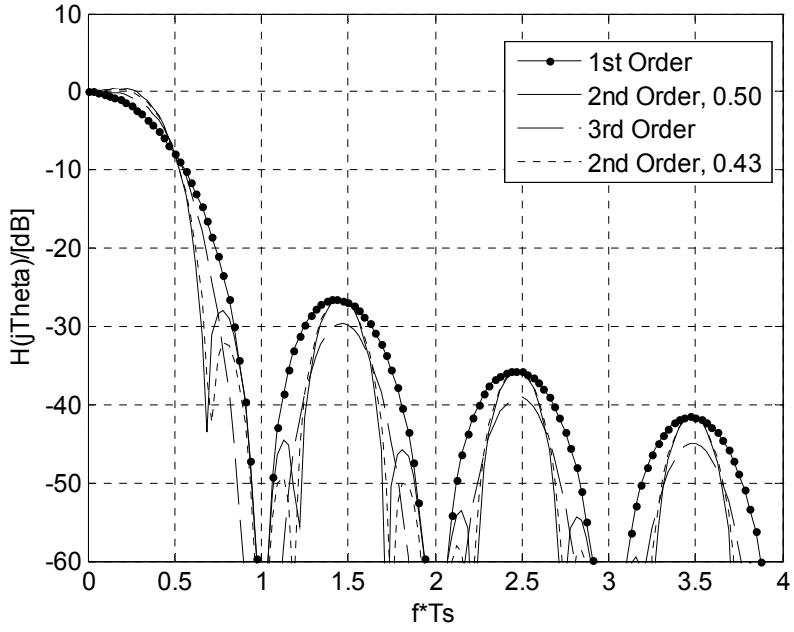

Figure 3.8 Frequency responses of Farrow filter implementations

The SER performance curves for each of the implementations are shown in Figure 3.9. It can be seen that all but one of the four interpolators lies close to the theoretical line, whereas the 1st-order filter is far worse: it intersects the shaded box in the top right corner, which represents the disallowed region and therefore discounts it from further consideration. Of the remaining candidates, the 3rd-order filter exhibits the lowest implementation loss, followed by the two 2nd-order interpolators. All three lines lie within the tolerance region.

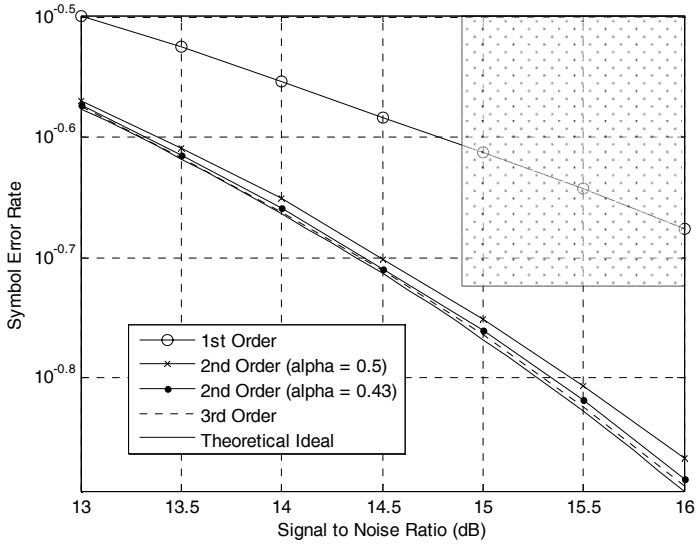

Figure 3.9 Comparison of interpolator implementations.

The theoretical curve is calculated according to:

$$\mathrm{SER}_{\min} = \frac{L-1}{L}\,\mathrm{erfc}\left(\sqrt{\frac{3\times\mathrm{SNR}}{(L^2-1)}}\right), \qquad 3.14$$

where L represents the number of symbol levels, and SNR is measured over the full 6MHz channel bandwidth [1].

3.4 Demodulator

The demodulator receives samples at (approximately) the correct sample rate, which are first processed by an equalizer and then converted by a demapper to a bitstream suitable for trellis decoding in the next unit. En route, signal analytics are carried out to which are used to control the various units in the front-end, such as the AGC, the mixer (for carrier recovery) and the interpolator (for timing recovery). The interconnections for the interpolator are illustrated in Figure 3.10.

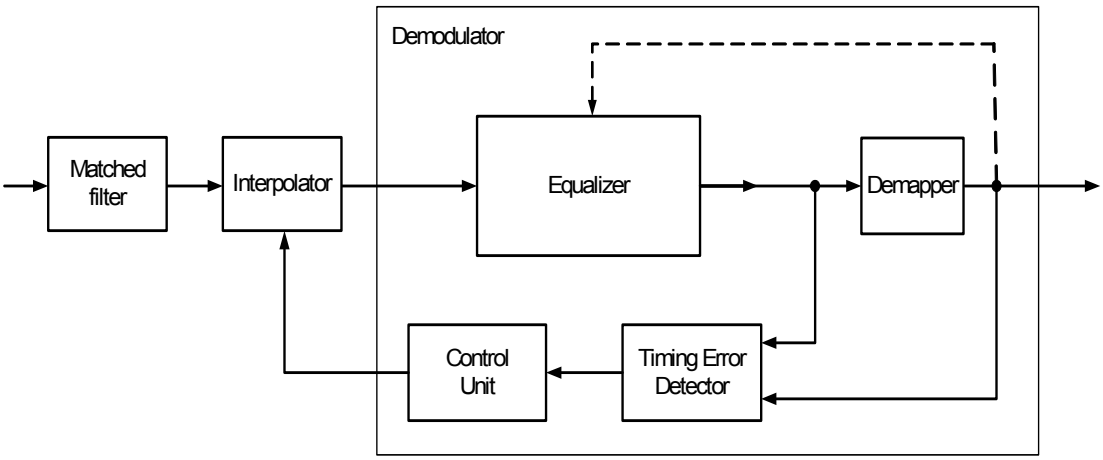

Figure 3.10 Generic demodulator structure

3.4.1 Timing Synchronization

Successful data reception is predicated on reconstructing symbols within the receiver at the same rate that they are transmitted. The symbols must also be strobed at the correct *timing phase* within the sampling interval, so as to maximise the average distance between levels in the *symbol alphabet*. Unlike many wired communication systems, no reference clock is available in the broadcast signal, and it is therefore necessary to derive it from the received modulated waveform; a process known as *self-timing* or s*elf-synchronization*. Timing recovery is the process whereby a clock signal at the correct rate is extracted within a receiver. The frequency and phase of the sampling clock is determined by a subsystem known as the timing recovery circuit.

The GA receiver samples the real signal synchronously at the symbol rate, using an analog PLL to ensure accurate frequency and phase lock. [9] This is necessary, because it has a symbol-spaced equalizer (SSE); namely, one coefficient corresponds to one symbol at the transmitted clock rate and the sample rate through the equalizer is the same as the symbol rate. Designs where the sample rate is higher (normally double) the symbol rate are described as fractionally-spaced equalizers (FSEs), because the spacing between coefficients corresponds to less than one symbol period. Therefore to cover a given echo span, a SSE requires fewer coefficients than a FSE. However, SSEs are more sensitive to the phase of the incoming signal than FSEs, which can perform interpolation as a by-product of their operation (assuming the sample rate is very close to an integer multiple of the equalizer sampling rate).

3.4.2 Equalization

As a multipath propagation channel consists of echoes with varying delays and attenuations, it can be modelled by a linear filter which processes the transmitted signal producing a non-uniform frequency response across the channel [6]. The role of the equalizer is to invert this channel (as effectively as possible) and thus restore the original signal. Although equalization can also be carried out in the frequency-domain, time-domain equalizers are the predominant solution for 8-VSB receivers. Due to the sample rate and large number of coefficients (and therefore multiplications) required for ATSC DTV, it is assumed that the equalization is implemented in programmable hardware: a fixed structure with configurable coefficient values.

3.4.3 Demapper

The values generated by the equalizer must be converted into a form that can subsequently be processed by the FEC decoder (section 3.5), the first stage of which is a trellis decoder. Depending on the implementation, this accepts either a stream of three-bit "hard-quantized" values corresponding to the eight allowable symbol levels, or a sequence of "soft-decisions". In the latter case, each symbol is represented by more bits so as to provide a confidence estimate for decisions carried internally within the trellis decoder and reduce the bit error rate at its output. It is the role of the demapper to calculate either the hard or soft decisions.

The values generated by the demapper may additionally be used by subsystems situated outside the main signal path; for example, in generating an error metric for a recursive equalizer coefficient adaptation algorithm, or passed back as the input an equalizer's feedback filter.

The demapper with the lowest computation complexity is an eight-level slicer: samples at its input are rounded to the nearest of the eight levels in the alphabet by simply quantizing from higher precision to three-bit words. The accuracy of such estimates deteriorates with increasing channel noise and ISI.

A more advanced approach uses an "Intelligent Slicer", which exploits redundant information within the trellis-coded signal to restrict the possible range of transitions between successive symbols, thereby reducing the probability of an incorrect decision. However, due to the 12-way convolutional interleaving employed during encoding, the delay incurred by a Viterbi decoder in reconstructing the data stream would be at least 168 symbols, assuming a trace-back depth (TBD) of 5 [16] and a constraint length of 3. Such a delay would be unacceptably long for use with a DFE or where an error metric is derived from the demapper decisions. An alternative would be to use a trellis decoder with a TBD of one [17] as the demapper, which imposes no delay. Compared to a slicer, this comes at the cost of extra complexity: 12 such decoders would be required due to the deinterleaving, each involving 8 path metric calculations followed by a search for the minimum. (However, the conventional difference of squares can be reduced by using absolute rather than squared values, as in [17]). Such an approach has been reported to be superior to a slicer in relatively benign channels, but less effective in hostile multipath conditions.

3.5 Decoder

The trellis decoder performs near-maximum-likelihood error detection and correction using a Viterbi algorithm on the received symbols. A convolutional interleaver restores the original order of the data bytes, thereby spreading any contiguous burst noise added in the transmission channel over many packets, giving the Reed-Solomon decoder a better chance at correcting errors. Following convolutional de-interleaving, a data de-randomizer puts the data back into its original form.

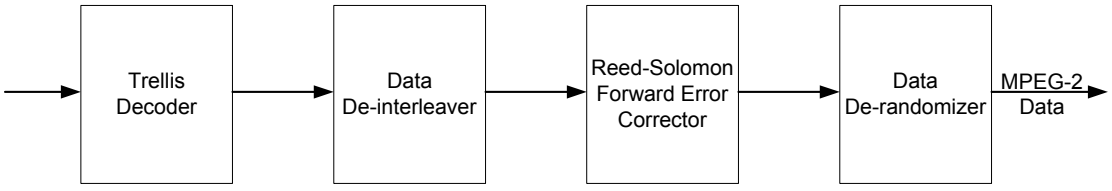

Figure 3.11 ATSC 8-VSB Receiver

4 Timing Recovery

The role of the timing recovery control system in a self-synchronizing receiver is to acquire and maintain the correct sample frequency and phase by extracting and utilizing timing information contained within the received signal. As the instant at which the samples are strobed directly affects the SER, the timing recovery system has a critical impact on the overall performance of a digital communications receiver. [16].

The sample rate must be continuously adapted because the frequency of the crystal oscillator driving the ADC is temperature-dependent. It also exhibits phase variation arising from physical effects that cause the phase angle of the oscillator to deviate from the ideal, thus broadening the spectrum from an infinitely narrow peak (Figure 4.1). Imperfections in the timing recovery system lead to "timing jitter", namely phase fluctuation around the ideal value which act as an internal noise source [18] which can be maintained within acceptable bounds through measures discussed in this chapter.

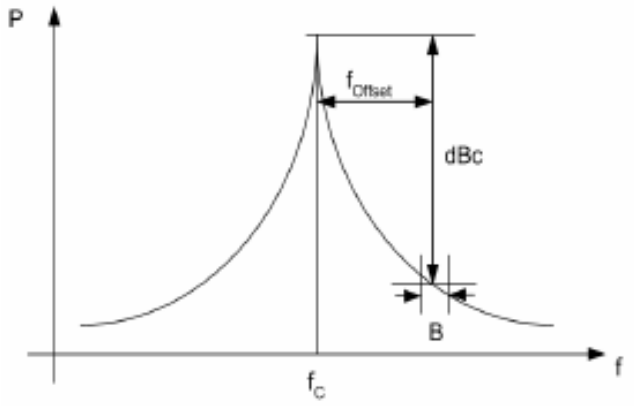

Figure 4.1 Illustration of Oscillator phase noise

The main concepts are briefly reviewed in the following sections, before different techniques applicable to ATSC DTV reception are discussed in detail.

4.1 Foundations

4.1.1 Structure

Timing recovery comprises two main steps: (i) generating a metric related to the timing error, and (ii) adjusting the sampling phase, either during sampling or subsequent processing, with the goal of minimizing ISI. Depending on the order in which these occur, the recovery system is said to have either a feedforward (Figure 4.2) or feedback (Figure 4.3) structure. The former is often used for "burst-like" transmissions where fast acquisition is required. Feedback systems typically possess superior steady-state tracking characteristics and consequently tend to be chosen for continuous transmission systems such as television broadcasting.

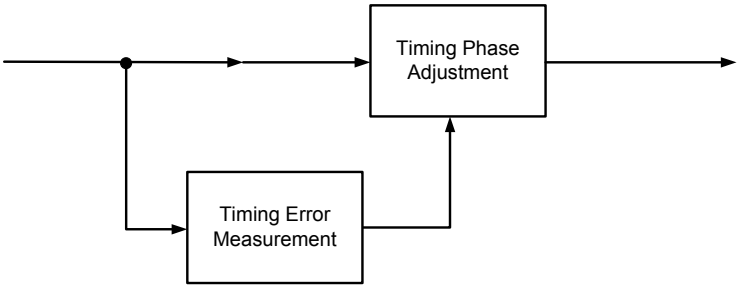

Figure 4.2 Feedforward Timing Recovery

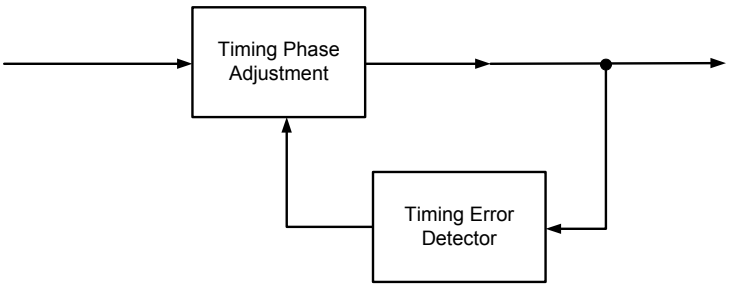

Figure 4.3 Feedback Timing Recovery

Timing measurement is performed by a timing error detector (TED), which generates an error signal as a function of the difference between the actual and desired timing phase. Some of the possible approaches are discussed later in this chapter. As the instantaneous values at the TED are imprecise estimates–or in the case of feedback schemes, delayed–the signal is typically bandpass filtered or integrated into a PLL in order to reduce sample-to-sample variation and consequently the steady-state timing jitter. In most cases, the resulting signal undergoes further processing before driving the actuator that alters timing phase (either the ADC or an interpolator).

Since the late 1980s, the processes associated with timing recovery have increasingly moved from the analog to the digital domain as the cost of programmable silicon (DSP, FPGA etc) has decreased [19, 20]. The following sections first briefly review analog and hybrid analog/digital approaches, which serve as an introduction to the main concepts. Then the final section concentrates on digital timing techniques that employ interpolation, which is used in contemporary receivers (including the proposed design).

4.1.1.1 Analog

In an entirely analog realization the sampling is *synchronous*, because it is locked to the incoming pulses which are sampled at–or close to–the ideal sampling instants. The clock is recovered by analog means from the received signal, and used to control the ADC sampling instants as depicted in Figure 4.4. Analog timing recovery is a feedforward process, because the timing function is generated in the analog domain before timing phase is controlled via the sampling rate at the ADC.

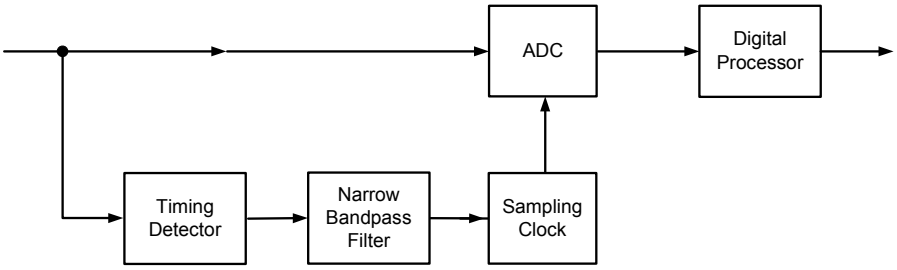

Figure 4.4 Analog Timing Recovery

4.1.1.2 Hybrid

Hybrid modems perform feedback synchronous sampling with an ADC driven by a numerically-controlled oscillator (NCO) in a phase-locked loop. The timing error is derived from the digital samples, and processed digitally through a loop filter and a NCO. The digital output from the NCO must be converted to a continuous signal via a DAC before adjusting the sampling phase of the ADC.

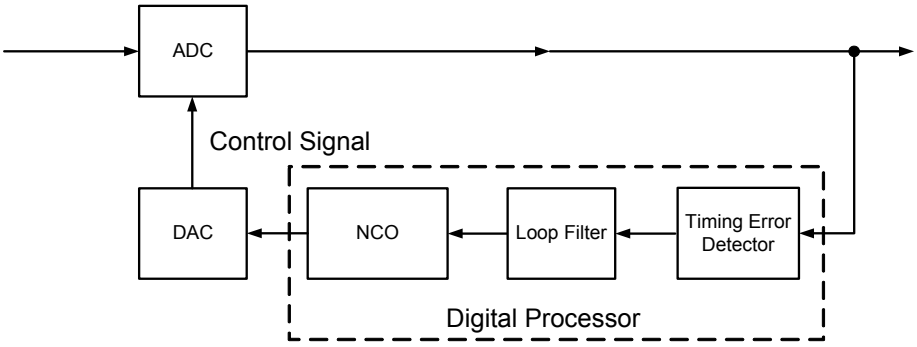

Figure 4.5 Hybrid Timing Recovery

The GA prototype uses hybrid timing recovery to perform phase control; frequency control is handled by a PLL locked to the periodic data segment sync.

4.1.1.3 All-Digital

The goal of the all-digital approach is to perform the same function as the hybrid approach, but with fewer analog components because the ADC is at the first point in the processing chain. [14] Consequently an all-digital approach is *non-synchronous*, because the clock is not locked to the incoming data. It runs at a multiple of the symbol rate, so that sampled values can be interpolated from the received stream to obtain values as though the clock frequency or phase had been different. Digital interpolation carried out in this way permits adjustment of the symbol rate and phase independently of the sampling rate of the quartz crystal by varying the phase on successive symbols. It is usually preferred, because it lowers the component and manufacturing costs and enables tracking of a wider frequency offset [21].

The discussion in the following sections is restricted to all-digital feedback structures, which are more cost-effective than their analog or hybrid counterparts and exhibit superior performance.

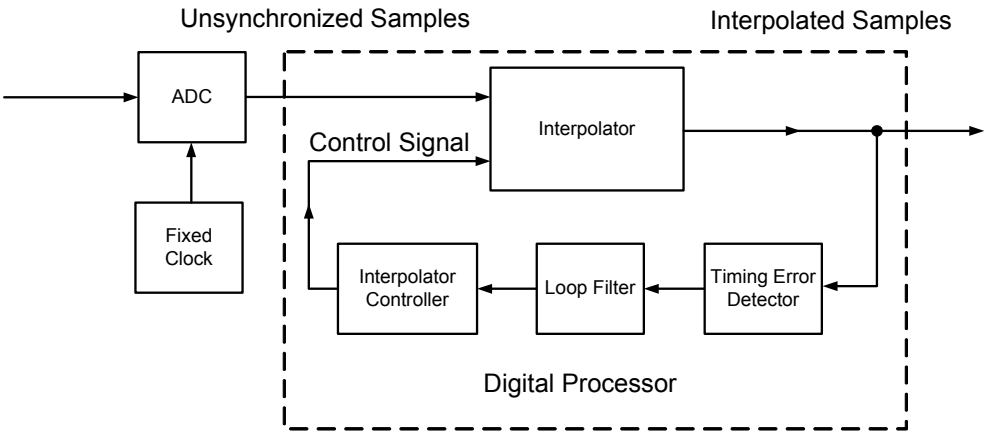

Figure 4.6 All-Digital timing control

4.1.2 Implementation Complexity

The direct cost of a timing recovery system is related to the sampling rate and the collective complexity of its components, namely: the TED; loop filter; controller and interpolator. However, it cannot be considered in isolation because of its interconnection with the channel equalizer. In situations where the signal is distorted due to non-flat channel frequency characteristics (such as in DSL or DTV), the TED measures the phase offset of the signal downstream of the interpolator, normally after the equalizer (Figure 4.7 Structure of Timing Recovery loop). In this position it operates on channel-compensated signals and so produces more accurate error estimates, resulting ultimately in lower timing jitter. [22]

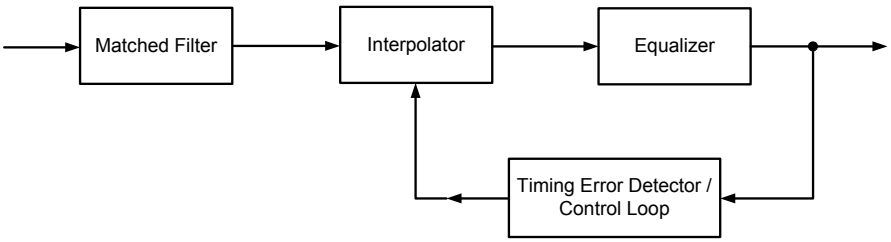

Figure 4.7 Structure of Timing Recovery loop

The complexity of the equalizer and other blocks located in the receiver prior to the TED is determined by the sampling rate required by the timing recovery system. Thus symbol rate receivers have a significantly lower implementation complexity than those operating at higher rates. However, a disadvantage of symbol-rate equalizers is that they are sensitive to timing phase, necessitating accurate synchronization algorithms. [18]

4.1.3 Performance Measures

Timing recovery systems can be judged by numerous criteria, such as their transient or steady-state performance. Examples of the former include the maximum tolerable frequency or phase offset that can be corrected during the initial acquisition period, or the time to reach a tolerance region. Alternatively (or additionally), following acquisition, the variance of the timing frequency or phase fluctuation may be measured. In a commercial digital television receiver, the main figures of interest are: (i) the conver-

gence time, as this affects how long it takes for a picture to appear when changing channels (shorter is better); (ii) the acquisition range, which determines the maximum tolerance of the crystal oscillator (and therefore its cost); and (iii) the variation of steady-state SER with input SNR, where a superior receiver exhibits a lower SER for a given SNR and thus providing a picture in a wider range of reception sites.

Analytical comparison of different timing recovery systems is usually very difficult; for this reason, simulation provides the best means of estimating how candidate approaches will perform under realistic operation conditions, as measured by the performance measures discussed above. [23]

4.2 Timing Error Detector

Many of the textbook TEDs rely on the signal being over-sampled (e.g. Zero-crossing) and/or a binary alphabet (e.g. Early-late). As discussed in section 3.4.2, a TED capable of operating at baud rate enables a lower sample rate through the equalizer, and therefore far fewer coefficients for a given echo span coverage and considerably reducing its implementation size. As this has a major impact on whether a demodulator can be classed as low-complexity, the following discussion is restricted to approaches that do not require the samples through the equalizer to be at a multiple of the symbol rate.

4.2.1 Fundamental Concepts

4.2.1.1 Data-Aided

Training sequences, such as the ATSC segment and field syncs, allow algorithms in the receiver to operate in Data-aided (DA) mode: received values can be compared with the known sequences when computing metrics for timing, carrier, gain control etc. (However, the transmission of regular training sequences occupies bandwidth, reducing the overall efficiency of the system.)

4.2.1.2 Decision-Directed

A TED operates in decision-directed (DD) or non-data-aided (NDA) mode if it estimates the transmitted symbol values from the received samples rather than using known values, and can thus be applied when training signals are unavailable or insufficient. (For example, the field syncs are too far apart (24ms) to be used for continuous tracking of the timing drift.) Many algorithms that function in DA mode may also be used in a DD sense, albeit with impaired performance due to estimation errors. These may repeatedly switch between the two modes when training signals are interspersed with useful data, such as in ATSC. Alternatively DD methods may be used in isolation; this saves hardware associated with searching for the training sequence and repeatedly enabling and disabling the DA TED.

4.2.1.3 Design Criteria

As mentioned in section 4.1.3, analytical performance evaluation of a complete timing recovery system is difficult; simulations prove more reliable when comparing candidate designs. Before a full timing recovery system simulation is carried out, isolated consideration of potential TEDs provides a useful insight into their relative suitability. Desirable characteristics include: (i) low self-noise (or “systematic jitter”), arising from the stochastic nature of the data signal; (ii) robustness to additive channel noise, enabling operation in the worst-case SNR conditions; (iii) unbiased estimates, such

that the expected metric value over a sufficiently long input sequence yield the true value of the unknown parameter; (iv) high information content relative to disturbances; and (v) non-ambiguity, preventing "false-lock" at incorrect phases or frequencies.

Other considerations include: (i) minimum required sample rate; (ii) constraints on the useable alphabet (e.g. many TEDs only function with binary signals); (iii) sensitivity to carrier offsets, because this affects whether carrier recovery must be performed before timing recovery (and therefore influences the range of applicable carrier recovery systems); and (iv) implementation, where a lower complexity is favoured, other factors being equal. Acquisition speed and tracking accuracy are conflicting properties, between which the most favourable compromise is the objective of any design.

The "S-Curve" is a plot of the TED output at different phase offsets, which enables off-line visual analysis of its behaviour. It is derived by driving the TED (open loop) with a constant known error for values over the range ±½ symbol period. Characteristics that are sought include: (i) a steep timing function slope, indicating sensitivity to phase offsets relative to noise sources; (ii) intersection of the origin with 180° rotational symmetry, ensuring unbiased error estimates; and (iii) same sign as the phase offset, implying non-ambiguity. As S-Curves are typically SNR-dependent (e.g. Figure 4.12), the plots in this document are calculated at the threshold SNR of 14.9dB, unless otherwise specified. All are averaged over 20ms.

4.2.2 Segment Sync-based Approaches

4.2.2.1 Correlator

The GA receiver identifies the repetitive data segment sync sequences within the data stream by a narrowband phase-lock loop centred on the nominal sample rate. A data segment sync detector containing a 4-symbol correlator {+1, +1, -1, -1} sequence searches for the periodic data segment sync sequences {-1, +1, +1, -1}.

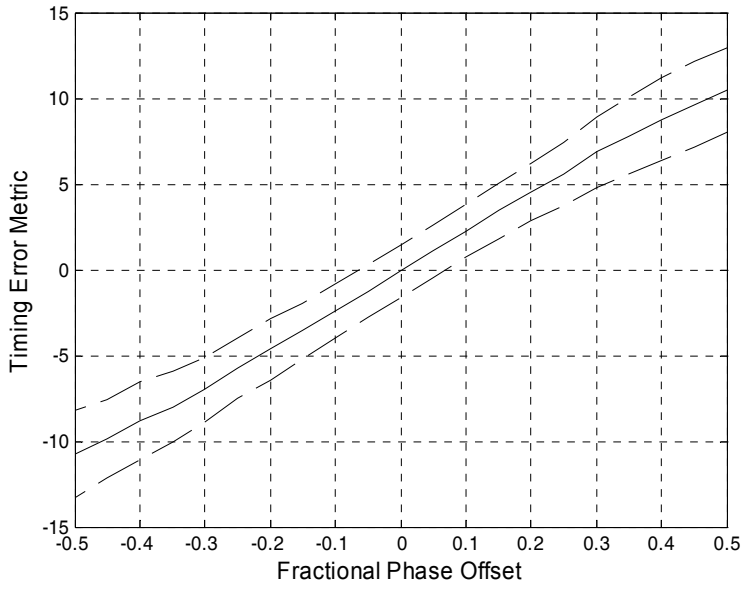

Figure 4.8 Segment sync correlator S-curve

The frequency of the output peaks can be used to synchronize the sampling frequency in an analog PLL. The correlation value is proportional to the phase error, enabling the receiver to sample synchronously (in phase) at the symbol rate [3].

Figure 4.8 illustrates the characteristics of the GA correlator. The error response is approximately linear over the full range of phase error and only crosses the horizontal axis at the origin. This indicates a very robust detector. It can be observed that the standard deviation is higher at larger offsets than in the central region, presumably because of the increasing influence of data samples outside the segment sync.

4.2.2.2 Early-Late

This timing recovery algorithm [16] generates an error signal using three samples: an estimate $\hat{c}_k$ of the transmitted symbol c_k at the current sample position and two sample values y either side of this, spaced approximately half a symbol period (factoring in their timing offsets $\hat{\tau}_k$ and $\hat{\tau}_{k-1}$) away thus:

$$\varepsilon_k = \hat{c}_k \cdot \left[y\left(kT + \frac{T}{2} + \hat{\tau}_k \right) - y\left(kT - \frac{T}{2} + \hat{\tau}_{k-1} \right) \right]. \qquad 4.1$$

The early-late clock recovery works well in conjunction with binary modulation schemes which have peaks in most of the symbol periods, but less satisfactorily with multilevel schemes because there are fewer distinctive peaks. However, it can be applied to the two-level segment syncs, which contains sufficient repetition to obtain the $\left(kT + \frac{T}{2} \right)$ and $\left(kT - \frac{T}{2} \right)$ without oversampling. This yields two possibilities:

1. Use values 1 and 3 from the SS as the mask {+1, 0, –1, 0}
2. Use values 2 and 4 from the SS as the mask {0, +1, 0, –1}

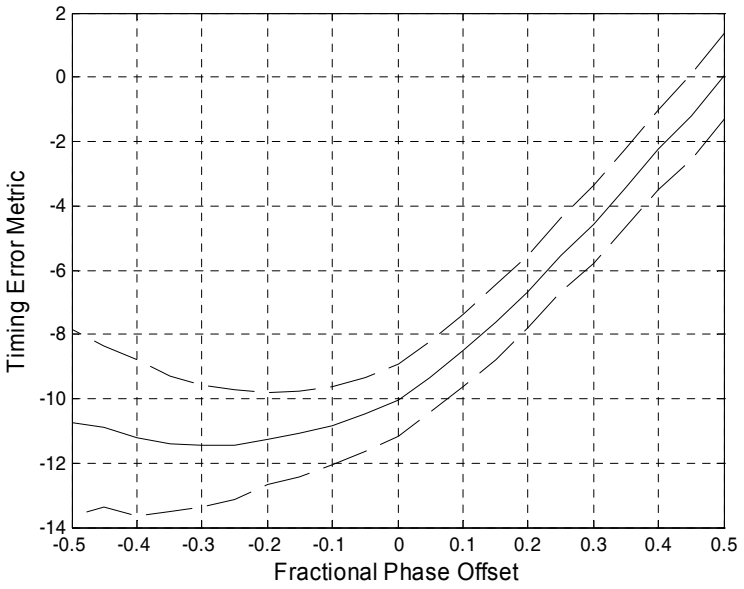

Figure 4.9 Early-Late Detector S-curve (values 1 and 3)

Figure 4.9 and Figure 4.10 illustrate that the two estimators are biased, because they are data-dependent; the data in this case being the same every time. (If the data were

different, e.g. alternating pulses, the result would be unbiased.) This can be achieved if both are calculated each segment sync and combined. This is equivalent to summing the correlator masks, resulting in the same mask as the segment sync correlator!

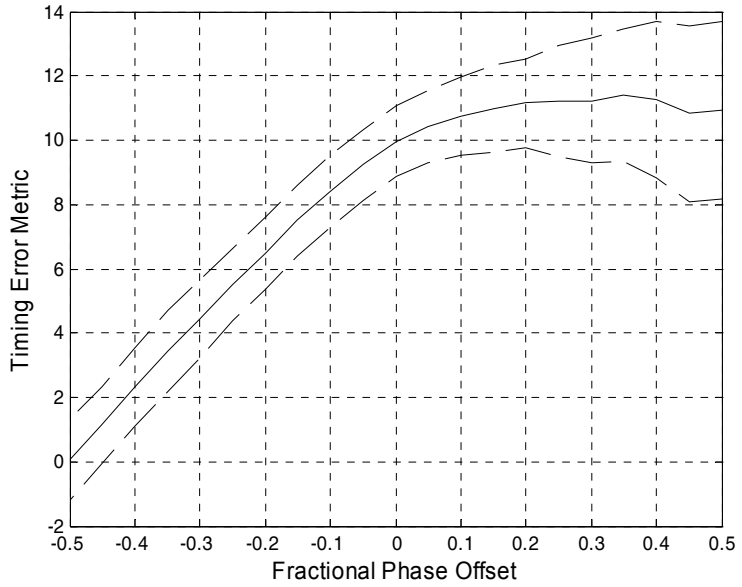

Figure 4.10 Early-Late Detector S-curve (values 2 and 4)

A second application of the early-late technique to the ATSC segment sync was proposed by Kim [24]. It takes an implicit value of unity for the $\hat{c}_k$ factor due to the symmetry of the sync pulse. Thus:

$$\varepsilon_k = y\left(kT + \frac{T}{2} + \hat{\tau}_k\right) - y\left(kT - \frac{T}{2} + \hat{\tau}_{k-1}\right). \qquad 4.2$$

This can be viewed as a mask of {0, +1, -1, 0}: the centre 2 values of the GA mask.

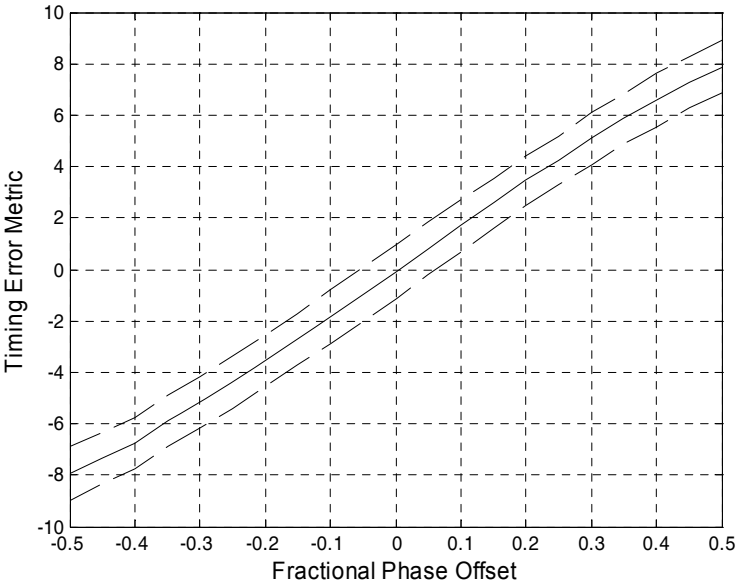

Figure 4.11 S-curve of Early Late Detector as applied by Kim

The S-curve for the Kim detector (Figure 4.11) is very similar to that of the GA correlator, albeit with a different gradient (which has little significance in this case, as it can be factored into the PLL gain). The broadening of the standard deviation bounds with increasing phase offset magnitude is less marked for the Kim detector than the GA correlator for larger offsets, presumably because the influence of neighbouring data samples is less due to their decreased proximity.

4.2.2.1 Zero-Crossing

The zero-crossing detector [25] computes the error metric thus:

$$\varepsilon_k = \left(\hat{c}_{k-1} - \hat{c}_k\right) \cdot y\left(kT - \frac{T}{2} + \hat{\tau}_{k-1}\right). \tag{4.3}$$

Similar to the ELD, it uses $T/2$ terms, which would restrict its use to segment syncs. However, as the $\left(\hat{c}_{k-1} - \hat{c}_k\right)$ term equates in ATSC to (+5 – (–5)) = 0, it provides no timing information.

4.2.3 Non-Segment Sync-based Approaches

4.2.3.1 Mueller & Mueller

The Mueller and Muller TED [26] is a maximum-likelihood technique (which applied to equiprobable 8-VSB symbols is equivalent to the maximum *a posteriori* (MAP) criterion [8]). It can operate on multiple-PAM signals and only requires samples to be at baud rate; thus it is not restricted to training data, unlike the techniques described previously. Other desirable characteristics are no self-noise with Nyquist pulses and good performance at small excess bandwidth factors, unlike that of the ELD which deteriorates as the rolloff decreases. (Mengali) However, the Mueller and Muller algorithm is sensitive to carrier offsets, and so must be performed after carrier recovery.

The second-order realization of the algorithm is appropriate where the channel impulse is not perfectly known *a priori*. In this case, the timing phase error estimate z at sampling instant k is calculated as follows:

$$\varepsilon_k = \frac{y_k \hat{y}_{k-1} - y_{k-1} \hat{y}_k}{2E\{c_k^{\,2}\}}, \tag{4.4}$$

where $E\{c_k^{\,2}\}$ is a scaling factor calculated from the statistics of the symbol alphabet values $c_k, k \in \{0...7\}$. This yields the S-curves shown in Figure 4.12, shown for three levels of SNR. All of these pass through the origin and have the same sign as the phase offset. However, the metric drops to zero for the noiseless case at ±0.15 sample period. This is no cause for concern, because even if the initial sampling frequency were exact and the phase offset at one of these points (which is extremely unlikely), it would move away due to thermal drift of the oscillator driving the ADC. No such point exists for the 14.9dB curve, although this has a much shallower slope than even the 22.0dB curve.

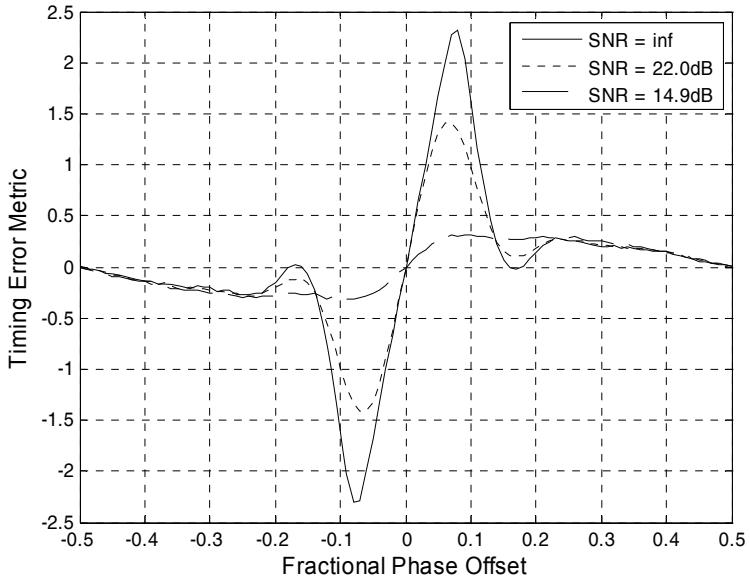

Figure 4.12 Mueller and Muller S-curve SNR variation

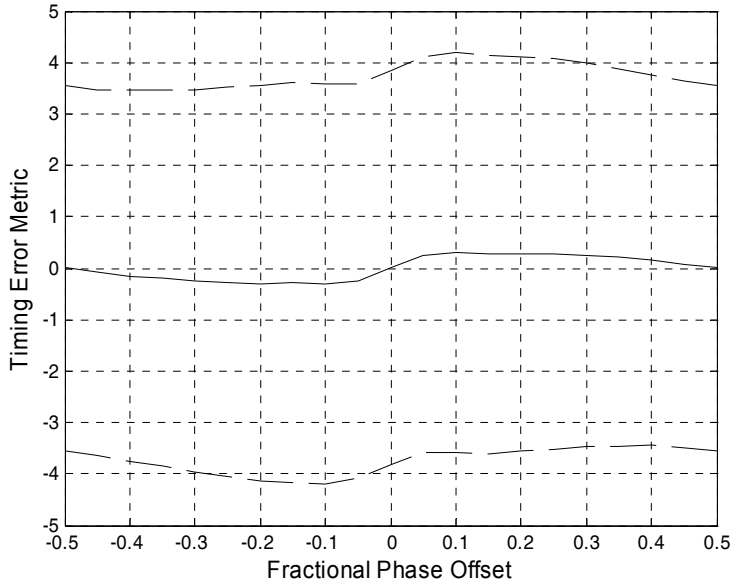

Figure 4.13 Mueller and Muller S-curve standard deviation

Figure 4.13 demonstrates that the standard deviation of the Mueller and Muller TED error metric at 14.9dB is very high relative to the information content in comparison with the segment sync techniques. This can be attributed to it operating DD mode on an eight-level alphabet, whereas the other approaches operated in DA mode on a binary sync pulse. Thus many more estimates are required to obtain the true timing error.

4.2.3.2 Band-Edge Filtering

After the folded aliases within the digitized signal have been removed by a bandpass filter, the isolated spectrum-reversed DTV signal lies between 3MHz and 9MHz (section 3.3). This is supplied to band-edge complex filters 2.69MHz above and below

its centre frequency. The filter cut-offs are set to be complementary to the DTV signal, so that conjugate convolution yields a complex signal whose real and imaginary components indicate the magnitude and direction of the timing frequency mistiming, respectively [5]. Alternatively, the clock phase can be adjusted by a gradient search algorithm to maximize the energy of the received signal at the symbol rate. Variations on this technique exploit the Nyquist sidebands one stage later in the signal processing chain, following demodulation of the signal to baseband [25, 27].

However, such algorithms rely on relatively undistorted band edges. Deviations from this can have undesirable consequences on the synchronization [28]. Based on recordings of received signal power spectral densities (PSDs) made in Philadelphia in March 2000, the extent of band edge distortion in ATSC reception conditions would be expected to impact the synchronization capability of 8-VSB receivers [29]. This technique is therefore not considered further.

4.3 Control Loop

4.3.1 Loop Filter

Unlike the smooth S-Curves in Figure 4.12, the instantaneous metric values are noisy due to: (i) stochastic jitter of the input data; (ii) delay within the control loop; (iii) signal distortion effects arising from the transmission channel, even when attenuated by the equalizer; (iv) non-ideal interpolation and anti-aliasing filtering; (v) ongoing adaptation of the equalizer coefficients; and (vi) numerical quantization.

For this reason, considerable averaging of the metric is required, typically by a proportional plus integral (PI) loop filter, which provides good steady state timing phase and frequency compensation. Suitable multiplier factors were determined empirically through simulations. The output of the loop filter is calculated from the current estimate of the instantaneous timing frequency $\Delta\phi_n$ and phase ϕ_n errors, scaled by proportional P and integral I factors, respectively:

$$LF_{out} = P \cdot \Delta\phi_n + I \cdot \phi_n \,. \tag{4.5}$$

4.3.2 Controller

The controller is responsible for determining suitable values of m_n and μ_n for the interpolator at instant n+1. These can be calculated efficiently according to Moeneclaey's approach [30] thus:

$$m_{n+1} = m_n + \text{int}\left[\hat{\mu}_n + \frac{T_i}{T_S}\left(1 + SAW\left(\hat{\varepsilon}_n - \hat{\varepsilon}_{n-1}\right)\right)\right] \tag{4.6}$$

and

$$\hat{\mu}_{n+1} = \text{frac}\left[\hat{\mu}_n + \frac{T_i}{T_S}\left(1 + SAW\left(\hat{\varepsilon}_n - \hat{\varepsilon}_{n-1}\right)\right)\right]. \tag{4.7}$$

$SAW\left(x\right)$ denotes the sawtooth function (Figure 4.14) and $\hat{\varepsilon}_n$ is the current estimate from the TED. int[x] represents the largest integer less than x, which takes care of incrementing or decrementing the index m when the value of μ wraps below 0 back to 1 or vice-versa, respectively (as frac[x] denotes the fractional part of x). This is an

efficient way of calculating the control values, because it avoids the need for a NCO [30]. (The resampling rate T_i/T_S is calculated using nominal values.)

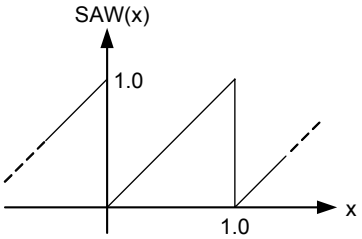

Figure 4.14 Sawtooth function

4.4 Proposed Approach

The proposed design employs the Mueller and Muller [26] algorithm as the TED, which for this application combines the benefits of simple implementation with satisfactory performance characteristics. Although the accuracy of instantaneous phase estimates is lower compared with the DD approach, the latter is restricted to the known data sequences and can therefore only be performed occasionally. Overall the proposed design exhibits lower jitter than comparable systems, as confirmed by simulations (section 6.2.1) that demonstrate its superior steady-state SER performance.

In combination with the Farrow interpolator, the timing recovery scheme incurs only a small implementation loss and is suitable for high-speed operation [31]. It was shown that a particularly simple realization of the Farrow interpolator yielded acceptable performance for ATSC DTV reception [32]. In addition, the ability of the timing recovery loop to operate at the symbol rate is advantageous in reducing the equalizer size, as will be seen in Chapter 5.

5 Equalization

The primary purpose of the equalizer is to remove linear distortions that close the data eyes of the received signal, such as spectral tilt or multiple path propagation in the transmission channel. A secondary benefit may also be the compensation of imperfections in transmitter/receiver hardware (e.g. non-ideal interpolation or filtering), potentially relaxing the specifications on sub-components and lowering costs.

The original "Grand Alliance" ATSC Receiver was built in 1993. With 256 equalizer coefficients its ghost echo range was limited to a maximum of 24μs, which satisfied the requirements of the prevailing opinion of expected multipath conditions experienced at an in-home receiver. Equalizer coefficients were determined via the periodic field sync sequence, allowing the channel impulse response (CIR) up to 24μs either side of the dominant path to be estimated.

Echo spans subsequently experienced "in the field" have significantly exceeded the initial estimates. Successive generations of receivers have exhibited increasing robustness to the delay and amplitude of single ghosts and ensembles of multiple signal paths. One of the ways in which this has been achieved is by extending the equalizer length, to the extent that it occupies in the region of 60% to 80% of the gate count associated with the signal processing between the antenna to and including the convolutional decoder [2]. Current ATSC recommendations [9] are for a minimum echo coverage of -10 to +40μs (corresponding to at least 538 coefficients), rendering the training signal too short for equalization [34] and motivating the search for high-performance, low-complexity techniques for adapting coefficients using the quasi-random data symbols, namely "blind" techniques.

As the equalizer interacts with other components within the demodulator, its design cannot be considered in isolation. Most significantly, it affects the timing synchronization system, because: (i) its group delay (and therefore control) is affected by whether a linear or feedback structure is chosen; (ii) use of symbol-spaced or fractionally-spaced filter coefficients has an impact on the equalizer's sensitivity to timing phase offsets, thereby restricting the type of timing error detector used but also constraining the requirements on its phase tracking performance; and (iii) the steady-state equalization capability affects the reliability of the timing control system. This interaction must therefore be factored into the design.

This chapter discusses the suitability of different equalizer structures and filter coefficient adaptation techniques applicable to ATSC terrestrial reception. Important design factors include complexity-versus-performance decisions, as measured by convergence speed, steady-state error rate and robustness to noise and challenging channel ensembles. Innovations in this area are then presented.

5.1 Model

If the response *h(t)* of a band-limited multipath propagation channel with frequency response *C(f)* to a similarly band-limited pulse *g(t)* is defined as

$$h(t) = \int_{-\infty}^{\infty} g(\tau)c(t-\tau)d\tau\,, \qquad 5.1$$

the signal *x(t)* observed at a receiver arising from a transmitted sequence s_n can be described thus:

$$x(t) = \sum_{n=0}^{\infty} s_n h\left(t - nT\right) + z(t)\,, \tag{5.2}$$

where *z(t)* represents additive noise and *c(t)* is the Fourier transform of *C(f)* [16]. Sampling the continuous signal *x(t)* at times $t = kT + \tau_0$, where τ_0 is the transmission delay through the channel and $k = 0, 1, ...$, results in the discrete sequence:

$$x(kT + \tau_0) \equiv x_k = \sum_{n=0}^{\infty} s_n h\left(kT - nT + \tau_0\right) + z(kT + \tau_0)\,. \tag{5.3}$$

Rearranged, equation 5.3 reads:

$$x_k = s_k h\left(\tau_0\right) + \sum_{\substack{n=0 \\ n \neq k}}^{\infty} s_n h_{k-n} + z_k\,. \tag{5.4}$$

It is clear that the first term represents a scaled version of the transmitted signal. The second term corresponds to ISI, and the third represents the additive noise at the *k*th sampling instant.

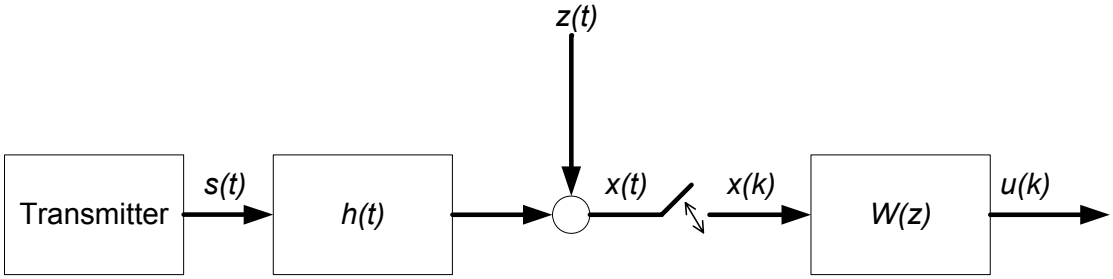

Figure 1 Simplified model of Channel and Equalizer

Figure 1 depicts how the samples x_k are then deconvolved by the equalizer with transfer function *W(z)*. The objective is therefore to choose coefficients such that the response of the equalizer minimizes the effect of ISI in the received samples and generates an output sequence *u(k)* that approximates the transmitted sequence as closely as possible. As high-amplitude echoes lead to deep notches in the frequency spectrum of the received signal, both noise and signal power at the spectral nulls are amplified when the equalizer inverts the channel frequency response perfectly. Thus both imperfect equalization and noise increase the SER.

5.2 Design Considerations

5.2.1 Structure

The most common structures are introduced in the following sections. In each case the performance and robustness are discussed in the context of the associated complexity. As adaptive time-domain equalizers comprise one or more adaptive FIR filters, the main considerations are the number of coefficients (which may depend on the sample rate of the incoming signal) and the wordlengths of coefficients and incoming samples. Together these specify the number of multiplication operations per second and their relative computational effort. Coefficient updates and error metric generation will be covered in later sections (5.3 and 5.4).

5.2.1.1 Linear

The simplest equalizer structure is a linear transversal FIR filter (Figure 5.2). Output values are calculated from a linearly-weighted sum of present and past input values according to equation 5.5:

$$u[n] = \sum_{k=0}^{N-1} w[k] \cdot x[n-k]. \qquad 5.5$$

One of the limitations of the linear equalizer is that cancellation of precursor echoes requires an infinite number of taps. [35]

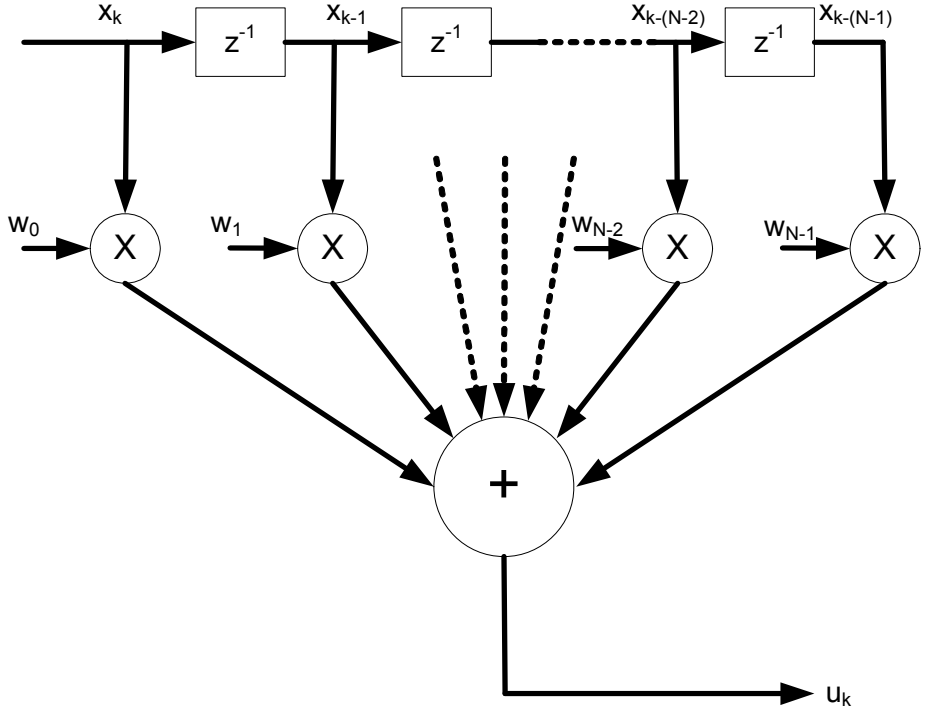

Figure 5.2 Linear transversal equalizer

5.2.1.2 Sparse

A sparse takes the form of a delay line with various clusters of FIRs at locations where echoes are expected. As DTV echo profiles are normally sparse, this type of equalizer was employed in some early ATSC receiver designs. However, setting the delays is a complex procedure requiring accurate knowledge of the full channel impulse response, which may be unobtainable. Prediction of tap positions is complicated by the higher order terms arising from pre-echoes. Sparse equalizers also experience problems in dynamic channels, and will be excluded from further consideration.

5.2.1.3 Feedback

A feedback equalizer structure consists of two FIR filters joined at a summing junction (Figure 5.3). In principle, the FF filter attenuates the pre-echo, leaving the post-echo contributions of the remaining CIR to be removed by the FB filter [2]. In a FSE, only the feedforward filter is typically fractionally-spaced, whereas the feedback filter is symbol-spaced.

Feedback equalizers offer several advantages compared with their linear counterparts: (i) shorter group delay, improving control within the timing recovery loop; (ii) lower

MSE for a given number of coefficients [36]; and (iii) improved compensation for spectral nulls arising from poor timing phase (only required in SS implementations) [37].

The choice of feedback signal determines the equalizer type: a linear feedback equalizer (LFE) processes the previous equalizer output values; a decision feedback equalizer (DFE) uses the sliced 3-bit values. A LFE tends to amplify noise as well as signal in spectral nulls, whereas a DFE limits this effect by only feeding back the actual symbol and not noise associated with the samples. A DFE also has a computational advantage, because it processes quantized (rather than full-precision) values in the feedback path; thus multiplications between data and coefficients in the FB filter can be replaced by simpler shift-and-add operations [35].

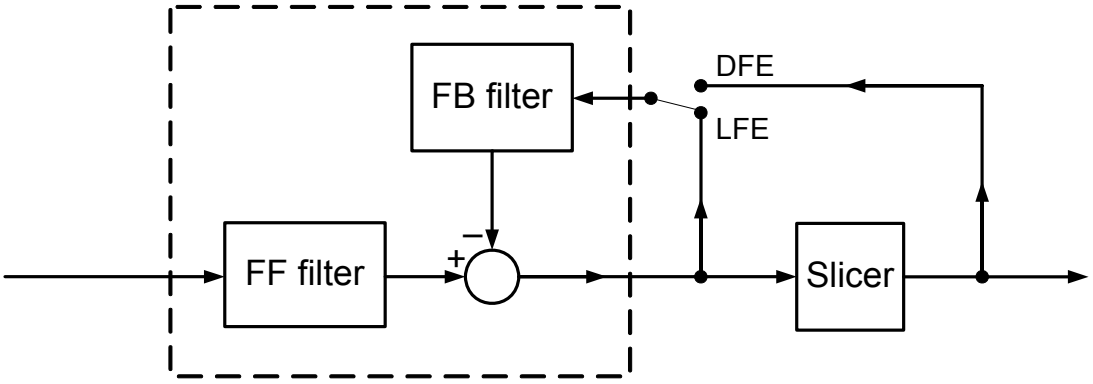

Figure 5.3 Feedback equalizer structure

Incorrect slicer decisions in the DFE lead to a phenomenon known as "error propagation". This occurs when an error at the slicer is fed back to the FB branch, introducing distortion during filtering and consequently increasing the probability of error on the next N-1 symbols [37]. Error propagation is most likely to occur: (i) at startup; (ii) when the SNR is low; (iii) when the multipath conditions are severe (particularly for SSEs when deep spectral nulls are present, as the feedback filter coefficient magnitudes become large); or (iv) a combination of these conditions. Despite its susceptibility to error propagation, the DFE architecture is employed in the vast majority of ATSC DTV receivers [2].

As feedback and nonlinearity complicate analytical performance comparisons with other schemes such as linear feedforward or fractionally spaced equalizers [38], simulation is essential in choosing the most suitable structure for a given application.

Hereafter, the discussion is restricted to feedback equalizers.

5.2.2 Data Types

Data and coefficient values may be either real or complex. A complex equalizer can compensate carrier phase offsets, whereas a real-only equalizer requires carrier recovery to precede equalization. However, adaptation of complex coefficients can be problematic when certain blind coefficient adaptation algorithms are used [39]. Use of complex values for either doubles the complexity compared with a real-real multiplication; in the worst case, namely complex-complex, the increase in complexity is a factor of four. Therefore, given the large number of coefficients associated with the equalizer, the use of real only data and coefficients is preferred, as in [36, 40].

5.2.3 Coefficient Spacing

If the received signal is sampled at the data symbol rate such that each coefficient corresponds to a single symbol, the equalizer is said to be symbol-spaced (SS). As the signal spectrum is folded at the sampling frequency prior to this, the equalizer can only compensate this signal, whose sidebands are aliased back into the main signal band. As a portion of the channel distortion is associated with its delay, the SSE exhibits timing phase-specific behaviour. In contrast, an equalizer whose input sample rate is higher than the symbol rate is said to be fractionally-spaced (FS), and has a bandwidth that extends beyond the sidebands. It can thus compensate for the component of distortion associated with timing phase; thus the performance of the FSE is insensitive to input phase [16].

This resilience of a FSE is particularly noticeable when deep spectral nulls are present, where otherwise for a SSE the feedback filter must develop a relatively long impulse response with large magnitude coefficients. This is indeed the case for an ATSC receiver, which operates under severe multipath channels and extremely long delay spread [29]. However, the additional complexity associated with the higher sample rate and longer FF filter in a phase-tolerant FSE is undesirable from an implementation perspective [41]. Although such designs with high-performance and complexity have been demonstrated [42], adequate equalization has been achieved with a SSE, which is the only choice for a low-complexity implementation [36, 40].

As mentioned in section 4.1.2, the coefficient spacing in the feedforward filter affects the type of timing recovery system that can be used. A SSE restricts the TED to symbol rate designs.

5.2.4 Filter Lengths

Early research on feedback equalizers assumed that a channel spread over N symbols would in total require N–1 taps for compensation, where the feedforward filter would be sufficiently long to cover the span from the furthest pre-echo up to the dominant path [43]. However, more recent work has identified that the feedforward filter must be extended if adequate pre-echo compensation is to be achieved, because cancellation of one pre-echo results in a more distant, lower-power alias echo which must also be attenuated if ISI is to be minimized [44]. Fortunately, echo aliases ~20dB below the main path signal have only a negligible impact on the total ISI, allowing the feedforward filter CIR to be truncated to a finite length. [42]

Inevitably not all coefficients are active for a given channel. Due to jitter in the coefficient adaptation process, redundant taps–which nevertheless adopt non-zero values–act as internal noise sources. This makes it not only undesirable to extend the filter lengths unnecessarily to avoid additional complexity: it also prevents a corresponding increase in the SNR threshold.

5.3 Coefficient Adaptation

Since the DTV channel characteristics are unknown *a priori* at the receiver, and may change slowly over time (Doppler rates of 0.05Hz are mentioned in the recommendations [9]), successful channel compensation requires the equalizer response to adapt automatically to sufficiently restore and maintain signal quality. [45].

With this objective, most approaches aim to optimize a specific performance index, of which the most common are introduced in section 5.3.1. Some of the practical means of adjusting coefficients based on these are discussed in section 5.3.3.

In the context of equalization, data-aided approaches refer to those that employ the training data within the field sync, and are typically faster than unsupervised adaptation. Decision-directed approaches take the output of the demapper as an estimate of the transmitted data.

5.3.1 Criterion

Receivers are often classified according to the criterion they seek to optimize [46]. Equalizers are a class of suboptimal receivers which are used instead of optimal structures such as the maximum likelihood receiver, for lower complexity and cost. The following paragraphs discuss some of the criteria available for setting equalizer coefficients, of which the zero-forcing and minimum mean-square error (MSE) are the most widespread. [16]. The SER at the receiver output directly affects the observed picture quality in the DTV system, and is therefore the ultimate measure of system performance [46].

5.3.1.1 Maximum-Likelihood (ML)

The ML decision criterion is based on determining the sequence of received symbols with the highest probability, given a transmitted sequence. It is theoretically optimal assuming an *a priori* noise distribution and a known symbol alphabet, but is prohibitively intensive computationally for long channels because the computational complexity grows exponentially with the length of the channel dispersion. [16]

5.3.1.2 Minimum Symbol Error Rate

The SER on the sliced output values is the ultimate measure of equalizer performance, and thus the quantity we wish to minimize. However, this cannot be achieved directly in a real system, because the correspondence between SER and the coefficients is nonlinear.

5.3.1.3 Peak Distortion

This criterion aims to minimize the peak distortion at the equalizer output, measured as the worst-case value of the ISI. According to this principle, the ideal equalizer in the absence of noise inverts the channel perfectly and error-free reception is possible. However, noise may be significantly amplified if the channel frequency response exhibits deep spectral nulls (as is common in fading channels), leading to poor performance in practice.

5.3.1.4 Minimum Mean-Square Error (MMSE)

The objective under the MMSE criterion is to minimize the mean-square difference between the transmitted symbol $\left(I_k\right)$ and the value at the equalizer output $\left(\hat{I}_k\right)$.

This leads to the cost function

$$J = E\left|\varepsilon_k\right|^2, \tag{5.6}$$

where the error is defined as

$$\varepsilon_k = I_k - \hat{I}_k \tag{5.7}$$

if the transmitted values are known (e.g. due to a training sequence); or

$$\varepsilon_k = \tilde{I}_k - \hat{I}_k \qquad 5.8$$

if estimates $\left(\tilde{I}_k\right)$ of the transmitted values are used instead.

Two highly-suited methods are LMS and RLS, the former being more widely used due to its simplicity. Even though MMSE is a suboptimal approach which trades off ISI reduction and output noise variance, the loss in SER performance compared to ML is often negligible [38].

5.3.2 Channel Estimation

The field sync sequence may be used to estimate directly the channel impulse response, from which suitable initial coefficients may be generated [42]. Because the range of the training sequence is insufficient to cover the echo span [47], and also the difficulty associated with setting of the precursor higher-order terms, it can be used to assist recursive approaches, but not to replace them.

Coefficient initialization typically reduces the total convergence time, because at the start of recursive adaptation many of the coefficients within ±24μs of the dominant path lie close to their final values. This may also help to ensure convergence to the global optimum, particularly when adaptation is performed "blindly" (sections 5.3.3.3 and 5.4).

The initial filter weights may be derived using the following procedure:

1. Locate a segment sync (832 symbols)
2. Compute the cross-correlation of the received values with the known values (stored in memory).
3. Determine the positions of the *N* highest peaks within the resulting vector.
4. Copy the points around the highest peak near to the end of the FF filter, using reverse indexing.
5. Place *M* impulses in the FB filter corresponding to their amplitudes and positions relative to those in the cross-correlation.
6. Convolve with the negative of the FF filter, compensating for any changes in position arising from the convolution.
7. Switch to a recursive adaptive algorithm to improve on the initial estimate and track slow changes of the channel.

Initialization of the coefficients therefore involves computation requiring dedicated hardware (such as a 832×832 cross-correlator), and control logic to govern the scheduling of the different stages. Given that it may only be used in addition to, rather than instead of, recursive approaches, its use cannot always be justified.

5.3.3 Iterative Adaptive Algorithms

The following iterative approaches seek to minimize a cost function over all possible values of equalizer coefficients [39]. Iterative learning is better suited to continuous processes such as broadcast transmissions [46]. The techniques are described in the context of PAM constellations; the extensions of many to 2-dimensional constellations are omitted for clarity.

5.3.3.1 Least Mean Squares

The least mean squares (LMS) algorithm is a stochastic steepest-descent algorithm used in many system identification problems due to its computational simplicity. On subsequent iterations, each coefficient is modified in the opposite direction to the gradient of its associated (estimated) error. The coefficient vector ***C*** at instant *(k+1)* is derived from its previous value at instant *k* thus:

$$\hat{\mathbf{C}}_{k+1} = \hat{\mathbf{C}}_k - \Delta\hat{\mathbf{G}}_k, \tag{5.9}$$

where estimates of the true gradient

$$\mathbf{G}_k = \frac{1}{2}\frac{dJ}{d\mathbf{C}_k} = -E\left(\varepsilon_k \mathbf{V}_k^*\right) \tag{5.10}$$

are chosen as

$$\hat{\mathbf{G}}_k = -\varepsilon_k \mathbf{V}_k^*, \tag{5.11}$$

where

$$\mathbf{V}_k^* = \mathbf{V}_{-k}. \tag{5.12}$$

This yields the basic LMS algorithm proposed by Widrow and Hoff [48]:

$$\hat{\mathbf{C}}_{k+1} = \hat{\mathbf{C}}_k + \Delta\varepsilon_k \mathbf{V}_k^*. \tag{5.13}$$

The values internal to the equalizer V_k depend on its structure. For a linear equalizer these are simply the buffered received samples:

$$\mathbf{V}_k = \left[v_k \ldots v_{k-n} \ldots v_{k-N}\right]. \tag{5.14}$$

A feedback structure in training mode additionally contains fed back values:

$$\mathbf{V}_k = \left[v_k \ldots v_{k-n} \ldots v_{k-K_1} \ldots I_{k-K1-1} \ldots I_{k-N}\right], \tag{5.15}$$

which in DD mode becomes

$$\mathbf{V}_k = \left[v_k \ldots v_{k-n} \ldots v_{k-K_1} \ldots \tilde{I}_{k-K1-1} \ldots \tilde{I}_{k-N}\right] \tag{5.16}$$

for a DFE and

$$\mathbf{V}_k = \left[v_k \ldots v_{k-n} \ldots v_{k-K_1} \ldots \hat{I}_{k-K1-1} \ldots \hat{I}_{k-N}\right] \tag{5.17}$$

for a LFE. In practice, LMS methods operating in DD mode are limited to a subset of "easy" channels, where the eye is initially almost open. [34]

The main advantage of the LMS algorithm is its computational simplicity. Yet simpler implementations can be derived by utilizing only the sign of the ε_k and/or $\mathbf{V}_k^*$ components, thereby reducing some of the (costly) multiplications to (inexpensive) sign-manipulations. For example, the full-precision update of the *j*th coefficient:

$$c_{(k+1)j} = c_{kj} + \Delta\varepsilon_k v_{k-j}^* \tag{5.18}$$

becomes

$$c_{(k+1)j} = c_{kj} + \Delta sign\left(\varepsilon_k\right) v_{k-j}^* \tag{5.19}$$

or

$$c_{(k+1)j} = c_{kj} + \Delta\varepsilon_k sign(v^*_{k-j}) \quad 5.20$$

or

$$c_{(k+1)j} = c_{kj} + \Delta sign\left(\varepsilon_k\right) sign(v^*_{k-j}) . \quad 5.21$$

Implementation complexity may be further simplified if the update parameter Δ is restricted to powers of two, allowing a shift-and-add operation to replace a multiplication.

Thus in theory, the coefficient update step could be multiplier-free. However, such loss of information would normally be expected to degrade adaptation performance.

5.3.3.2 Recursive Least-Squares

The LMS algorithm exhibits a slow convergence because a single parameter Δ governs the update rate of all the coefficients. The recursive least-squares (RLS) algorithm achieves faster convergence by employing a gain *vector* ***K***:

$$\mathbf{C}_{k+1} = \mathbf{C}_k + \mathbf{K}_k \varepsilon_k , \quad 5.22$$

where

$$\mathbf{K}_k = \frac{\mathbf{P}_{k-1}\mathbf{V}^t_k}{w + \mathbf{V}^t_k \mathbf{P}_{k-1}\mathbf{V}^*_k} \quad 5.23$$

$$\mathbf{P}_k = \frac{1}{w}\left[\mathbf{P}_{k-1} - \mathbf{K}_k \mathbf{V}^t_k \mathbf{P}_{k-1}\right], \quad 5.24$$

and w is a user-defined factor which governs the weighting of past data in the updates.

The superior performance of the RLS over the LMS algorithm comes at the expense of considerable increased complexity (even in "fast RLS" variants). In addition, when implemented as a transversal structure it is sensitive to round-off noise, avoidance of which requires long wordlengths for the internal computation.

5.3.3.3 Blind

The term "blind equalization" means *unsupervised* adaptation of the coefficients, without knowledge (or estimates) of the transmitted data values, for example by exploiting higher order signal statistics (e.g. [49]). However, in DTV systems where the ISI spans many symbols, implementation constraints make the class of stochastic-gradient blind algorithms the most applicable. These warrant a detailed discussion in the following section.

5.4 Blind Equalization

Blind equalization techniques do not require accurate knowledge of the transmitted symbols. For this reason they are often applied to systems where no training sequence is transmitted (e.g. due to the overhead or in audio systems etc), and the eye is initially closed thus preventing DD adaptation. The eye may be closed due to ISI arising from multipath propagation, noise introduced in the transmission channel, or–more commonly–a combination of the two.

As ATSC DTV channels often exhibit a delay spread exceeding the length of the 511-symbol pseudo-noise equalizer training sequence, blind algorithms have become standard in the more recent generations of receivers with longer echo span coverage. They are reported to satisfy the majority of expected multipath environments [34], and have also been successfully combined with DD adaptation to improve steady-state performance when the SNR is sufficiently high [29].

The discussion is restricted to the class of Bussgang algorithms, which are the most commonly used methods in blind equalization due to their high performance/complexity characteristics [39]. They are analogous to stochastic gradient algorithms, because during convergence the equalizer parameter vector traverses a cost surface in the direction of steepest descent. [10]

5.4.1 Bussgang Algorithms

Bussgang algorithms exploit higher-order statistics of the received signal in an implicit sense, by passing the equalizer output $y(n)$ through a zero-memory nonlinearity which supplies the desired response [46]. If the nonlinearity is denoted by $g(\cdot)$, and y is real-valued, a Bussgang process satisfies the following condition for all k if:

$$E\left[y(n)\cdot y(n-k)\right] = E\left[y(n)\cdot g\left(y(n-k)\right)\right]. \tag{5.25}$$

or expressed another way [16]:

$$E\left[\hat{I}_n g^*\left(\hat{I}_n\right)\right] = E\left[\left|\hat{I}_n\right|^2\right]. \tag{5.26}$$

Namely, the autocorrelation of the (unsliced) equalizer output equals the cross-correlation between the equalizer output and a nonlinear transformation $g(\cdot)$ of it. Bussgang algorithms converge when this property of the equalizer output signal is satisfied. Their different behaviours arise from how the nonlinear function $g(\cdot)$ is defined; the most common algorithms are described in the following sections.

5.4.1.1 Sato Algorithm

The Sato cost function is:

$$J(w) = E\left\{\varepsilon_S^2\right\} = E\left\{\left(\gamma.sign(\hat{I}_k) - \hat{I}_k\right)^2\right\} = E\left\{\left(\left|\hat{I}_k\right| - \gamma\right)^2\right\}, \tag{5.27}$$

leading to the Sato error:

$$\varepsilon_S = -\left(\gamma.sign\left(\hat{I}_k\right) - \hat{I}_k\right), \tag{5.28}$$

with a dispersion constant γ defined as

$$\gamma = \frac{E\left\{I_k{}^2\right\}}{E\left\{\left|I_k\right|\right\}}. \tag{5.29}$$

5.4.1.2 Godard Algorithm

This [50] is a generalization of Sato's algorithm, which minimises the cost function

$$J(w) = E\left\{\left(\left|\hat{I}_k\right|^p - R_p\right)^2\right\}, \tag{5.30}$$

leading to the error estimate

$$\varepsilon_G = \left|\hat{I}_k\right|^{p-2}\left(\left|\hat{I}_k\right|^p - R_p\right). \tag{5.31}$$

The Godard dispersion coefficient R_p acts as a scaling parameter and normalizes the output of the equalizer

$$R_p = \frac{E\left\{\left|I_k\right|^{2p}\right\}}{E\left\{\left|I_k\right|^p\right\}}. \tag{5.32}$$

For the case (p=1) these are the same as the Sato algorithm.

5.4.1.3 Constant Modulus Algorithm (CMA)

The CMA is the case (p=2) of Godard's algorithm:

$$\varepsilon_{CMA} = \left(\left|\hat{I}_k\right|^2 - R_2\right). \tag{5.33}$$

It is the most widely established blind equalization algorithm [16], due to its relatively efficient implementation and performance close to that of MMSE receivers [51].

5.4.1.4 Benveniste-Goursat-Ruget Algorithm

The Sato algorithm can be expanded by introducing a function *f()*:

$$\varepsilon_{BGR} = -\left(\gamma \cdot sign\left(\hat{I}_k\right) - f\left(\hat{I}_k\right)\right), \tag{5.34}$$

where

$$\gamma = \frac{E\left\{f\left(I_k\right).I_k\right\}}{E\left\{\left|I_k\right|\right\}}. \tag{5.35}$$

It will be obvious to the reader that this reduces to the Sato algorithm for $f\left(x\right) = x$.

5.4.1.5 Benveniste-Goursat Algorithm

This is a combination of the Sato and a DD algorithm [52]:

$$\varepsilon_{BG} = k_1\varepsilon_{DD} + k_2\left|\varepsilon_{DD}\right|\varepsilon_S, \tag{5.36}$$

where ε_S is the Sato error and

$$\varepsilon_{DD} = \tilde{I}_k - \hat{I}_k \tag{5.37}$$

is the DD error.

Before the symbol transition eye is opened, the $\left|\varepsilon_{DD}\right|$ term is large and thus the blind algorithm dominates. If the ISI is sufficiently compensated by the equalizer steady-state and the SNR high, the DD error dominates. As DD typically experiences less excess noise in good conditions compared with the Sato algorithm, the MSE at the

equalizer output is further improved [29]. Thus a smooth automatic changeover between blind and DD mode is achieved; if the channel characteristics change abruptly, adaptation is automatically switched back to the blind mode. A variant of this [40] uses the CMA instead of the Sato algorithm, reportedly achieving superior performance.

5.4.1.6 Stop-and-Go Algorithm (SGA)

The SGA was devised by [53] to reduce the likelihood of convergence to local minima in the cost function, which would result in poor performance. It combines the advantages of the Sato and DD algorithms: as the former is more robust when the eye is closed, it provides a confidence indicator for whether to enable DD adaptation (with superior convergence and steady-state properties) on each iteration.

$$\varepsilon_{SG} = \frac{1}{2}\varepsilon_{DD} + \frac{1}{2}\left|\varepsilon_{DD}\right| sign(e_S), \tag{5.38}$$

which is only non-zero if the signs of ε_S and ε_{DD} are the same. Variations exist with different combinations of error metrics; for example ε_{CMA} instead of ε_S [54].

5.4.2 Convergence

In noisy channels, the CMA minima are near those of the MMSE for a FSE [55]. However, for a SSE, the possibility of false minima exists, degrading the SER [56]. As convergence behaviour of adaptive algorithms is less amenable to theoretical analysis when feedback and non-linearities are present, practical implementations of blind equalizers still employ heuristic measures to improve their convergence characteristics. [39] One such approach is to initialize the equalizer coefficients (section 5.3.2) in order to "steer" the convergence towards the global minimum; this increased robustness (and often convergence speed) naturally comes at the expense of extra hardware and design complexity.

As with non-blind stochastic-gradient algorithms, a larger step size favours more rapid convergence and tracking of time-varying channels, whereas a low step size is preferable to avoid excess noise in steady-state. Dynamic adjustment of the step size can be employed to obtain the benefits of both. This may take the form of a so-called "gear-shift" after a specified period of time, or when a given SER threshold is crossed. Some more advanced approaches regulate the step-size based on the spread of received points on the constellation (e.g. [57]).

5.5 Improved Blind Equalization for ATSC

At one extreme, the objective of equalizer design could be viewed as complexity minimization for a given performance criterion; at the other, performance maximization for a given architecture. In designing effective commercial receivers, both of these competing factors must be considered.

Whereas impressive robustness to very hostile multipath propagation channels can be achieved by highly sophisticated receivers [34], the contributions of the thesis are motivated by limitations of existing low-complexity schemes, and are presented in the context of a low-complexity ATSC receiver. (The objective was not to devise an equalizer that exceeds the current performance of the latest generation of receivers.)

Thus the number of coefficients is chosen to cover the minimum recommended channel span: with 20 coefficients at each end to absorb “ripple”, this corresponds to 364 feedforward and 472 feedback coefficients. In-phase samples are processed in a symbol-spaced feedback equalizer with real-only coefficients (as recommended in [40]), which are adapted by a stochastic gradient algorithm whose error metric is computed using the CMA. No DD adaptation is performed; at TOV it would degrade performance due to the inaccuracy of slicer decisions, whereas at higher SNRs it would lower the SER compared with blind adaptation. As the MPEG-2 error rate is already very low, the additional benefit of DD adaptation would be negligible.

Initially a LFE is demonstrated to provide superior SNR performance at TOV, due to the avoidance of error propagation associated with a DFE [58]. The findings are relevant to other systems employing FEC, where the SER/ SNR curve is steep. As the LFE incurs increased numerical precision (particularly in the feedback path), the relationship between wordlength and performance is explored with the goal of an acceptable trade-off. Further reductions in complexity are proposed by simplifying the coefficient update procedure and computation associated with the error metric [59].

An additional enhancement arises out of an analysis of the dispersion coefficient associated with the constant modulus algorithm. A modified value is considered initially from a theoretical perspective; empirical results then confirm its superiority [60]. These conclusions have a wider applicability to other types of communication receivers that employ blind Bussgang-type equalization.

5.5.1 LFE

The main performance advantage of the DFE over the LFE is due to its lower noise enhancement at higher SNRs. As the SNR drops and slicer decisions become less reliable, the occurrence of error propagation in the DFE increases. The relationship between these two factors is such that there is a threshold SNR, below which noise enhancement of the LFE has a lesser effect on SER than error propagation in the DFE [6]. Simulations confirm that for a representative collection of channels this crossover point occurs above TOV; thus a DFE has a lower area coverage than a LFE.

Assuming 10-bit numerical precision of the LFE output symbols compared with 3-bit precision for a DFE, use of the LFE incurs the following additional complexity:

Table 4 Computational increase of a LFE relative to a DFE

Bits	Number of instances	Description
(10-3)	472	bits of precision in the FB delay line
(10-3)	472	shift-and-adds associated with multiplication by 17-bit coefficients within the FB filter
(10-3)	472	shift-and-adds arising from multiplication by the combined (error × update-factor), for which 10 bits is a reasonable estimate, assuming a 10-bit error metric and an update factor <1.

The more significant figures here are the latter two, which involve multiplications. A first approximation to the increase in complexity would therefore be:

7 x 472 x 17 + 7 x 472 x 10 = 89208 bit additions.

Relative to the total (approximate) computation associated with additions in the DFE:

Table 5 Computational complexity of a DFE

Bits (data)	Bits (coeffs)	Number of instances	Description
10	17	364	shift-and-adds for the FF filter
3	17	472	shift-and-adds for the FB filter
10	17 x 3	364	shift-and-adds or additions in the update equation (assuming a 3-bit update factor) for the FF filter
3	17 x 3	472	shift-and-adds or additions in the update equation (assuming a 3-bit update factor) for the FB filter.

use of the LFE represents a percentage computational increase relative to the DFE of:

$$100 \times 89208 / \{61880 + 16048 + 185640 + 72216\} = 26.6\%,$$

which would be hard to justify in the context of a low-complexity receiver. However, it was found through simulation that the wordlength at the output of the equalizer could be reduced significantly (down to 5 bits) without compromising performance. Thus the corresponding increase would be approximately 7.6%, which is more commensurate with the performance enhancement.

5.5.2 Reduced-Complexity Coefficient Updates

Further efforts to reduce the overall equalizer complexity were pursued in the area of coefficient adaptation.

5.5.2.1 Sign-Error Algorithms

The potential of sign-error algorithms to reduce implementation complexity was introduced in section 5.3.3.1 in the context of the simple LMS algorithm. This principle of hard-limiting ε_k to $\{-1, 0, +1\}$ is extensible to other LMS-type adaptation schemes, such as the blind stochastic gradient algorithms covered in section 5.4. Signed-error updates have received much attention due to their potential for considerable complexity savings [e.g. 61, 62, 57].

5.5.2.2 Sign-Error SGA for LFE

For the LFE described in the previous section, the update calculation:

$$c_{(k+1)j} = c_{kj} + \Delta \varepsilon_k v^*_{k-j} \qquad 5.39$$

involves:

Table 6 Complexity of full-precision coefficient update

Bits	Number of instances	Description
(1 + 3 x 10 x 10)	364	additions / shift-and-adds for the FF FIR
(1 + 3 x 10 x 3)	472	additions / shift-and-adds for the FB FIR

which equates to 152516 such operations. In contrast, the sign-error version:

$$c_{(k+1)j} = c_{kj} + \Delta sign(\varepsilon_k) v^*_{k-j} \tag{5.40}$$

involves:

Table 7 Complexity of sign-error coefficient update

Bits	Number of instances	Description
(1 + 3 x 1 x 10)	364	additions / shift-and-adds for the FF FIR
(1 + 3 x 1 x 3)	472	additions / shift-and-adds for the FB FIR

which equates to 16004 such operations (ignoring the sign check and inversion). Although the figures are approximate, they illustrate that the complexity is an order of magnitude lower for the sign-error version. It is trivial to see that further savings may be obtained if the update factor Δ is chosen to be a power of two.

However, the deterioration in performance due to information loss is in most cases severe, as seen for 8-VSB in section 6.3.5. It is therefore proposed to compensate for the impaired accuracy by improving the information content of the error metric using a stop-and-go algorithm (SGA), where it is combined with the DD errors thus:

$$\varepsilon_k = \begin{cases} \text{sgn}(\varepsilon_{CMA}(k)), & \text{sgn}(\varepsilon_{CMA}(k)) = \text{sgn}(\varepsilon_{DD}(k)) \\ 0, & \text{sgn}(\varepsilon_{CMA}(k)) \neq \text{sgn}(\varepsilon_{DD}(k)) \end{cases}, \tag{5.41}$$

where sgn() is the signum function and $\varepsilon_{DD}(k)$ is the slicer error.

As only the sign of $\varepsilon_{CMA}(k)$ is used, the error metric calculation can be reduced from:

$$\varepsilon_{CMA}(k) = \hat{I}_k \cdot (R_2 - \hat{I}_k^2) \tag{5.42}$$

to

$$\text{sgn}(\varepsilon_{CMA}(k)) = \text{sgn}(\hat{I}_k) \times \text{sgn}(\sqrt{R_2} - \hat{I}_k) \times \text{sgn}(\sqrt{R_2} + \hat{I}_k), \tag{5.43}$$

which is similar to that in [57], except with a third term. Thus two multiplications and an addition are replaced by two additions and three sign comparisons. Performance of the resulting algorithm is superior to the original version. An additional benefit of the proposed sign-error algorithm is stable adaptation with a larger update parameter, thereby enabling the convergence time to be reduced.

5.5.3 Dispersion Coefficient

The dispersion coefficient calculated according to equation 5.41 refers to the transmitted constellation comprising the discrete 8-VSB values {-7, -5, -3, -1, +1, +3, +5, +7}. However, the received symbols are subject to noise introduced in the transmission channel, leading to a continuous range of values with a wider probability density function (PDF). In this case the value calculated according to:

$$R_2 = \frac{E\left\{\left|I_k\right|^4\right\}}{E\left\{\left|I_k\right|^2\right\}}. \qquad 5.44$$

may result in a suboptimal choice of target modulus unless modified to consider the PDF of the expected received signal thus:

$$R_2 = \frac{E\left\{\left|\hat{I}_k\right|^4\right\}}{E\left\{\left|\hat{I}_k\right|^2\right\}}. \qquad 5.45$$

Under the assumption that the values at the equalizer output are corrupted by AWGN–either due to the channel, or the residual noise arising from amplified noise or uncompensated within the equalizer–a modified value of the dispersion can be calculated. This has an obvious dependence on SNR, which is normally unknown *a priori*. However, in a practical system it is sufficient to use the value at the threshold of operation, where the *effective* SNR is 14.9dB, regardless of the SNR as measured at the ADC; at higher effective SNR, the picture quality is unaffected, whereas at lower effective SNR there is no picture.

The effectiveness of this approach is confirmed through simulations in section 6.3.6.

6 Simulations

System simulation was essential for evaluating performance characteristics due to the high level of complexity of subsystems and the interaction between them [14]. It facilitated exploration of the design space, assisted decision-making in subsystems where parameters could be chosen (such as the interpolator), and enabled verification of the proposed designs against the performance requirements.

6.1 Models

Matlab was used to design the critical sub-systems, where development and analysis in isolation was most practical. The resulting algorithms were then implemented in SystemC and integrated into a full system model of the modulator, channel and receiver front-end and demodulator (the last two are depicted in Figure 6.1). This enabled *in situ* development and analysis of the equalizer and timing recovery system, and inspired confidence that the techniques could be applied to real signals.

The fixed-point libraries in SystemC enabled wordlengths to be determined for the critical sections in the context of the complete system. As the equalizer and timing synchronization system were under test, other parts of the system (such as the bandpass and lowpass filters) were deliberately over-specified in order to minimize their contribution to the implementation loss. (In a real receiver, these would be optimized for performance/cost.) Figure 6.1 illustrates the interconnections and wordlengths in the SystemC model, showing both the signal (black) and control paths (grey).

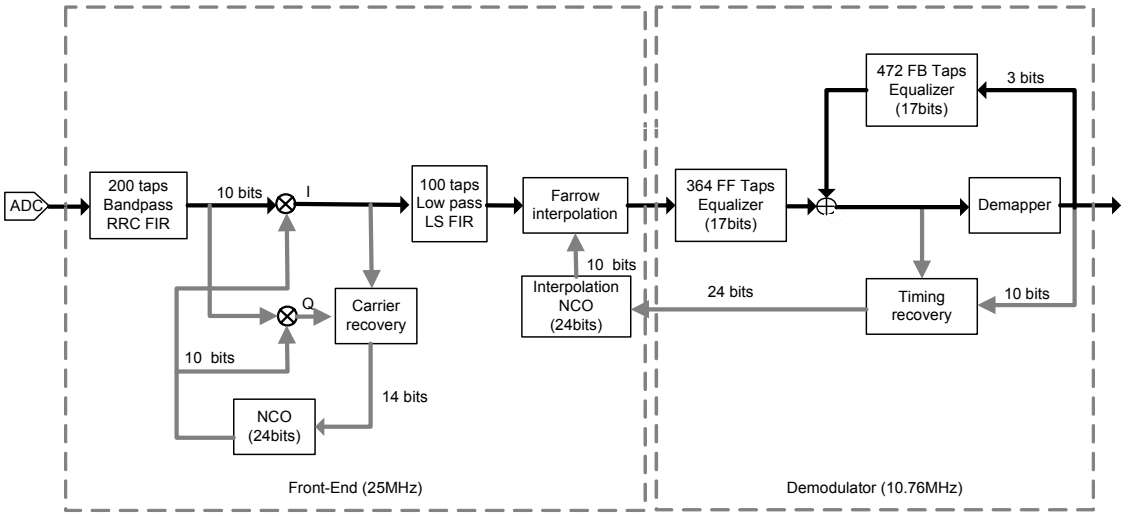

Figure 6.1 SystemC Front-End and Demodulator implementation

6.2 Timing Recovery

6.2.1 Steady-State Performance

The waterfall plots shown in Figure 6.2 provide a useful means of performance comparison between the different approaches. In each case, the simulations were carried out with PLL parameters that yielded the best performance (determined empirically through exhaustive search).

It can be seen that the GA Correlator has the highest implementation loss of the three TEDs under test. Its slight inferiority to the Kim Early-Late TED is not surprising,

because of the increased variance of its S-curve (Figure 4.8 and Figure 4.11). A less obvious result is that the Mueller and Muller algorithm exhibits the best performance of the three systems under test. Its S-curve (Figure 4.13) based on all symbols is not directly comparable with the others which apply only to segment syncs; only simulation of the full timing recovery loop for each case demonstrates its superiority.

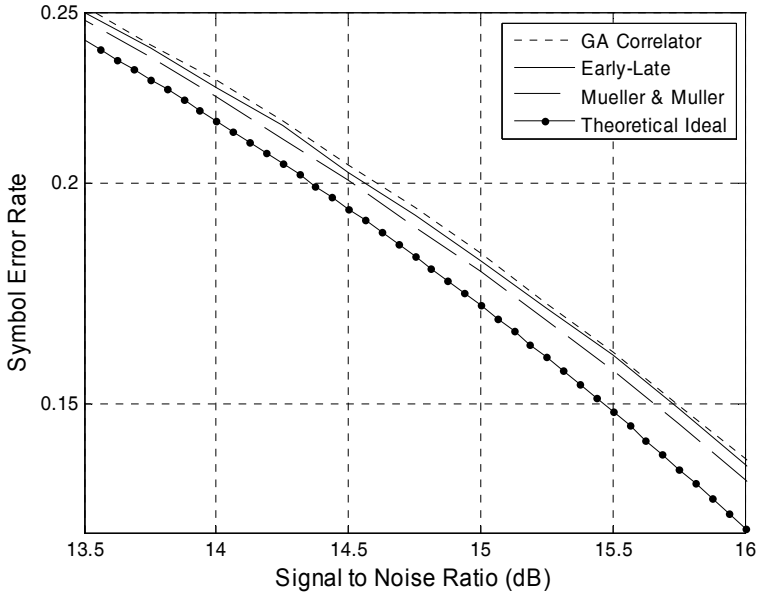

Figure 6.2 Comparison of Timing Error Detectors

Figure 6.3 illustrates the ability of the equalizer to compensate for the non-flat passband of the Farrow interpolator. A simulation was first run with the equalizer coefficients initialized to all zeros except for a single "1" near the end of the FF filter, and then allowed to adapt automatically. Following convergence, they were saved for use on subsequent runs (with adaptation disabled). The waterfall curves obtained using either the initialization or saved coefficients illustrate the superiority of the latter.

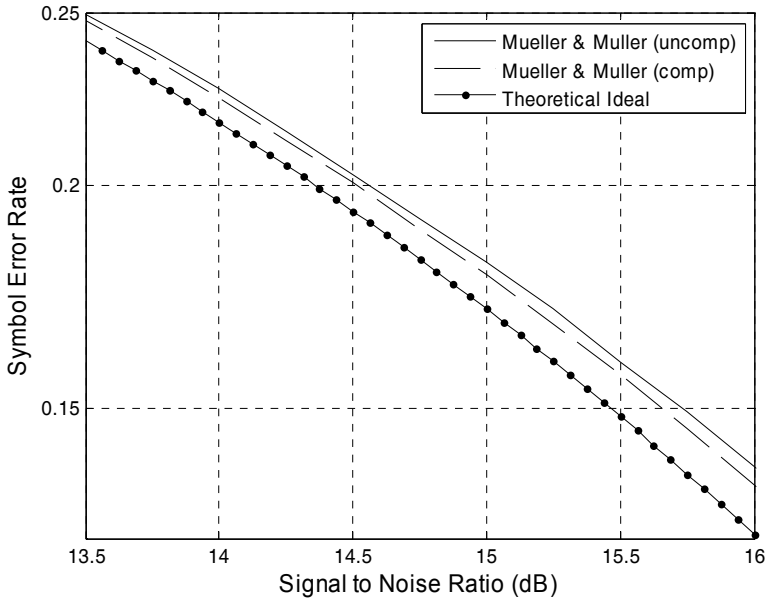

Figure 6.3 Effect on SER of Interpolator compensation

This improvement can be better understood by considering the coefficients obtained by allowing the equalizer to adapt. Figure 6.4 depicts the frequency responses when second (α=0.5) and third order interpolators were used. Besides the obvious dependence on frequency, one notes that the third order interpolator has a lower variation than the second order implementation. This is because–without compensation–it has a flatter passband; this also explains why its performance is superior.

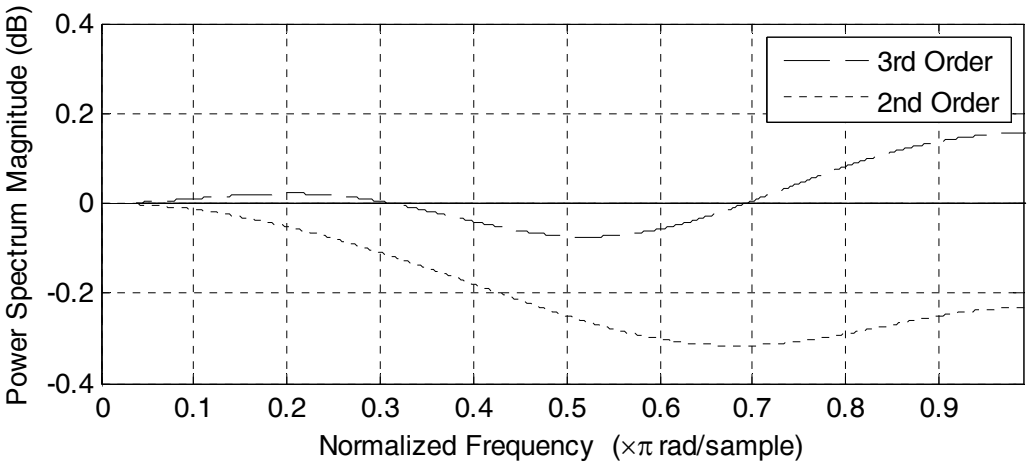

Figure 6.4 Equalizer frequency response for Interpolator compensation

6.2.2 Transient Performance

So far the steady-state performance of the timing recovery loop has been considered, because the system must be able to track small variations of the incoming sample rate. Another important consideration is its ability to lock to an unknown offset when the television is first switched on or when a channel is changed. As a typical crystal oscillator tolerance is 100ppm, testing the system with a larger offset of 200ppm provides confidence in its robustness, as illustrated in Figure 6.5. (The plot has been smoothed to facilitate viewing.) Convergence occurs in less than 5ms, which is negligible in the context of the total lock-in time of a receiver.

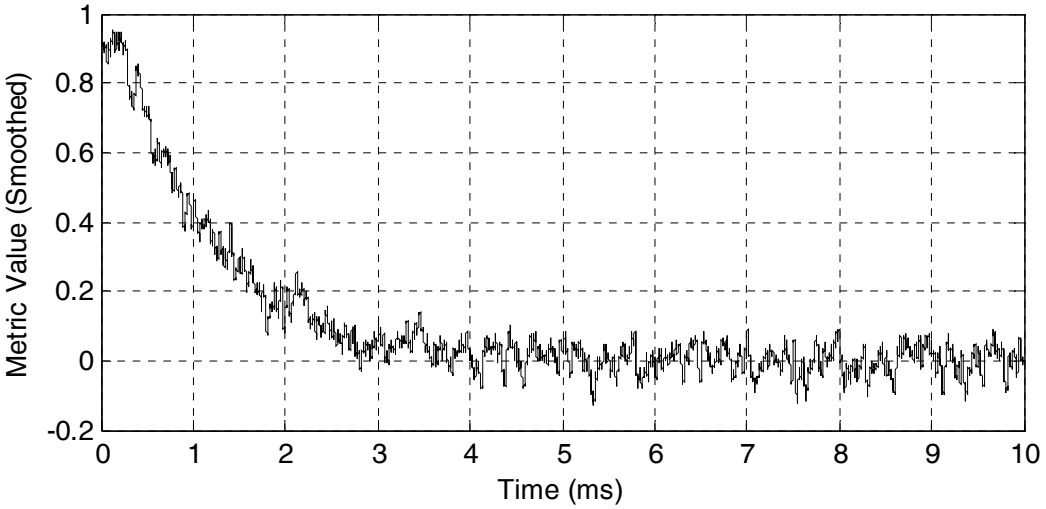

Figure 6.5 Convergence of Timing Recovery loop

6.3 Equalization

An adaptive DFE was first developed in Matlab. This provided as a platform for making the experiments and innovations described in the remainder of this chapter. To speed up simulations (by an order of magnitude), the core of the equalizer was coded in C as a "mex" file, and then compiled and linked to the Matlab code. Later this module was incorporated into a SystemC model of the entire modulator/demodulator, which enabled its system-level behaviour to be verified, including interaction with other functions such as synchronization, bandpass filtering and AGC and carrier recovery. An additional benefit was the facility to experiment with quantization, as described in section 6.3.2.

The SystemC modulator up-converts the signal to IF, as it would be impractical to simulate this section at RF (where DTV signal are in reality transmitted). Multipath propagation profiles were therefore modelled at baseband by a FIR filter containing coefficients generated offline, as in [63].

For each simulation (unless otherwise specified), the coefficients were initialized by the following procedure:

1. Set all FF and FB weights to zero, except a single 1 near the end of the FF filter.

2. Run the 8-VSB data through the simulation, with the recurrent update algorithm.

6.3.1 Extended Feedforward Filter

As described in section 5.2.4, attenuation of pre-echoes within the FF filter leads to alias echoes of lower power further back in time. Figure 6.6 illustrates the converged coefficients of a greatly-extended FF to the -5dB, -10μs echo specified by the standard. For a single echo such as this, the reflections are of diminishing amplitude–in this case as the square of the previous echo–and opposite sign, each spaced apart by the time interval of the original pre-echo. (For multiple pre-echoes the situation is more complicated, but the minimum required FF filter length is the same.)

Echoes that are not covered by the equalizer manifest as noise sources. Fortunately, as the echoes diminish fairly rapidly in amplitude, the filter can be truncated after 30μs, after which the sum of the residual echoes is below -20dB (and would have negligible effect on overall performance).

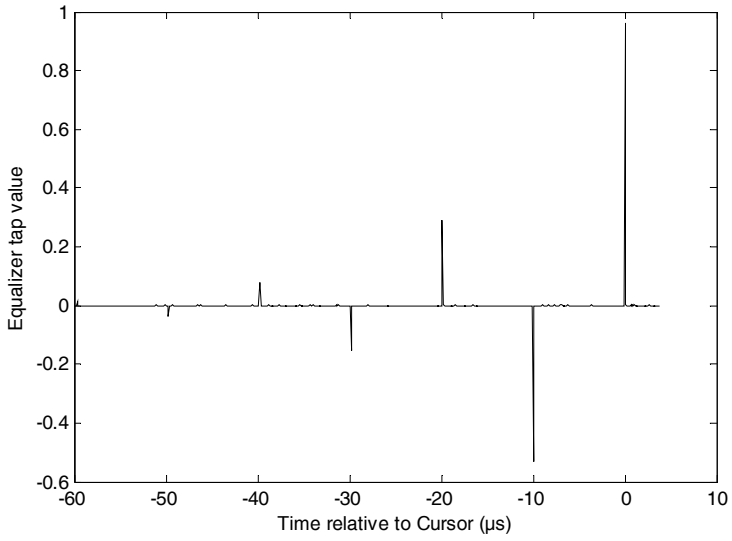

Figure 6.6 Feedforward coefficient values

This conclusion is reinforced by considering the equalizer output for two FF filters: one "short", which covers only the first pre-echo; and a "long" one, covering the first three pre-echoes. As the eye is almost closed at TOV, the histogram at its central (sampling) position is a more insightful means of comparing performance. Figure 6.7 illustrates clearly that the correct symbol values are much easier to identify with the longer filter.

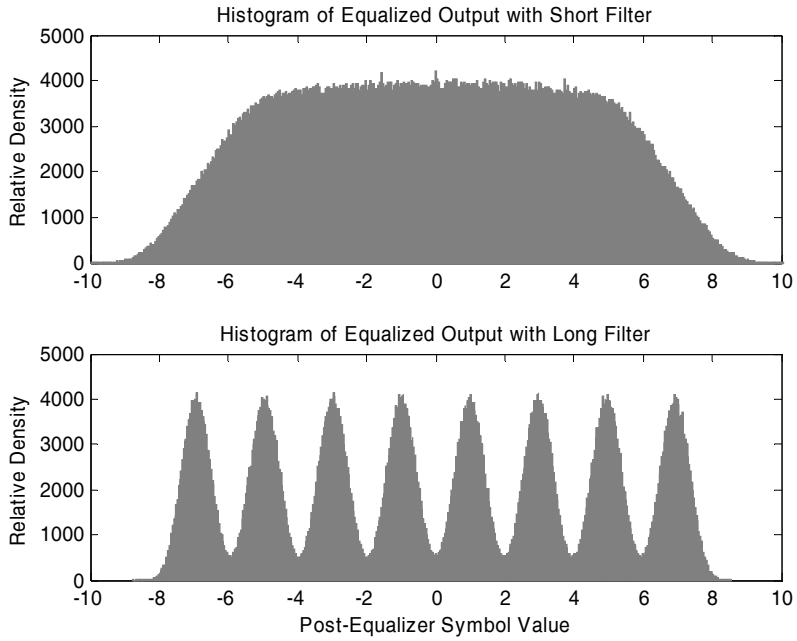

Figure 6.7 Histogram of Equalizer output symbols

6.3.2 Coefficient Quantization

As seen in chapter 5, two types of process involve the equalizer coefficients: (i) multiplying the incoming sample values; and (ii) updating of the coefficient values by an adaptive algorithm. As both necessitate multiplication operations, and there are so many coefficients, it is advantageous to restrict their wordlength. Reduction limits the ability of the equalizer to accurately invert the transmission channel and introduces noise which contributes to the implementation loss.

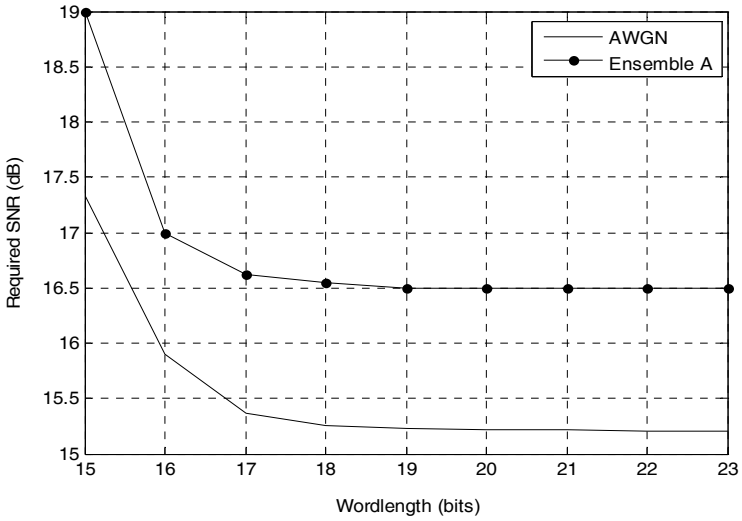

Figure 6.8 Required SNR at TOV versus coefficient wordlength.

Figure 6.8 and Figure 6.9 illustrate the simulated effect (SystemC) on steady-state and transient performance, respectively. The results suggest that 17 bits per coefficient may provide a reasonable trade-off between performance and implementation cost, below which both the required SNR at TOV and convergence time increase dramatically. Above 18 bits a slight improvement is visible, but this might be hard to justify for the added implementation cost: the final decision would depend on the intended market positioning, where a higher-priced DTV might use a longer wordlength.

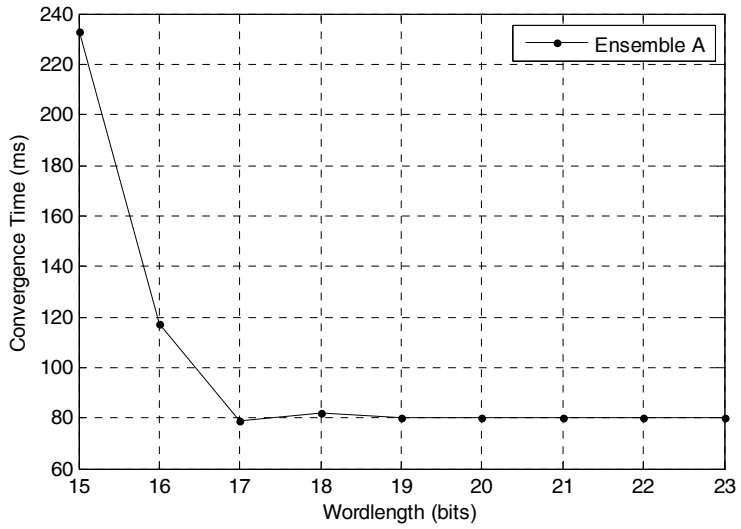

Figure 6.9 Effect of coefficient wordlength on convergence time

6.3.3 Phase Offset Compensation

A SSE is considered to be less robust to incoming timing phase than a FS equivalent. The adapted coefficients of a SSE to different timing phases of the incoming signal are shown in Figure 6.10. These illustrate the ability of an adaptive SSE to interpolate the incoming samples so as to readjust the phase to the optimal position. For no fractional offset (μ = 0 or 1), only one equalizer tap is active. As μ increases from 0 to 1, the coefficients adopt appropriate values to ensure that the output signal is restored to a unit impulse.

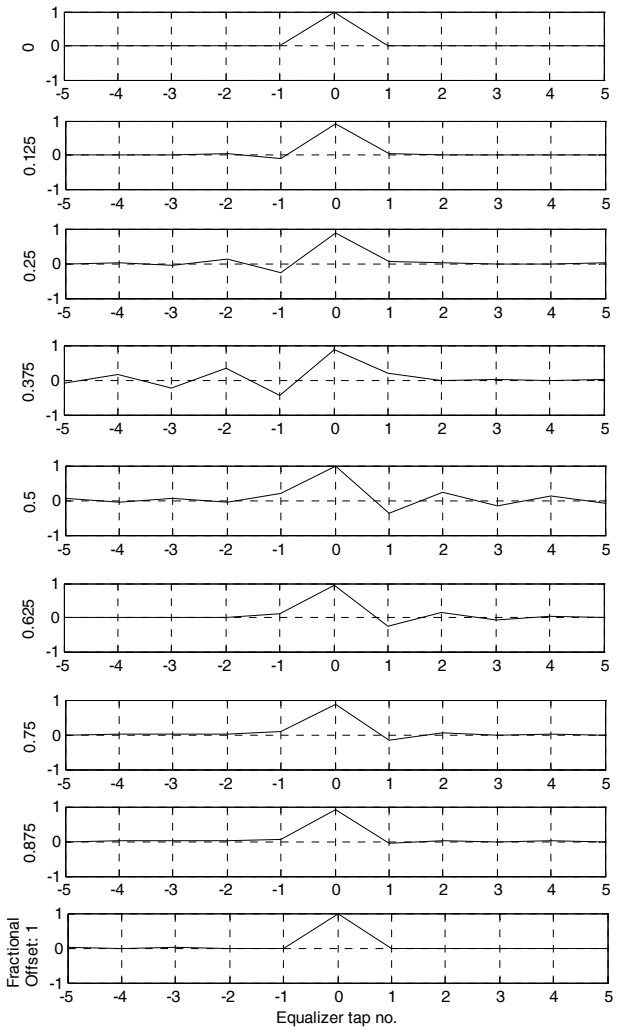

Figure 6.10 Variation of coefficients with symbol timing phase

6.3.4 ATSC Channels

A number of multipath propagation models taken from two sources were used to compare equalizer performance in the following sections. Table 8 lists the seven Advisory Committee on Advanced Television Service (ACATS) echo ensembles [64]. ACATS specified the tests to be carried out by the Advanced Television Test Centre (ATTC) on the GA prototype and many commercial receivers since. In each case, one dominant path has a nominal power of 0dB, while five echoes exhibit varying levels of attenuation and phase rotations.

It is apparent from Figure 6.11 that for each of the ACATS ensembles, the equalizer converges in less than 2×10^6 samples (200ms).

Table 8 ACATS Echo Ensembles used by ATTC

Ensemble A				**Ensemble B**			
Path	Delay (μs)	Phase (degrees)	Atten (dB)	Path	Delay (μs)	Phase (degrees)	Atten (dB)
1	0.00	288	20	1	0.00	288	20
2	1.80	180	0	2	1.75	180	0
3	1.95	0	20	3	1.947	0	20
4	3.60	72	10	4	3.60	72	10
5	7.50	144	14	5	7.50	144	14
6	19.80	216	18	6	19.70	216	18
Ensemble C				**Ensemble D**			
Path	Delay (μs)	Phase (degrees)	Atten (dB)	Path	Delay (μs)	Phase (degrees)	Atten (dB)
1	0.00	288	18	1	0.00	288	20
2	1.80	180	0	2	1.80	180	0
3	1.95	0	20	3	1.95	0	20
4	3.60	72	20	4	3.60	72	18
5	7.50	144	10	5	7.50	144	14
6	19.80	216	14	6	19.80	216	10
Ensemble E				**Ensemble F**			
Path	Delay (μs)	Phase (degrees)	Atten (dB)	Path	Delay (μs)	Phase (degrees)	Atten (dB)
1	0.00	288	20	1	0.00	288	0
2	1.80	180	0	2	0.20	180	10
3	1.95	0	14	3	1.90	0	14
4	3.60	72	10	4	3.90	72	18
5	7.50	144	20	5	8.20	144	20
6	19.80	216	18	6	15.0	216	20
Ensemble G							
Path	Delay (μs)	Phase (degrees)	Atten (dB)				
1	0.00	180	19				
2	0.20	0	0				
3	0.28	180	22				
4	0.35	180	17				
5	0.50	180	22				
6	0.80	180	19				

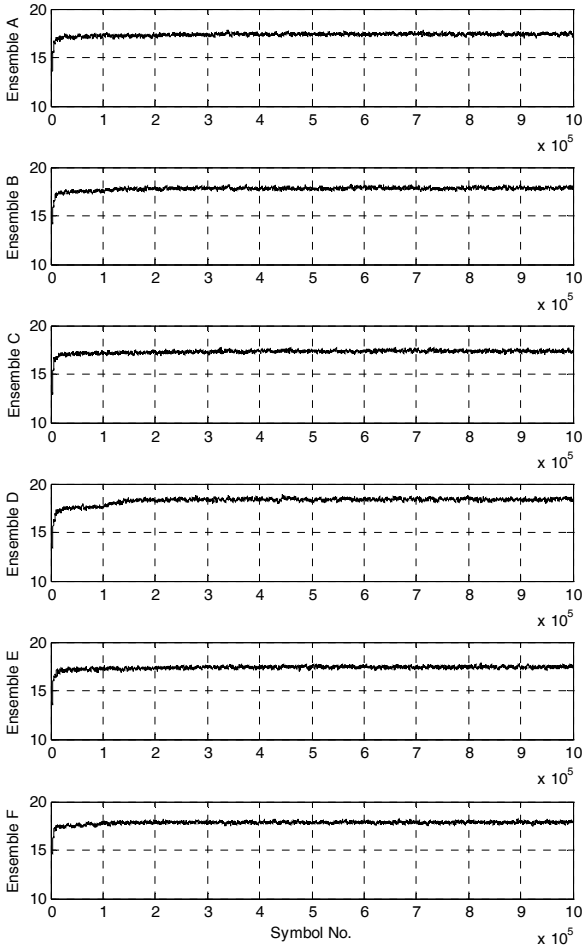

Figure 6.11 Equalizer output SNRs for ACATS Ensembles A-F

The ACATS and so-called "Brazil" profiles (Table 10) are the most commonly-cited tests in the literature associated with ATSC equalization [65]. The Brazil ensembles are more challenging, and are not a requirement of the standard: they contain one relatively easy case (Brazil A), plus three cases of increasing complexity (Brazil B, C, D), and one pathological case of a worst case multiple transmitter scenario (Brazil E). The last of these is of limited relevance to receivers for use in the US, where such single frequency networks are not planned. The minimum SNRs at TOV for the five channels are listed in Table 9. In each case, the SNR refers to the first acquisition (re-acquisition is less challenging).

Table 9 Equalizer (LFE) performance at TOV

Channel	SNR(dB)	Convergence Time (s)
Brazil A	16.7	0.9
Brazil B	20.7	1.1
Brazil C	21.5	1.3
Brazil D	Fail	Fail
Brazil E	30.5	1.5

Table 10 Brazil Echo Ensembles

Ensemble A				**Ensemble B**			
Path	Delay (μs)	Phase (degrees)	Atten (dB)	Path	Delay (μs)	Phase (degrees)	Atten (dB)
1	0.00	0	0.0	1	0.00	0	0.0
2	0.15	0	13.8	2	0.30	0	12.0
3	2.22	0	16.2	3	3.50	0	4.0
4	3.05	0	14.9	4	4.40	0	7.0
5	5.86	0	13.6	5	9.50	0	15.0
6	5.93	0	16.4	6	12.70	0	22.0
Ensemble C				**Ensemble D**			
Path	Delay (μs)	Phase (degrees)	Atten (dB)	Path	Delay (μs)	Phase (degrees)	Atten (dB)
1	0.00	0	2.8	1	0.15	0	0.1
2	0.089	0	0.0	2	0.63	0	3.8
3	0.419	0	3.8	3	2.22	0	2.6
4	1.506	0	0.1	4	3.05	0	1.3
5	2.322	0	2.5	5	5.86	0	0.0
6	2.799	0	1.3	6	5.93	0	2.8
Ensemble E							
Path	Delay (μs)	Phase (degrees)	Atten (dB)				
1	0.00	0	0.0				
2	1.00	0	0.0				
3	2.00	0	0.0				
4	-						
5	-						
6	-						

6.3.5 Choice of Feedback Signal

Figure 6.12 illustrates superior performance of the LFE at TOV [58]. This is a typical relationship for all but the most challenging channels, whose deep spectral nulls are susceptible to noise enhancement by a LFE. In the region of the TOV, the LFE has a lower SER than the DFE; at higher SNRs, the DFE is superior. However, improvements in SER at (and above) the crossover point would be imperceptible to the consumer, because it is more than 1dB above the TOV where the MPEG-2 error rate is negligible. Thus the transition to a DFE following convergence–as in some receiver designs–is unnecessary.

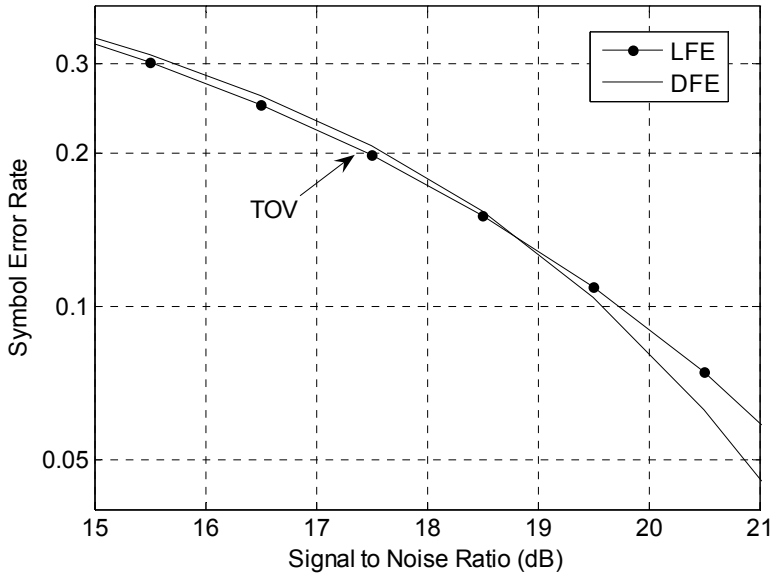

Figure 6.12 SER curves for ACATS Ensemble A channel

However, the performance gain comes at the cost of extra computation in higher-precision feedback filtering and in the coefficient update procedure. A low-complexity adaptation scheme was developed in order to offset this impact: a Sign-Error, Stop-and-Go algorithm, with comparable performance to the full-precision LFE (Figure 6.13). It is also apparent that Sign-Error adaptation in isolation results in significant degradation (due to information loss).

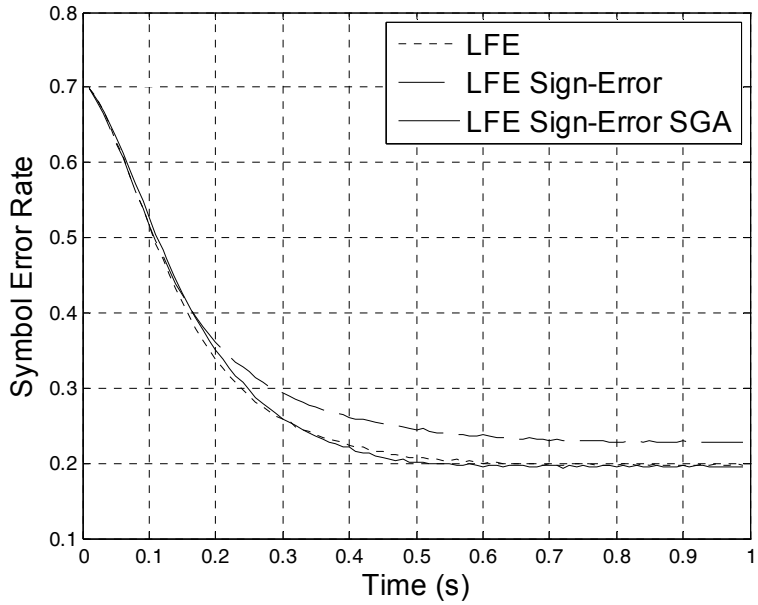

Figure 6.13 Comparison of LFE implementations (Brazil B, 21.1dB SNR)

In each case, the update parameter was set to yield similar convergence times (2^{-17} for the full Godard algorithm and 2^{-18} for the signed algorithms), with steady-state SER values close to TOV, thus allowing comparison of relative performance (the actual values are less significant). Of course, in a real system, the step size could be gear-

shifted after convergence, in order to reduce the steady state SER further. Monte-Carlo simulations smoothed the lines, facilitating comparison of the three algorithms.

6.3.6 Dispersion Coefficient

The modified dispersion coefficient proposed in section 5.5.3 varies with the SNR of the incoming signal. For AWGN this relationship is shown in Figure 6.14: close to the TOV (~14.9dB), the dispersion coefficient is highly sensitive to the SNR; below this the magnitude of the gradient increases, whereas above it tends towards the conventional value.

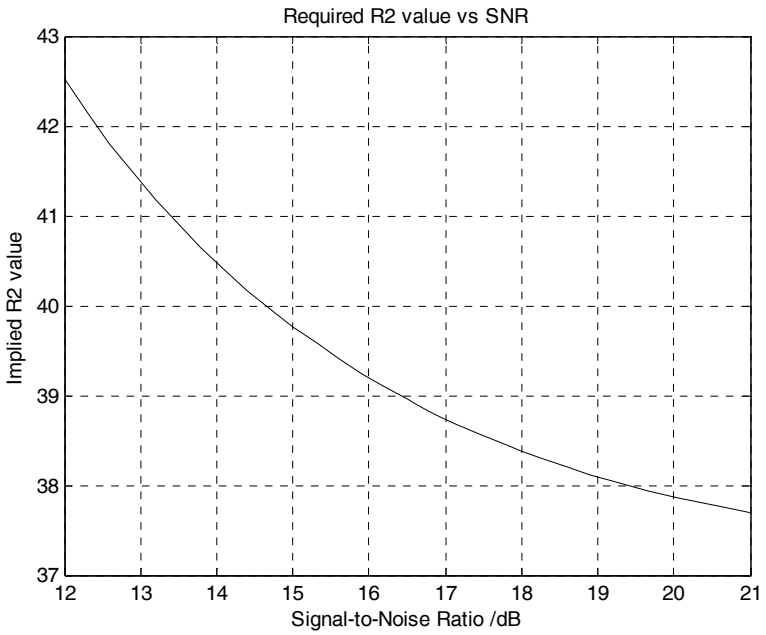

Figure 6.14 Implied Dispersion Coefficient

The SER improvement due to the modified value is shown in Figure 6.15 (AWGN).

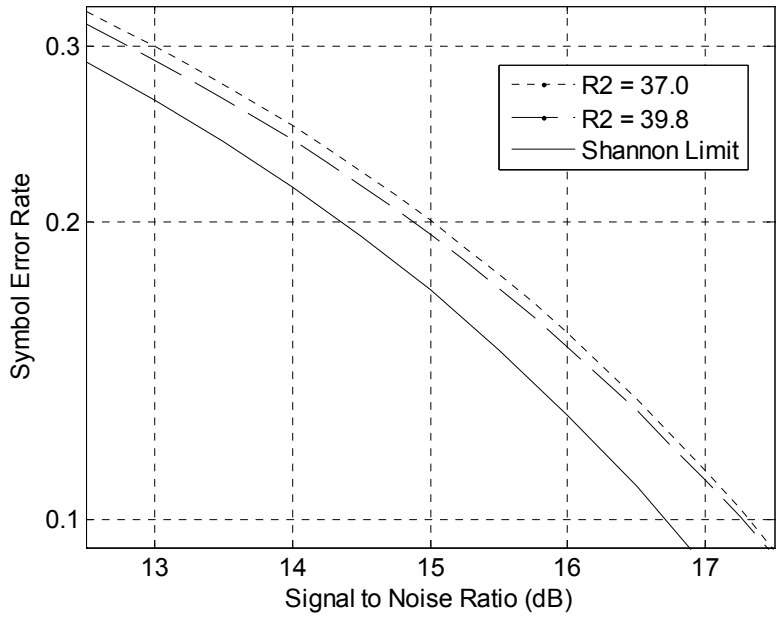

Figure 6.15 AWGN performance of DFE

If the received signal is subjected to multipath propagation, the line in Figure 6.14 shifts to the right, because a practical receiver cannot perfectly compensate the channel and the residual has the effect of an added noise source [13]. In this context it is practical to consider the *effective* SNR: the signal to interference-plus-noise ratio (SINR). If plotted against the SINR on the horizontal axis, the line would appear close to the same position as in Figure 6.14 independent of the channel.

In a commercial receiver it would be impractical to continually measure or estimate the SINR and modify the dispersion coefficient accordingly. Furthermore there is a circular dependence: the residual noise affects the SINR, leading to a different optimal coefficient, which in turn influences the SINR. Due to the "cliff effect" discussed previously, there is no perceptible penalty for using a sub-optimal value above TOV, because errors are corrected by the decoder. At lower SINRs (or SNRs), there is no picture to improve. Thus optimizing for the SINR at TOV (which is a constant ~14.9dB) yields a satisfactory solution in a practical receiver, where the SNR and the contribution of the uncompensated multipath are unknown.

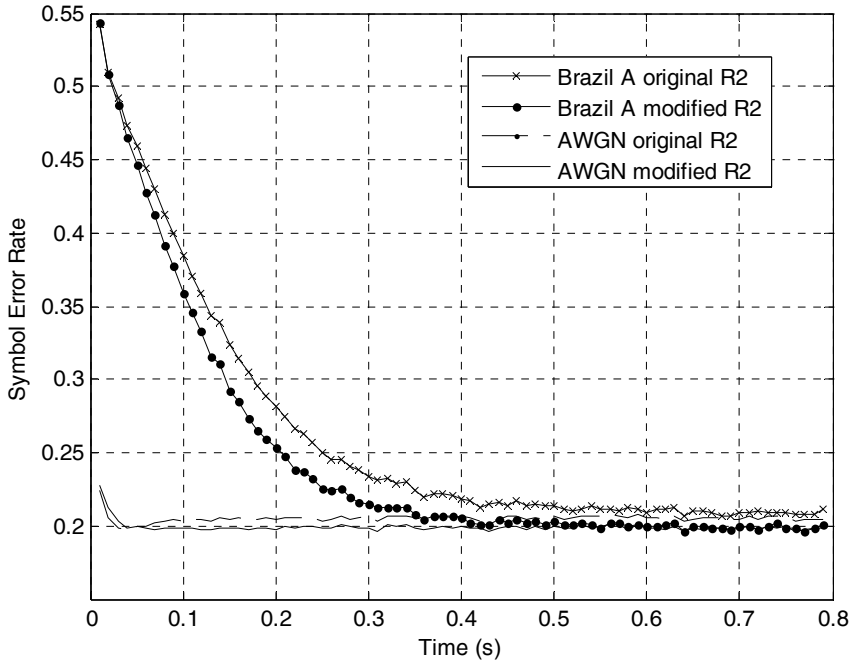

Figure 6.16 Further simulations with optimal Dispersion Coefficient

The effectiveness of this strategy is demonstrated by the simulation results shown in Figure 6.17. Although the SNRs close to the TOV (16.7dB, 20.7dB and 21.5dB) differ for the three channels shown, the relationship between SER and dispersion coefficient value is similar for each: the minimum lies close to the predicted value[2], whereas the SERs for the unmodified value (37.0) are significantly worse. The asymmetry of the curve suggests that it is better to err on the side of too large a value than too small.

[2] Based on a TOV of 14.6dB, because in the simulation there was no implementation noise within the receiver upstream of the equalizer.

The SNRs used in this experiment are taken from the TOV values reported in Table 9 for a LFE. As the corresponding DFE performance is inferior, the minimum SERs seen in Figure 6.17 are above the TOV value (0.2).

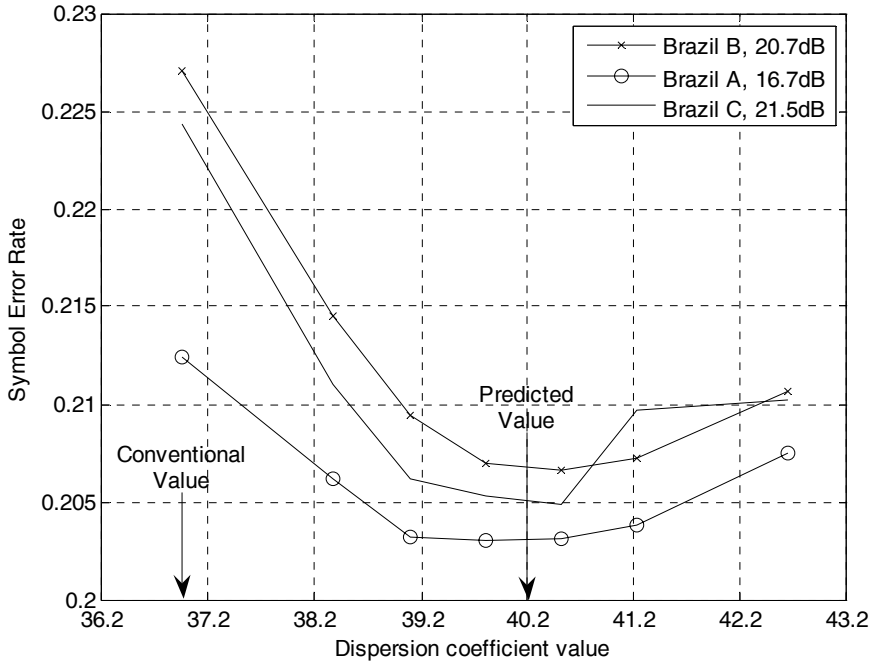

Figure 6.17 Variation of (DFE) SER with dispersion coefficient close to the TOV.

7 Conclusions and Outlook

The focus of this work was on synchronization and equalization techniques for vestigial sideband ATSC DTV receivers. The state of knowledge in all-digital timing recovery systems and blind equalization techniques was advanced.

All-digital timing recovery permits the ADC to run with a free clock, which lowers its specifications and is more cost-effective than controlling it from the digital portion of the receiver. Symbols at the correct sample rate and strobe phase are then derived from this signal via digital interpolation. A digital realization of the entire timing recovery system leads to better control characteristics and ultimately a lower error rate. A Farrow structure is used for interpolation, yielding an efficient implementation because the filter parameters remain constant during operation. The choice of a piecewise-parabolic structure further reduces the computational complexity at the cost of a small increase in MSE, which is shown to be tolerable in the context of a commercial ATSC receiver. In addition, interpolation carried out this way attenuates the out-of-band frequencies, obviating the need for a separate anti-aliasing filter.

A symbol-rate timing error detector allows symbol-spacing of equalizer coefficients. This significantly reduces its implementation complexity for a given echo range, because a smaller spacing would require more coefficients, translating to a larger silicon area occupied by the equalizer. The timing recovery scheme employs a Mueller and Muller detector operating in decision-directed mode on all samples, and exhibits lower timing jitter compared with a data-aided approach on segment syncs.

Linear and feedback equalizer symbol-spaced structures were considered; the latter is preferable when ISI and susceptibility to timing phase are considered. It was demonstrated how the feedforward coefficients of a feedback structure adapt to interpolate the incoming signal in the presence of a timing phase offset.

During the training sequence or if the signal transition eye is open, the equalizer coefficients may be adapted in decision-directed mode; otherwise, blind equalization must be employed. Of the various common techniques the CMA was found to be the best choice for this application. A computationally-efficient sign-error version of the algorithm was developed, and demonstrated to yield superior (and stable) convergence and steady-state error characteristics compared with both its full-precision counterpart and other similar approaches.

Blind adaptation of a DFE is more troublesome than a linear equalizer, because if the coefficient weights initially lie far from the ideal values, a high proportion of the slicer decisions in the feedback path are incorrect, leading to suboptimal adaptation of coefficients. A LFE is not susceptible to this phenomenon because it does not use decisions in the feedback path, and is thus sometimes used at start-up until the eye is sufficiently open for the DFE to be used. Simulations verified that a LFE would tolerate a lower SNR at TOV than a DFE; as the SNR increases above this level, the relative difference first decreases, and then the DFE error rate becomes lower. Due to the error correction techniques employed in the ATSC DTV system, the effect of errors above the crossover point is nearly invisible; thus there is no need to switch to the DFE to improve performance in this region.

The techniques developed in the course of this thesis allow reception of 8-VSB signals without using a training sequence; thus the findings are not restricted to ATSC, but are applicable to any 8-VSB communications system.

7.1 Main Advancements

Enhancements in the fields of timing synchronization and blind equalization have been presented in the context of a low-complexity ATSC DTV receiver. These lead to a lower tolerable SNR at the threshold of operation and consequently a wider range of reception sites. Alternatively, the reduction in implementation loss in these areas could offset the use of low-specification components in other parts of the system (e.g. oscillator or filters), thereby reducing the overall cost for a given performance requirement. As the proposed advancements do not require training sequences they are applicable to other PAM communications systems.

7.1.1 Timing Synchronization

A robust and efficient timing recovery system for use in practical ATSC standard HDTV receivers was presented. The proposed solution operates at baud rate, thereby enabling use of a symbol-spaced channel equalizer and simplifying the demodulator architecture.

A Mueller and Muller timing error detector is used in decision-directed mode; thus timing recovery is not restricted to training sequences. This leads to favourable control characteristics, obviates the need for a training sequence detector and reduces the lock-in time.

The design complexity is further reduced by the selection of a Farrow interpolator, whose non-flat passband response is compensated to some extent by the equalizer.

7.1.2 Blind Feedback Equalization

An adaptive DFE for ATSC DTV receivers was first developed. Low complexity was achieved by real-only filtering of in-phase, baud rate symbols. An extended feedforward filter was confirmed to sufficiently attenuate pre-echo aliases and thus reduce the steady-state MSE. Computer simulations demonstrated that stable convergence and favourable steady-state SNR performance in representative channel conditions could be attained by adapting filter coefficients using a blind algorithm.

The theoretical value of the blind CMA dispersion coefficient was then examined within the context of a noisy channel, and a modification proposed to take into account the reduced SNR of the received signal. The superiority of the new theoretical value was confirmed, as was a close correspondence between theory and empirical results.

Comparisons of DFE and LFE performance were carried out in the region of TOV. Due to error propagation in the DFE, it is found that a QEF picture may be obtained at a lower SNR with a LFE. At higher SNRs, the DFE exhibits a lower SER, but because of the strong error correction techniques employed in ATSC, picture improvements are imperceptible; thus it was proposed that a transition between LFE and DFE is unnecessary, leading to a higher design complexity without a corresponding performance improvement.

Increased computation associated with higher numerical precision within the LFE feedback path–compared with only three bits per symbol in a DFE–motivated the search for reduced-complexity update techniques. A novel hard-limited stop-and-go algorithm generates the error signal used in updating coefficients.

It was demonstrated by means of simulations that the proposed combination of equalizer and timing recovery system satisfies the requirements of the ATSC standard at a

low implementation cost, and consequently lower production and operational costs. Improvements in SNR performance translate to a wider range of sites at which a consumer would experience acceptable picture quality.

7.2 Outlook

This subject is a fertile area of research with further scope for technical advances. Potential improvements fall into two broad categories: those that would be expected to raise the performance with a minor increase in complexity; and those that would reduce the implementation cost without significantly impairing performance.

For little additional cost, the CMA algorithm could be extended to a "multi-mode" implementation [66] employing more than one constant modulus dispersion coefficient. A decision is made when the equalizer output is fed into the algorithm: depending on whether it is above or below the centre point of the four possible absolute values (from eight signed values), one of two different dispersion coefficients is used. This would be expected to shorten the convergence time by reducing the high probability of error during the initial adaptation period.

The slicer decisions passed to the FB filter of a DFE could be supplemented by (more accurate) outputs from the trellis decoder (i.e. Viterbi) in order to reduce the likelihood of error propagation (as in [17]). This would however, add to the overall complexity of the system.

As most DTV channels are typically sparse and rarely span the worst-case echo range, many coefficients are effectively inactive on a given channel (different for each channel). Random fluctuations in their (small) values introduce noise and raise the combined MSE. Identification and de-activation of the "idle" coefficients would therefore improve performance by lowering the SNR threshold.

The matched filter and interpolator have been described as separate units; this is conceptually simpler and reflects the architecture of conventional systems. However, as they both consist of linear filtering operations they could potentially be combined in order to reduce the overall effort and reduce complexity, as in [67].

It has been seen that much of the computational effort within a feedback equalizer is associated with the FF filter. Both filtering and calculation of new coefficients have a higher complexity than in the FB filter, because the precision of the input samples is much higher than that of the fed-back data. Scope for using a lower precision in the adaptation of the FF coefficients might therefore exist. A second possibility for computational reduction concerns the number of coefficients. The FF length was extended from 10µs to 30µs in order to cancel the first two "aliases" of a -5dB pre-echo located 10µs before the dominant path, leaving aliases below -20dB which contribute directly to the MSE. This constraint could potentially be relaxed, because the TOV lies in the region of 15dB (for white noise and simple channels), where such echoes (or aliases) would have minimal impact. Thus cancellation of the first alias at -10dB, 20µs would leave the -20dB, 30µs alias (and others) with minimal performance impairment. This trade-off decision would be made depending on the intended market positioning of the ATSC DTV receiver.

Enhancements in these and other areas of ATSC demodulator design can be expected to contribute to continual improvements in the performance/cost characteristics of future televisions far beyond the digital transition in the US on February 19th, 2009.

References

1. *ATSC Digital Television Standard*, Doc. A/53C, Advanced Television Systems Committee, May 2004.
2. Henderson, J.G.N.; Bretl, W.E.; Deiss, M.S.; Goldberg, A.; Markwalter, B.; Muterspaugh, M.; Touzni, A., "ATSC DTV Receiver Implementation," *Proceedings of the IEEE,* vol.94, no.1, pp.119-147, Jan. 2006.
3. *Recommended Practice: Guide to the Use of the ATSC Digital Television Standard*, Doc. A/54A, Advanced Television Systems Committee, Dec. 2003.
4. Sgrignoli, G., "History of ATSC Digital Television Transmission System," *Consumer Electronics, 2007. ICCE 2007. Digest of Technical Papers. International Conference on,* 10-14 Jan. 2007.
5. *ATSC Technology Group Report: DTV Signal Reception and Processing Considerations*, Doc. T3-600r4, Advanced Television Systems Committee, Sept. 2003.
6. Schreiber, W.F., "Advanced Television Systems for Terrestrial Broadcasting: Some Problems and some Proposed Solutions," *Proceedings of the IEEE,* vol.83, no.6, pp.958-981, Jun 1995.
7. George, D.; Bowen, R.; Storey, J., "An Adaptive Decision Feedback Equalizer," *Communications, IEEE Transactions on [legacy, pre - 1988]*, vol.19, no.3, pp.281-293, Jun 1971.
8. Proakis, J.G.; Salehi, M., *Communication Systems Engineering*. Upper Saddle River, NJ: Prentice-Hall, 1994.
9. *ATSC Recommended Practice: Receiver Performance Guidelines*, Doc. A/74, Advanced Television Systems Committee, Jun 2004.
10. Cornell University Blind Equalization Research Group, *DTV Channel Characterization*: signal captures available online at http://bard.ece.cornell.edu/downloads/data/dtv/dtv.html.
11. Gumm, L., "Signal to Noise Relationships in 8-VSB," Tektronix technical brief, Sept. 1999.
12. Sparano, D., "What Exactly is 8-VSB Anyway?," Harris Corporation Broadcast Division, 1997.
13. Sgrignoli, G.; Bretl, W., "Summary of the Grand Alliance VSB Transmission System Field and Laboratory Tests," *Consumer Electronics, ICCE 1996. Digest of Technical Papers. International Conference on,* 5-7 Jun 1996.
14. Meyr, H.; Moeneclaey, M.; Fechtel, S.A., *Digital Communication Receivers*, New York: Wiley, 1997.
15. Farrow, C.W., "A Continuously Variable Digital Delay Element," *Circuits and Systems, 1988. IEEE International Symposium on*, vol.3, pp.2641-2645, 7-9 Jun 1988.
16. Proakis, J.G., *Digital Communications*, 3rd ed. New York: McGraw-Hill, 1995.
17. Kim, H.-N.; Park, S.I.; Kim, S.W., "Performance Analysis of Error Propagation Effects in the DFE for ATSC DTV Receivers," *Broadcasting, IEEE Transactions on*, vol.49, no.3, pp.249-257, Sept. 2003.
18. Daecke, D.; Haar, S.; Schenk, H., "Symbol-rate Timing Error Detectors for DSL Transceivers," *Communications, 2004 International Zurich Seminar on,* pp.144-147, 2004.
19. Ahmed, H.M.; Kline, R.B., "Recent advances in DSP systems," *Communications Magazine, IEEE,* vol.29, no.5, pp.32-45, May 1991.
20. Ahmed, H.M., "Directions in DSP Processors," *Selected Areas in Communications, IEEE Journal on,* vol.8, no.8, pp.1420-1427, Oct. 1990.
21. Li, X.; Kwok, H.K.-C., "Interpolation Based Timing Recovery," U.S. Patent Appl. 10/422,316, Pub. no. US 2004/0213337, Oct.28, 2004.
22. Tzeng, C.-P.; Hodges, D.; Messerschmitt, D., "Timing Recovery in Digital Subscriber Loops Using Baud-Rate Sampling," *Selected Areas in Communications, IEEE Journal on,* vol.4, no.8, pp.1302-1311, Nov. 1986.
23. Lee, E.A.; Messerschmitt D.G., *Digital Communication*, 2nd ed. Boston, MA: Kluwer Academic, 1994.
24. Kim, K.; Shin, H.; Song, D., "A Symbol Timing Recovery using the Segment Sync Data for the Digital HDTV GA VSB system," *Consumer Electronics, IEEE Transactions on*, vol.42, no.3, pp.651-656, Aug. 1996.
25. Gardner, F., "A BPSK/QPSK Timing-Error Detector for Sampled Receivers," *Communications, IEEE Transactions on [legacy, pre - 1988]*, vol.34, no.5, pp.423-429, May 1986.
26. Mueller, K.; Muller, M., "Timing Recovery in Digital Synchronous Data Receivers," *Communications, IEEE Transactions on [legacy, pre - 1988]*, vol.24, no.5, pp. 516-531, May 1976.
27. Lou, H., "Timing Recovery Methods for VSB Receivers," *Consumer Electronics, IEEE Transactions on,* vol.53, no.2, pp.310-312, May 2007.
28. Godard, D., "Self-Recovering Equalization and Carrier Tracking in Two-Dimensional Data Communication Systems," *Communications, IEEE Transactions on [legacy, pre - 1988]*, vol.28, no.11, pp.1867-1875, Nov. 1980.
29. Garrison, I.M., Martin, R.K., Sethares, W.A., Hart, B., Chung, W., et al., "DTV Channel Characterization", *Information Sciences and Systems, 2001 Conference on*, 2001.
30. Gardner, F.M., "Interpolation in Digital Modems. I. Fundamentals," *Communications, IEEE Transactions on,* vol.41, no.3, pp.501-507, Mar 1993.
31. Wilson, T.G.B., "Method and Apparatus for Timing Recovery of PAM signals," U.S. Patent Appl. 60/824,306, Sept.1, 2006.
32. Wilson, T.G.B., "Baud Rate Symbol Timing Synchronization for 8-VSB ATSC DTV Receivers," *Consumer Electronics, 2007. ISCE 2007. IEEE International Symposium on,* 20-23 Jun 2007.
33. Erup, L.; Gardner, F.M.; Harris, R.A., "Interpolation in Digital Modems. II. Implementation and Performance," *Communications, IEEE Transactions on,* vol.41, no.6, pp.998-1008, Jun 1993.

34. Dehghan, H.; Heidari, S., "Demonstration of a Terrestrial TV Receiver with Optimized Equalizer," *Consumer Communications and Networking Conference, 2006. CCNC 2006. 3rd IEEE,* vol.2, pp.1299-1300, 8-10 Jan. 2006.
35. Kurzweil, J., *An Introduction to Digital Communications*, New York: Wiley, 2000.
36. Ghosh, M., "Blind Decision Feedback Equalization for Terrestrial Television Receivers," *Proceedings of the IEEE*, vol.86, no.10, pp.2070-2081, Oct. 1998.
37. Qureshi, S.U.H., "Adaptive Equalization," *Proceedings of the IEEE*, vol.73, no.9, pp.1349-1387, Sept. 1985.
38. Casas, R.A.; Johnson, C.R., Jr.; Harp, J.; Caffee, S., "On Initialization Strategies for Blind Adaptive DFEs," *Wireless Communications and Networking Conference, 1999. WCNC. 1999 IEEE,* vol.2, pp.792-796, 21-24 Sept., 1999.
39. Ding, Z., "Adaptive Filters for Blind Equalization", in *IEEE DSP Handbook*, Douglas B. Williams, ed., pp.24.1-24.17, IEEE Press, 1998.
40. Deshpande, N., "Fast Recovery Equalization Techniques for DTV Signals," *Broadcasting, IEEE Transactions on*, vol.43, no.4, pp.370-377, Dec. 1997.
41. Chung, W., Blind Parameter Estimation for Data Acquisition in Digital Communication Systems, PhD thesis, Cornell Univ., NY, 2002.
42. Wu, Y.; Wang, X.; Citta, R.; Ledoux, B.; Lafleche, S.; Caron, B., "An ATSC DTV Receiver with Improved Robustness to Multipath and Distributed Transmission Environments," *Broadcasting, IEEE Transactions on,* vol.50, no.1, pp.32-41, Mar. 2004.
43. Chen, W.Y., *DSL: Simulation Techniques and Standards Developments for Digital Subscriber Line Systems*, New York: Macmillan, 1988.
44. Ozen, S.; Hillery, W.; Zoltowski, M.; Nereyanuru, S.M.; Fimoff, M., "Structured Channel Estimation Based Decision Feedback Equalizers for Sparse Multipath Channels with Applications to Digital TV Receivers," *Signals, Systems and Computers, 2002. Conference Record of the 36th Asilomar Conference on*, vol.1, pp.558-564, 3-6 Nov. 2002.
45. Endres, T.J.; Strolle, C.H.; Hulyalkar, S.N.; Schaffer, T.A.; Shah, A.; Gittings, M.; Hollowell, C.; Bhaskaran, A.; Roletter, J.; Paratore, B., "Carrier Independent Blind Initialization of a DFE," *Signal Processing Advances in Wireless Communications, 1999. SPAWC '99. 1999 2nd IEEE Workshop on,* pp.239-242, 1999.
46. Haykin, S., "Adaptive Digital Communication Receivers," *Communications Magazine, IEEE*, vol.38, no.12, pp.106-114, Dec. 2000.
47. Baek, J.-S.; Park, S.-W.; Seo, J.-S., "Fast Start-Up Decision Feedback Equalizer Based on Channel Estimation for 8VSB DTV System," *Broadcasting, IEEE Transactions on,* vol.53, no.1, pp.38-47, Mar. 2007.
48. Widrow, B.; Hoff, M.E., Jr., "Adaptive Switching Circuits," *IRE WESCON Convention Record,* pt 4, pp.96-104, 1960.
49. Shalvi, O.; Weinstein, E., "New Criteria for Blind Deconvolution of Nonminimum Phase Systems," *Information Theory, IEEE Transactions on,* vol.36, no.2, pp.312-321, Mar. 1990.
50. Godard, D., "Self-Recovering Equalization and Carrier Tracking in Two-Dimensional Data Communication Systems," *Communications, IEEE Transactions on [legacy, pre - 1988]*, vol.28, no.11, pp.1867-1875, Nov. 1980.
51. Schniter, P.; Johnson, C.R., Jr., "Bounds for the MSE Performance of Constant Modulus Estimators," *Information Theory, IEEE Transactions on,* vol.46, no.7, pp.2544-2560, Nov. 2000.
52. Benveniste, A.; Goursat, M., "Blind Equalizers," *Communications, IEEE Transactions on [legacy, pre - 1988]*, vol.32, no.8, pp.871-883, Aug. 1984.
53. Picchi, G.; Prati, G., "Blind Equalization and Carrier Recovery Using a "Stop-and-Go" Decision-Directed Algorithm," *Communications, IEEE Transactions on [legacy, pre - 1988]*, vol.35, no.9, pp.877-887, Sept. 1987.
54. Hatzinakos, D., "Blind Equalization using Stop-and-Go Adaptation Rules," *Optical Engineering*, vol.31, no.6, pp.1181–1188, Jun 1992.
55. Zeng, H.H.; Tong, L., "The MSE Performance of Constant Modulus Receivers," *Acoustics, Speech, and Signal Processing, 1997. ICASSP-97., 1997 IEEE International Conference on*, vol.5, pp.3577-3580, 21-24 Apr. 1997.
56. Johnson, R., Jr.; Schniter, P.; Endres, T.J.; Behm, J.D.; Brown, D.R.; Casas, R.A., "Blind Equalization using the Constant Modulus Criterion: a Review ," *Proceedings of the IEEE,* vol.86, no.10, pp.1927-1950, Oct. 1998.
57. Weerackody, V.; Kassam, S.A.; Laker, K.R., "A Simple Hard-limited Adaptive Algorithm for Blind Equalization," *Circuits and Systems II: Analog and Digital Signal Processing, IEEE Transactions on*, vol.39, no.7, pp.482-487, Jul 1992.
58. Wilson, T.G.B., "Blind Equalization for ATSC DTV Receivers using Feintuch's IIR LMS Algorithm," *Intelligent and Advanced Systems, 2007 11th International Conference on,* 25-28 Nov. 2007.
59. Wilson, T.G.B., "Low-Complexity Linear-Feedback Equalization for ATSC DTV," *Consumer Electronics, 2008. ICCE 2008. IEEE International Conference on,* 9-13 Jan. 2007.
60. Wilson, T.G.B., "Robust Baud Rate Blind Equalization for ATSC DTV Receivers," *Information, Communications & Signal Processing, 2007 6th International Conference on,* 10-13 Dec. 2007.
61. Brown, D.R., Schniter, P., Johnson, C.R., Jr., "Computationally Efficient Blind Equalization," *Communications, Control and Computing, 35th Annual Allerton Conference on*, pp.54-63, Sept. 1997.
62. Ghosh, M., "A Sign-error Algorithm for Blind Equalization of Real Signals," *Acoustics, Speech and Signal Processing, 1998. Proceedings of the 1998 IEEE International Conference on,* vol.6, pp.3365-3368, 12-15 May 1998.
63. Kim, H.-N.; Lee, Y.-T.; Kim, S.W., "Mathematical Modeling of VSB-based Digital Television Systems," *ETRI Journal*, vol. 25, no. 1, pp.9-18, Feb. 2003.
64. *Field Test Results of the Grand Alliance HDTV Transmission Subsystem*, ACATS, SSWP2-1354, Sept. 1994.

65. Mackenzie, ABERT, and SET, "General Description of Laboratory Tests," DTV Field Test Report in Brazil, Jul 2000.
66. Yang, J.; Werner, J.-J.; Dumont, G.A., "The Multimodulus Blind Equalization and its Generalized Algorithms," *Selected Areas in Communications, IEEE Journal on*, vol.20, no.5, pp.997-1015, Jun 2002.
67. Vesma, J.; Saramaki, T.; Renfors, M., "Combined Matched Filter and Polynomial-based Interpolator for Symbol Synchronization in Digital Receivers," *Circuits and Systems, 1999. ISCAS '99. Proceedings of the 1999 IEEE International Symposium on,* vol.3, pp.94-97, Jul 1999.
68. Austin, M.E., "Decision-feedback Equalization for Digital Communication over Dispersive Channels," MIT Lincoln Lab., Lexington, MA, Tech. Rep. 437, Aug. 1967.
69. Peloso, R.A., "Adaptive Equalization for Advanced Television," *Consumer Electronics, IEEE Transactions on,* vol.38, no.3, pp.119-126, Aug. 1992.
70. Zukunft, R.; Haar, S.; Magesacher, T., "A Comparison of Different Blind Equalization Techniques for xDSL-Transceivers," *Broadband Communications for the Internet Era Symposium Digest, 2001 IEEE Emerging Technologies Symposium on,* pp.7-11, 10-11 Sept., 2001.
71. Godard, D., "Passband Timing Recovery in an All-Digital Modem Receiver," *Communications, IEEE Transactions on [legacy, pre - 1988]*, vol.26, no.5, pp.517-523, May 1978.
72. Treichler, J.R.; Fijalkow, I.; Johnson, C.R., Jr., "Fractionally Spaced Equalizers," *Signal Processing Magazine, IEEE,* vol.13, no.3, pp.65-81, May 1996.
73. Baek, J.-S.; Park, S.-W.; Seo, J.-S., "Novel Techniques to Minimize the Error Propagation of Decision Feedback Equalizer in 8VSB DTV System," *Broadcasting, IEEE Transactions on,* vol.53, no.2, pp.504-513, Jun 2007.
74. Dehghan, H.; Heidari, S., "Blind Iterative Linear Cancellation of Multipath for Terrestrial Digital Television Receivers," *Consumer Communications and Networking Conference, 2006. CCNC 2006. 3rd IEEE,* vol.2, pp.859-863, 8-10 Jan. 2006.
75. Firnoff, M., Ozen, S., Nereyanuru, S. M., Zoltowski, M.D., Hillery, W., "Using 8-VSB Training Sequence Correlation as a Channel Estimate for DFE Tap Initialization," *Communications, Control and Computing*, *39th Annual Allerton Conference on*, Sept. 2001.
76. Watkins, G., "Optimal Farrow Coefficients for Symbol Timing Recovery," *Communications Letters, IEEE,* vol.5, no.9, pp.381-383, Sept. 2001.
77. Qureshi, S., "Timing Recovery for Equalized Partial-Response Systems," *Communications, IEEE Transactions on [legacy, pre - 1988]*, vol.24, no.12, pp.1326-1331, Dec. 1976.

Tom Wilson MEng (Oxon) CEng MIET MIEEE

Curriculum Vitae

Key Skills

- Project management
- System architecture design
- Simulation and modelling of complex systems
- Algorithm development, implementation and optimization for real-time embedded systems
- Extensive knowledge and experience of digital signal processing (DSP) systems
- Programming: Matlab, C, C++, SystemC and DSP Assembler (TI, AD, plus proprietary DSPs)
- Applications: Speech / Audio, Communications and Image Processing.

Experience

2008-present ***Senior Algorithm Systems Designer***, On Demand Microelectronics, Vienna

Responsible for development of Digital Image Processing algorithms and their implementation on a proprietary fixed-point DSP. To date these include Edge Detection, Auto-Focus, Automatic White Balance and Colour Correction.

2005-2007 ***Algorithm Systems Designer***, On Demand Microelectronics, Vienna (2.2 years)

System architecture and algorithm designer for a multistandard digital television receiver chip, managing three engineers in software and hardware development and responsible for project planning. Sole author of four academic papers and a US patent application related to technological innovations during the project.

2003-2005 ***Design Engineer***, Imagination Technologies plc, King's Langley (2.8 years)

Design of algorithms for QPSK and OFDM acquisition and demodulation for digital television standards: DVB-T, DVB-S and DVB-H, and implementation on a proprietary fixed-point DSP. Four innovative designs were considered for patent applications. Supervised one engineer for 15 months.

2000-2002 ***Systems Engineer***, Noise Cancellation Technologies Ltd, Cambridge (2.5 years)

Development and implementation of frequency-domain algorithms for noise and echo filtering of audio signals (in a team). Sole designer of an automatic gain controller, line echo canceller, speech detector and a voice-operated switch, all of which were demonstrated on fixed-point DSPs. Partially responsible for creating group project plans.

1998 Noise Cancellation Technologies (Europe) Ltd, Cambridge (vacation)

1997 Sunrise Systems Ltd, Cambridge (vacation)

The Automation Partnership, Melbourn Science Park (vacation)

1995 Pi Research Ltd, Cambridge (vacation)

Education

1995-1999 New College, Oxford University, UK

2:1 in Engineering Science

Specialist subjects: Digital Comms, Optoelectronics, Artificial Intelligence

Final Year sponsorship by NCT (Europe) Ltd

1990-1995 Eton College, Windsor, UK

A-levels: 5 As, 1 B

AOs: 2 As

GCSEs: 11 As

Publications and Training

2007 Presented Paper: “Low-Complexity Linear-Feedback Equalization for ATSC DTV” at the International Conference on Consumer Electronics 2008, Las Vegas, Nevada, USA (sole author).

2007 Presented paper: “Robust Baud-Rate Blind Equalization for ATSC DTV Receivers” at the 6th International Conference on Information, Communications and Signal Processing 2007, Singapore (sole author).

2007 Presented paper: “Blind Linear-Feedback Equalization for ATSC DTV Reception” at the International Conference on Intelligent and Advanced Systems 2007, Kuala Lumpur, Malaysia (sole author).

2007 Presented Paper: “Baud Rate Symbol Timing Synchronization for 8-VSB ATSC DTV Receivers” at the 11th Annual IEEE International Symposium on Consumer Electronics, Dallas, Texas, USA (sole author).

2006 US Patent Application 6 082 4306, “Efficient Method and Apparatus for Timing Recovery of PAM Signals” (sole author).

2005 Attended Rohde & Schwarz Seminar on DVB-H, the standard for digital broadcasting to mobile receivers.

2004 Training course: “Real Time Embedded Systems”, by Ensigma Technologies.

2003 Training course: “Stylish Software”, by Ensigma Technologies.

2002 Attended IEE Seminar on Wireless Technologies and Applications, held at Cambridge University Engineering Department.

2001 Attended ‘Designing Systems on Silicon’ IEE Seminar, held at Cambridge University Engineering Department.

2001 Attended DSP Implementation Course at Oxford University Department for Continuing Education.

1999 2nd prize in IEE Young Members’ Section for Oxfordshire Short Papers.

1999 Management Course at Oxford University.

Personal Details

Date of birth: 22.11.1976

Languages: English (native speaker)

French (A at AS level)

German (certificate in Technical German from TU Wien, Austria)

Tel: (+43) 699 81633146

Email: twilson@iee.org

Address: Nordwestbahnstrasse 35a/13, 1020 Vienna, Austria

Clean driving licence

References

Academic and Professional references are available on request.